Theoretical Notes
Note 325

DC-TN-1298-1
(AFWL-TR-79-93)

TN

GAMMA-RAY AND NEUTRON EMP SOURCE COMPARISONS AND UNCERTAINTIES FOR SURFACE BURST EMP CODES

C. W. Jones
W. M. Folkner

Technical Note
on
Contract No. F29601-78-C-0052

Prepared for

Air Force Weapons Laboratory (ELT)
Air Force Systems Command
United States Air Force
Kirtland AFB, New Mexico 87117

Partially Supported by

Defense Nuclear Agency (DNA)

October 20, 1978

Dikewood
INDUSTRIES, INC.

1009 BRADBURY DRIVE, S.E. / TELEPHONE (505) 243-9781
UNIVERSITY RESEARCH PARK
ALBUQUERQUE, NEW MEXICO 87106

UNCLASSIFIED

SECURITY CLASSIFICATION OF THIS PAGE (When Data Entered)

REPORT DOCUMENTATION PAGE	READ INSTRUCTIONS BEFORE COMPLETING FORM
1. REPORT NUMBER: AFWL-TR-79-93	2. GOVT ACCESSION NO. / 3. RECIPIENT'S CATALOG NUMBER
4. TITLE (and Subtitle): GAMMA-RAY AND NEUTRON EMP SOURCE COMPARISONS AND UNCERTAINTIES FOR SURFACE BURST EMP CODES	5. TYPE OF REPORT & PERIOD COVERED: Technical Note - 1978
	6. PERFORMING ORG. REPORT NUMBER: DC-TN-1298-1
7. AUTHOR(s): C.W. Jones, W.M. Folkner	8. CONTRACT OR GRANT NUMBER(s): F29601-78-C-0052
9. PERFORMING ORGANIZATION NAME AND ADDRESS: Dikewood Industries, Inc., 1009 Bradbury Drive, S.E., Albuquerque, New Mexico 87106	10. PROGRAM ELEMENT, PROJECT, TASK AREA & WORK UNIT NUMBERS: Program Element 63305F, Project 672A
11. CONTROLLING OFFICE NAME AND ADDRESS: Air Force Weapons Laboratory (ELT), Air Force Systems Command, Kirtland AFB, New Mexico 87117	12. REPORT DATE: October 20, 1978
	13. NUMBER OF PAGES: 103
14. MONITORING AGENCY NAME & ADDRESS (if different from Controlling Office)	15. SECURITY CLASS. (of this report): UNCLASSIFIED
	15a. DECLASSIFICATION/DOWNGRADING SCHEDULE

16. DISTRIBUTION STATEMENT (of this Report)

17. DISTRIBUTION STATEMENT (of the abstract entered in Block 20, if different from Report)

18. SUPPLEMENTARY NOTES

This work partially supported by the Defense Nuclear Agency (DNA)

19. KEY WORDS (Continue on reverse side if necessary and identify by block number)

EMP Source Uncertainties TIG2
Gamma-Ray
LEMP 2
Neutron
SCX

20. ABSTRACT (Continue on reverse side if necessary and identify by block number)

Values of the EMP source terms due to gamma and neutron scattering which are used in two surface burst EMP codes, SCX and LEMP 2, are compared. Estimates of the uncertainties of various portions of the source specification are made. Data presented may also be useful for the estimation of EMP source terms in surface burst scenarios.

DD FORM 1 JAN 73 1473 EDITION OF 1 NOV 65 IS OBSOLETE

UNCLASSIFIED

SECURITY CLASSIFICATION OF THIS PAGE (When Data Entered)

ACKNOWLEDGMENT

The authors wish to acknowledge the cooperation of R. M. Hamilton of Mission Research Corporation who helped with the descriptions of the LEMP-2 sources.

CONTENTS

ILLUSTRATIONS

ILLUSTRATIONS (Cont'd.)

ILLUSTRATIONS (Cont'd.)

ILLUSTRATIONS (Cont'd.)

ILLUSTRATIONS (Cont'd.)

TABLES

SECTION I

INTRODUCTION

This report discusses the methods used to compute prompt and scattered gamma-ray sources and the neutron-induced EMP source terms in the codes SCX (refs. 1, 2) and LEMP-2 (ref. 3). Although absolute error estimates cannot be made on the basis of presently available data, conclusions concerning the uncertainties of several parameters are presented.

Prompt (direct) gamma contributions to the EMP sources are computed directly from the relevant cross sections and the weapon gamma output time history. The gamma output spectrum is normally modeled by one to eight separate energy groups. SCX normally treats eight energy groups (1, 2, 3, 4, 5, 6, 7, 8 MeV), and LEMP-2 includes three or more groups (normally, 0.5, 1.5, 5 MeV). Section II compares the cross sections used in these two codes with other sources of data. The effects of using these cross sections at various ranges for the computation of direct gamma sources are also compared.

The scattered gamma sources in SCX are based on curve fits by Knutson (ref. 4) to TIG2 Monte Carlo data (ref. 5). LEMP-2 scattered gamma sources are computed using fits to data of Chilton (ref. 6) and LeLevier (ref. 7). These sources and other Monte Carlo data are discussed in section III.

Neutron-induced source terms are discussed in section IV. Although implemented differently, the neutron sources in SCX

and LEMP-2 are mainly based on the Monte Carlo data of Sargis, et al. (ref. 8). Basic aspects of the source specifications and sample results are given.

Miscellaneous topics related to these sources and conclusions are given in section V. Recommendations for improvements in the sources are also presented.

In addition to the uncertainty estimates provided by this report, the basic descriptions of the techniques used to compute surface burst EMP sources may be of interest. The data provided will enable the evaluation of low altitude EMP source terms for a wide range of problems. In addition, the parameter variations given provide insight into the behavior of these source terms under various conditions.

SECTION II

DIRECT PROMPT GAMMA RESPONSES

Direct prompt gamma sources, as the name implies, are due to the initial gamma rays emitted by the device, and for the purposes of this report, they will include only that portion of the gamma flux undergoing a first scatter at any given observer location. If the device gamma output is specified by $\dot{\gamma}$ (γ MeV/s), the average gamma-ray energy is E_γ(MeV), and the range to an observer location is r (meters), the Compton current and ionization rate are computed by SCX and LEMP-2 using the relations:

$$J_{p,r}(\tau)[\text{electrons}/(m^2\text{-s})] = \frac{\dot{\gamma}(\tau)\, e^{-\mu_t \rho r 10^2} R_e \mu_c}{4\pi r^2 \; E_\gamma} \qquad (1)$$

$$Q_p(\tau)(\text{ion pairs}/(m^3\text{-s})) = \frac{\dot{\gamma}(\tau)\, e^{-\mu_t \rho r 10^2} \mu_a \rho 10^2}{4\pi r^2 \; (34 \times 10^{-6})} \qquad (2)$$

μ_t is the total interaction cross section for gammas of energy E_γ, μ_c is the Compton cross section, and μ_a is the energy absorption coefficient. μ_t, μ_c and μ_a are all dependent on E_γ and have units of (cm^2/g). R_e is the mean forward range of the average electron created by a scatter of a gamma ray of energy E_γ and has units of g/cm^2. ρ is the air density in g/cm^3.

In SCX, $(10^{+2}\mu_t\rho)^{-1}$ is usually expressed as λ_{γ_t}(m), the mean free path of the gamma ray. Similarly, $(10^{+2}\mu_c\rho)^{-1} = \lambda_{\mu_c}$(m), $(10^{-2}R_e/\rho) = R_e'$(m), and $(10^2\mu_a\rho) = E_e/(\lambda_{\gamma_t}E_\gamma)$ where E_e is the average energy of the electron created by a gamma scatter.

Tables 1, 2, 3, and 4 give values of μ_t, μ_c, μ_a, and R_e used in SCX, LEMP-2, in the TIG2 Monte Carlo used as the basis of SCX scattered gamma sources (refs. 4 and 5), data published by the National Bureau of Standards (NBS) (ref. 9), and curve fit values used in Monte Carlo calculations completed at the Los Alamos Scientific Laboratory (LASL) (ref. 10).

The SCX values of μ_t and μ_c are based on the NBS data of reference 9. Values of μ_a and R_e in SCX are based on numerical calculations reported by Jones (ref. 11).

Differences in parameter values are generally 20 percent or less, often much less. For calculations of the Compton current, the product $\mu_c R_e$ is used (values compared in table 5).

Uncertainties in μ_c, R_e and μ_a will have a linear effect on the computed current and ionization. It appears, based on reference 9 and other sources, that this uncertainty is probably 25 percent or less, except at very low energies (e.g., 0.5 MeV of table 5). Comparing values of μ_c and R_e (tables 2 and 4), it appears that the low energy variations seen in table 5 are due to different values of R_e.

μ_t is present in an exponential function of range and thus uncertainties in μ_t (or the air density) can have a more significant impact on the predicted source terms. For large yield problems, gamma source terms may be important out to a range of several kilometers (on the order of 10-30 gamma mean-free-paths). For example, at a range of 3 kilometers ($\rho = 1.225 \times 10^{-3}$), the 1.2 percent difference in the SCX (NBS) and TIG2 values of μ_t

Table 1

TOTAL GAMMA SCATTER CROSS SECTIONS, $\mu_t(cm^2/g)$

E_γ (MeV)	SCX	LEMP-2	TIG2	NBS	LASL
0.5	0.0870	0.0869	0.0885	0.0870	0.0911
1.0	0.0636		0.0631	0.0636	0.0635
1.5	0.0518	0.0516	0.0512	0.0518	0.0514
2.0	0.0445		0.0448	0.0445	0.0443
3.0	0.0358		0.0363	0.0358	0.0359
4.0	0.0308		0.0310	0.0308	0.0309
5.0	0.0275	0.0274	0.0274	0.0275	0.0275
6.0	0.0252		0.0249	0.0252	0.0250
7.0	0.0235		0.0231		0.0231
8.0	0.0223		0.0218	0.0223	0.0215

Table 2

COMPTON GAMMA SCATTER CROSS SECTIONS, $\mu_c(cm^2/g)$

E_γ (MeV)	SCX	LEMP-2	TIG2	NBS
0.5	0.0870	0.087	0.0885	0.0870
1.0	0.0636		0.0631	0.0636
1.5	0.0517	0.0516	0.0511	0.0517
2.0	0.0441		0.0444	0.0441
3.0	0.0347		0.0352	0.0347
4.0	0.0289		0.0291	0.0289
5.0	0.0250	0.0249	0.0249	0.0250
6.0	0.0221		0.0219	0.0221
7.0			0.0196	
8.0	0.0181		0.0179	0.0181

Table 3

GAMMA ENERGY ABSORPTION CROSS SECTIONS, $\mu_a(cm^2/g)$

E_γ (MeV)	SCX	LEMP-2	TIG2	NBS	LASL
0.5	0.0298	0.0296	0.0302	0.0297	0.0348
1.0	0.0280		0.0280	0.0280	0.0283
1.5	0.0257	0.0256	0.0251	0.0257	0.0251
2.0	0.0236		0.0237	0.0238	0.0230
3.0	0.0201		0.0216	0.0212	0.0204
4.0	0.0175		0.0193	0.0194	0.0187
5.0	0.0160	0.0182	0.0177	0.0182	0.0175
6.0	0.0142		0.0166	0.0174	0.0166
7.0			0.0158		0.0159
8.0	0.0122		0.0153	0.0162	0.0153

Table 4

MEAN FORWARD ELECTRON RANGE
OF COMPTON ELECTRON DISTRIBUTION, $R_e(g/cm^2)$

E_γ (MeV)	SCX	LEMP-2	TIG2
0.5	0.0206	0.0264	0.0208
1.0	0.083	0.1028	0.084
1.5	0.175	0.204	0.172
2.0	0.276	0.319	0.267
3.0	0.515	0.571	0.490
4.0	0.783	0.839	0.717
5.0	1.040	1.114	0.951
6.0	1.358	1.395	1.19
7.0	1.675	1.679	1.43
8.0	1.967	1.963	1.68

Table 5

$\mu_c R_e$ PRODUCT
(Factor Proportional to Compton Current)
(Dimensionless)

E_γ (MeV)	SCX	LEMP-2	TIG2	LASL
0.5	0.00179	0.00230	0.00184	0.00328
1.0	0.00528		0.00530	0.00655
1.5	0.00905	0.0105	0.00879	0.00980
2.0	0.0122		0.0119	0.0130
3.0	0.0179		0.0172	0.0190
4.0	0.0226		0.0209	0.0242
5.0	0.0260	0.0277	0.0237	0.0282
6.0	0.0300		0.0261	0.0307
7.0			0.0280	0.0318
8.0	0.0356		0.0301	0.0315

for E_γ = 1.5 MeV result in a 25 percent difference in the exponential attenuation. Fortunately, uncertainties in this parameter are small. For many problems, the uncertainty in the specified air density may be of more importance. If the air density is decreased by only 5 percent in the above example (increase in altitude of ~525 meters), the current or ionization rate would be increased by a factor of 2.6. Plots of factors of equations (1) and (2) as a function of range for different gamma energies are given by figures 1 and 2 using SCX parameters. The use of other parameters provides very similar results. It may be seen from figures 1 and 2 that for ranges less than 1 kilometer and for a constant gamma yield, the EMP source terms may be larger for smaller gamma energies (there are more gammas interacting in a given volume). At larger ranges, the higher energies are of

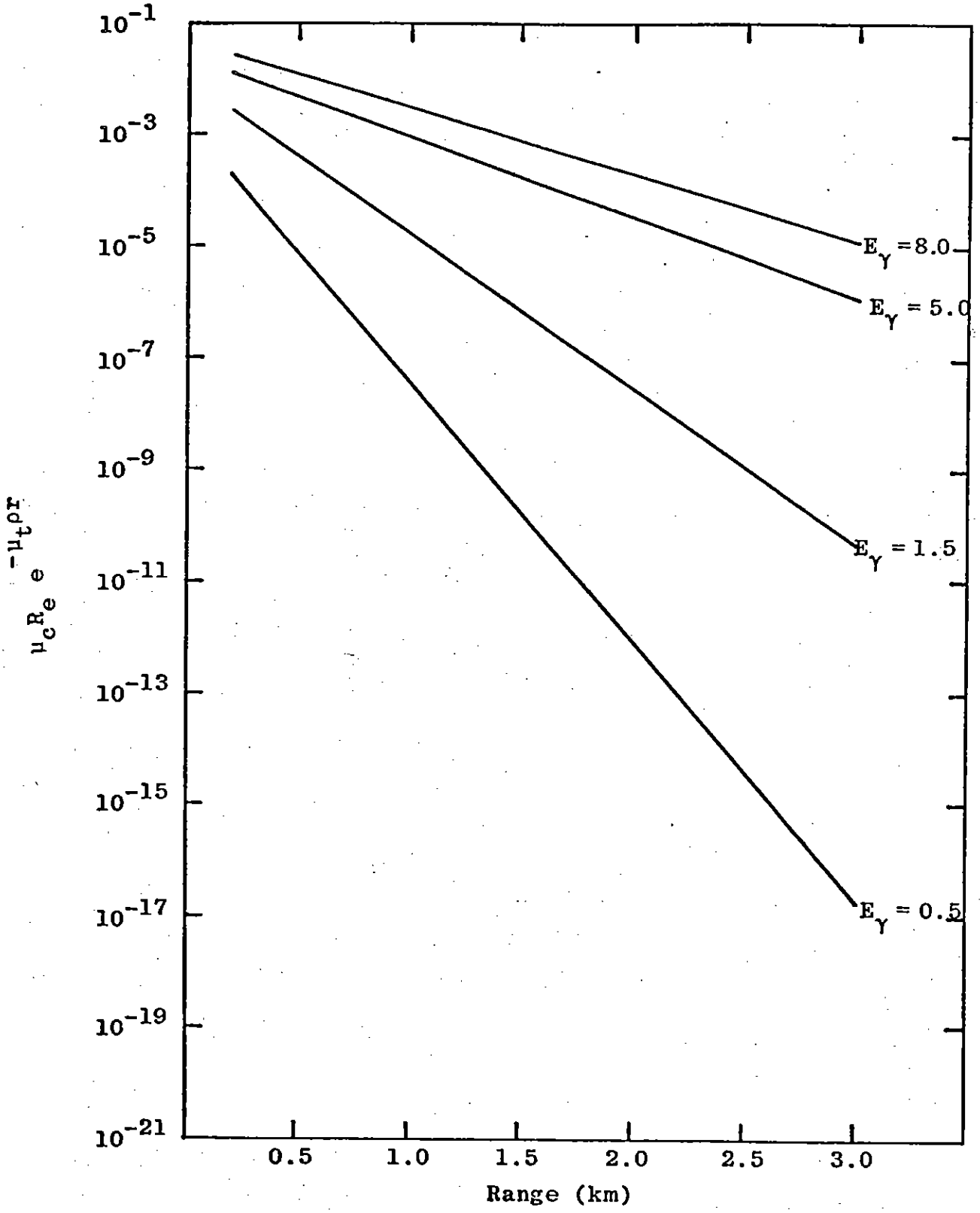

Figure 1. Direct Gamma Current vs. Range at Sea Level ($\rho = 1.225 \times 10^{-3}$ g/cm^3)

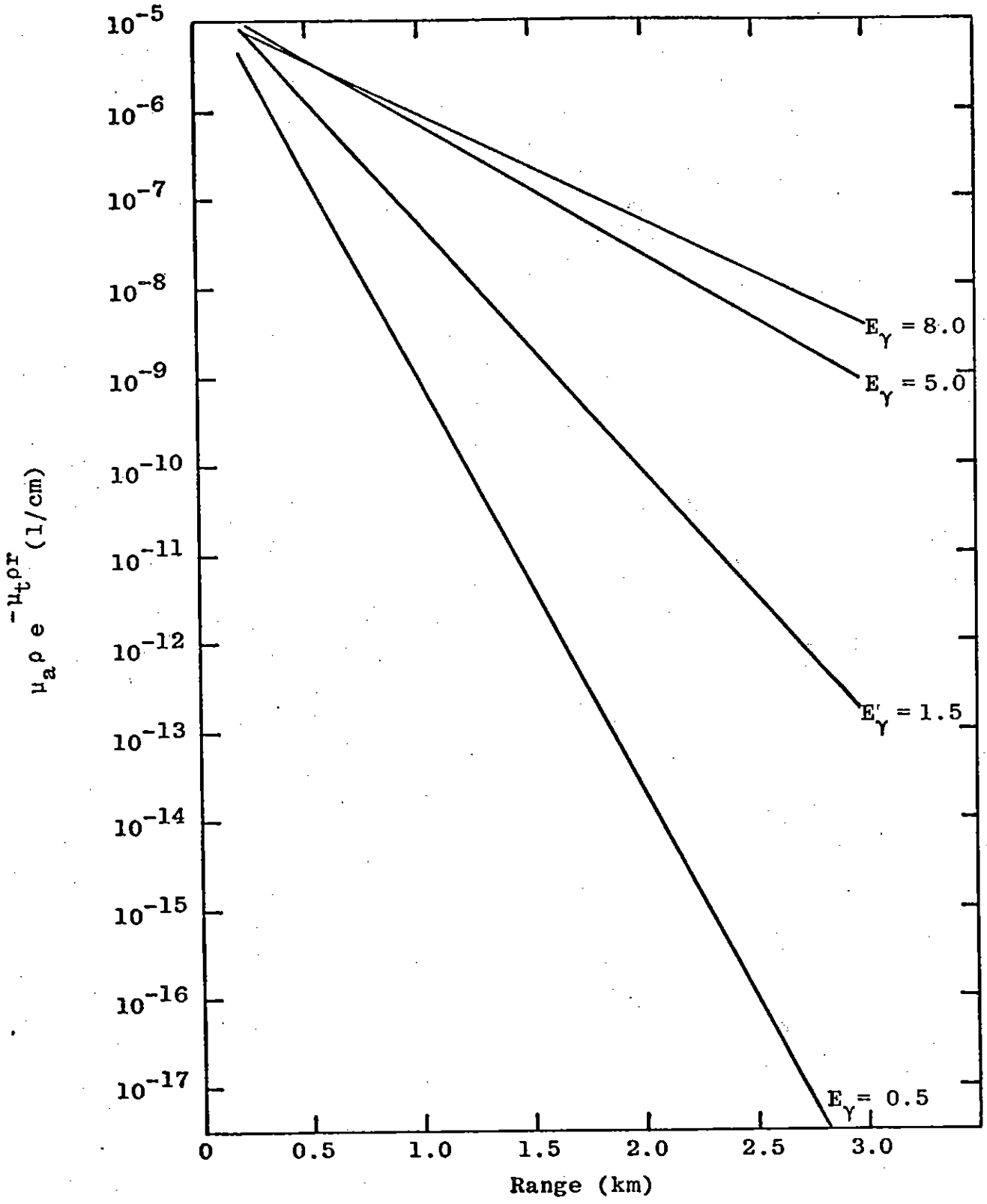

Figure 2. Direct Gamma Energy Deposition vs. Range at Sea Level ($\rho = 1.225 \times 10^{-3}$ g/cm^3)

much greater importance due to their longer mean-free-paths, even though there are fewer of them emitted from the bomb per unit yield.

Self consistency, the effects of the EMP fields on the source electrons, will normally cause a decrease in the prompt source current. However, the method used to treat this effect in SCX and LEMP-2 affects all source contributions and is discussed in section V.

The use of equations (1) and (2) assumes that the electron lifetime is short compared to the time required for significant variations in $\dot{\gamma}(\tau)$. Figures 3 and 4 (from ref. 12) compare currents and ionization rates computed using equations (1) and (2) with those computed by convoluting $\dot{\gamma}(\tau)$ with electron delta function current and ionization responses. For this $\dot{\gamma}(\tau)$ pulse the peak J is reduced ~18 percent and the current pulse is broadened. There is a larger decrease in the ionization rate peak. For slower pulse rise rates, the effect is less pronounced.

Over a region the size of the source region of a surface burst, surface irregularities are likely to be of importance for many geographical locations. This uncertainty is obviously scenario dependent.

The final uncertainty in the prompt gamma sources which is discussed here is that due to the geomagnetic turning of the source electrons. Due to the short lifetime of the electrons at sea level (on the order of 1 shake), the electrons are not turned to the extent seen in a high-altitude case. Figure 5 compares

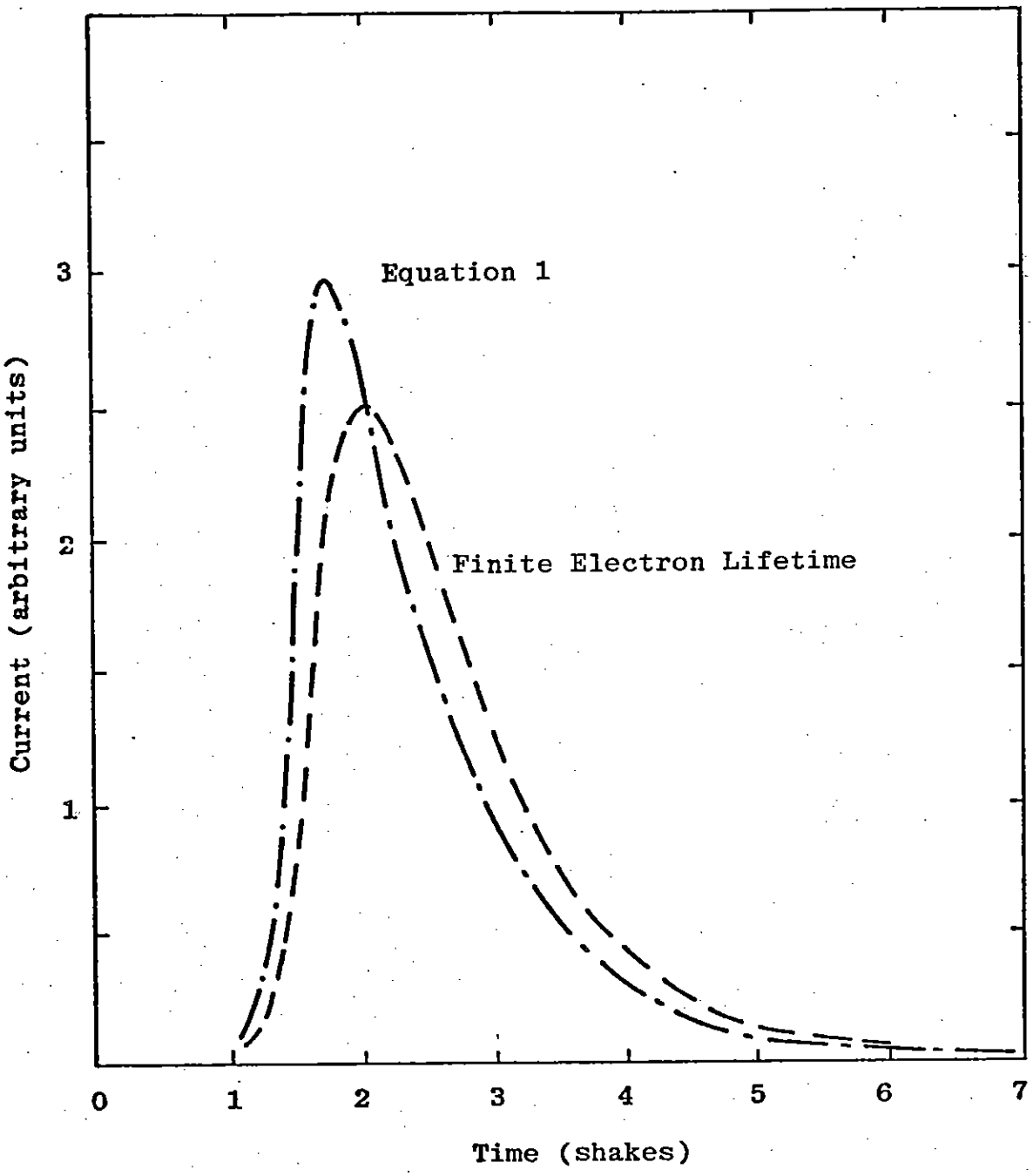

Figure 3. Finite Electron Lifetime Effects on Compton Current

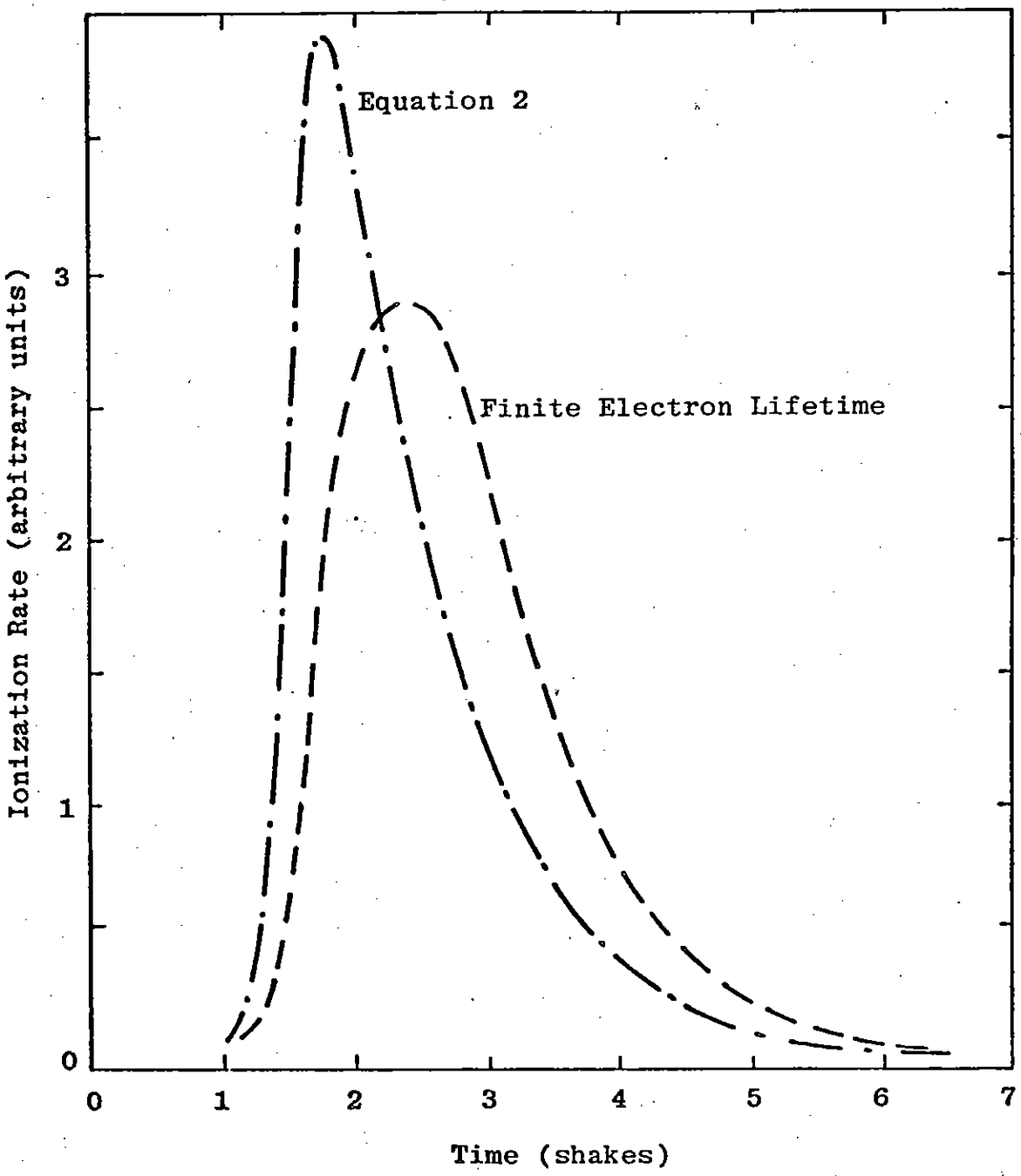

Figure 4. Finite Electron Lifetime Effects on Ionization Rate

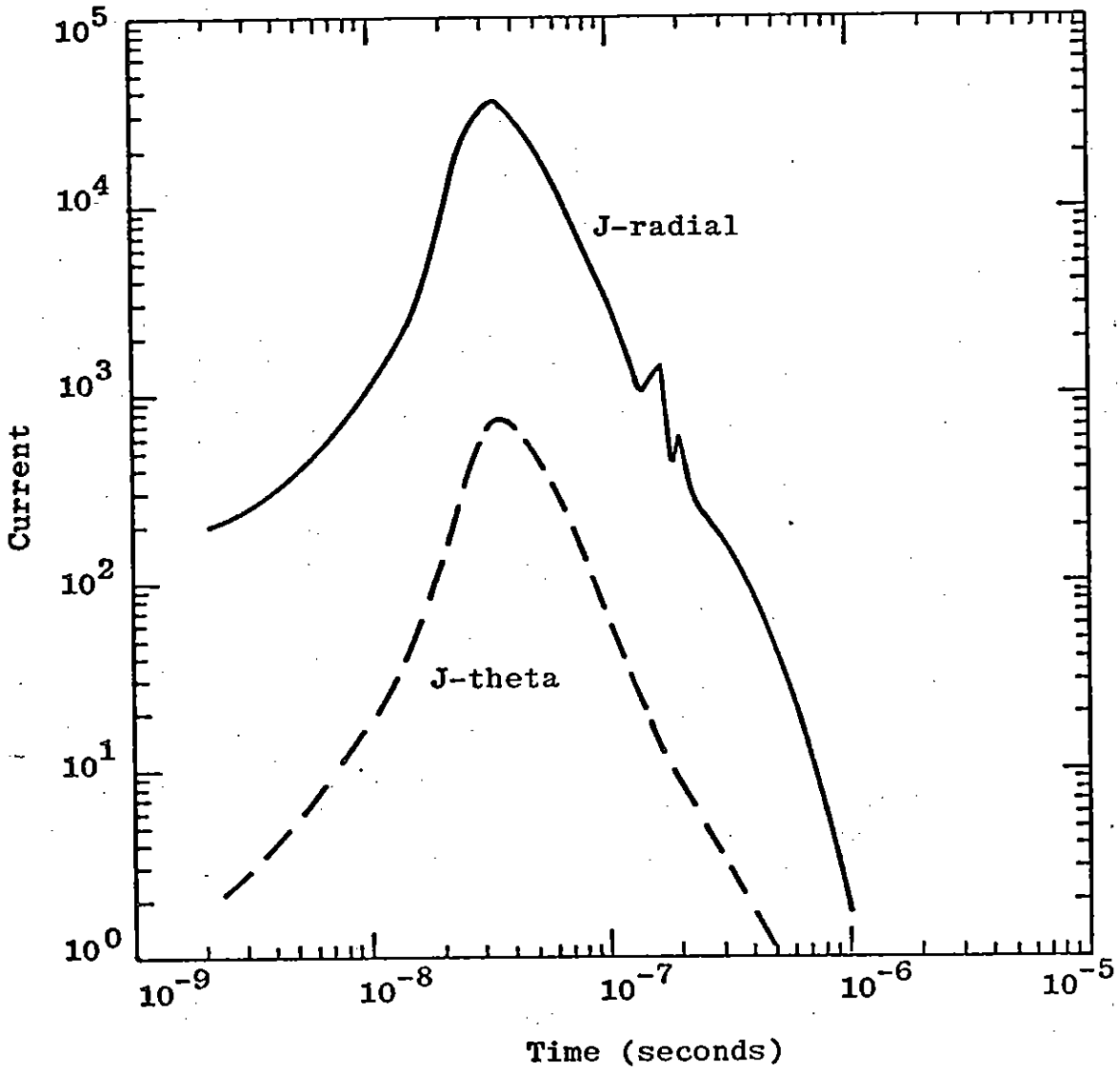

Figure 5. Geomagnetic Turning Current at Sea Level

the turning current (transverse to the line-of-sight from the burst) with the current of equation (1). The direction of this current is dependent on both the burst and observer locations, and thus this component may either add to or subtract from the J_θ due to scattered gammas, or it may be in a direction parallel to the earth but transverse to the line-of-sight. Changes in the radial current produced by the fields are normally less than a factor of two. Because of the large "drag forces" on the Compton electrons due to air scattering, self-consistency is of most importance for electric field values larger than 10^5 V/m and magnetic fields larger than a few gauss.

SECTION III

SCATTERED GAMMA RESPONSES

The scattered gamma source terms are those sources produced by the second or subsequent scatter of the gamma rays, and specifically exclude the first scatter (direct) sources discussed in section II. The following paragraphs discuss the SCX, LEMP-2 and LASL scattered gamma sources, angular variations, and code-code comparisons.

1. SCX SCATTERED GAMMA SOURCES

The radial and transverse currents and ionization rate, as computed by the AFWL gamma-ray Monte Carlo code TIG2 (ref. 5), were curve fit by Knutson (ref. 4) for use in SCX. In the TIG2 Monte Carlo, the cross section values of tables 1 through 4 were used for the current and ionization scoring, with the proper gamma energy used to compute the source contribution for each scatter in the Monte Carlo. TIG2 treated Compton scattering and pair-production. The neglect of the photoelectric effect should only affect results for late times when low energy photons ($\tilde{<}$0.03 MeV) become of greater importance.

Each of the three functions (J_r, J_θ, Q) is fit as a function of range and time for source gamma energies of 1, 2, 3, 4, 5, 6, 7 and 8 MeV. The data used in SCX is for a scoring bin centered at an angle of 2.87 degrees above the surface of the ground, with J_r radially outward and J_θ pointing into the ground at the surface. TIG2 also computed data in other bins in the air and ground but

these are not used at the present time. All three parameters are fit using the functional form

$$F(t,r) = Ae^{BT}\ (t + 1)^{c} \tag{3}$$

where

$$A = F(t = 0) \tag{4}$$

$$B = D\left[\ell n\ \frac{F(t = 10^{-7})}{A}\ \ell n(71) - \ell n\ \frac{F(t = 7 \times 10^{-7})}{A}\ \ell n(11)\right] \tag{5}$$

$$C = D\left[10\ell n\ \frac{F(t = 7 \times 10^{-7})}{A} - 70\ell n\ \frac{F(t = 10^{-7})}{A}\right] \tag{6}$$

$$D = \left[10\ell n(71) - 70\ell n(11)\right]^{-1} \tag{7}$$

$F(t = 0)$, $F(t = 10^{-7})$, $F(t = 7 \times 10^{-7})$ are found from fits to the data as a function of range:

$$F(t = 0) = a_1\ e^{a_4 r}\ r^{a_7} \tag{8}$$

$$F(t = 10^{-7}) = a_2\ e^{a_5 r}\ r^{a_8} \tag{9}$$

$$F(t = 7 \times 10^{-7}) = a_3\ e^{a_6 r}\ r^{a_9} \tag{10}$$

The units of t are seconds and r is in meters. Thus for each of the eight energy groups, there are nine curve-fit coefficients for each of the three functions. The time dependence of the delta-function responses is, in general, a function of range and gamma energy. The values of curve-fit coefficients of equations (8) through (10) are given by reference 4.

The curve fits for J_r, J_θ, and Q are compared with the Monte Carlo data in figures 6 through 11 at ranges of 475, 1475 and 2475 meters for the 2 and 5 MeV bins. The vertical tic marks on the Monte Carlo curves represent the statistics of the TIG2 calculations. The agreement between data and fits shown by these figures is fairly typical of a majority of the data, which is available for ranges on the interval of 0.1 to 3 kilometers. The curve fits are valid to times of approximately 70 shakes. With the exception of J_θ, the fits appear to be good to within a factor of 2 or better (especially at the smaller ranges). The Monte Carlo statistics are typically 50 percent or less. Smoothing of the data in range by the curve fits probably improves the accuracy of the range dependence of the fits with respect to the statistical variations of the TIG2 data.

J_θ responses are typically about two orders of magnitude less than the J_r responses. However, this component can be important in EMP calculations since it directly drives E_θ, the radiated field component. There is no J_θ component in the prompt (direct) gamma source, unless geomagnetic field and/or self-consistent effects are included. The curve-fit form used in SCX describes a J_θ scattered component which has its maximum value at t = 0. Physically, this is only correct at the ground. Shaefer (ref. 13) presented results of Monte Carlo calculations for air over ground gamma transport. The J_θ waveform of figure 12 resulted from smoothed data for an angular bin just above the ground. The accuracy of the early time SCX J_θ gamma

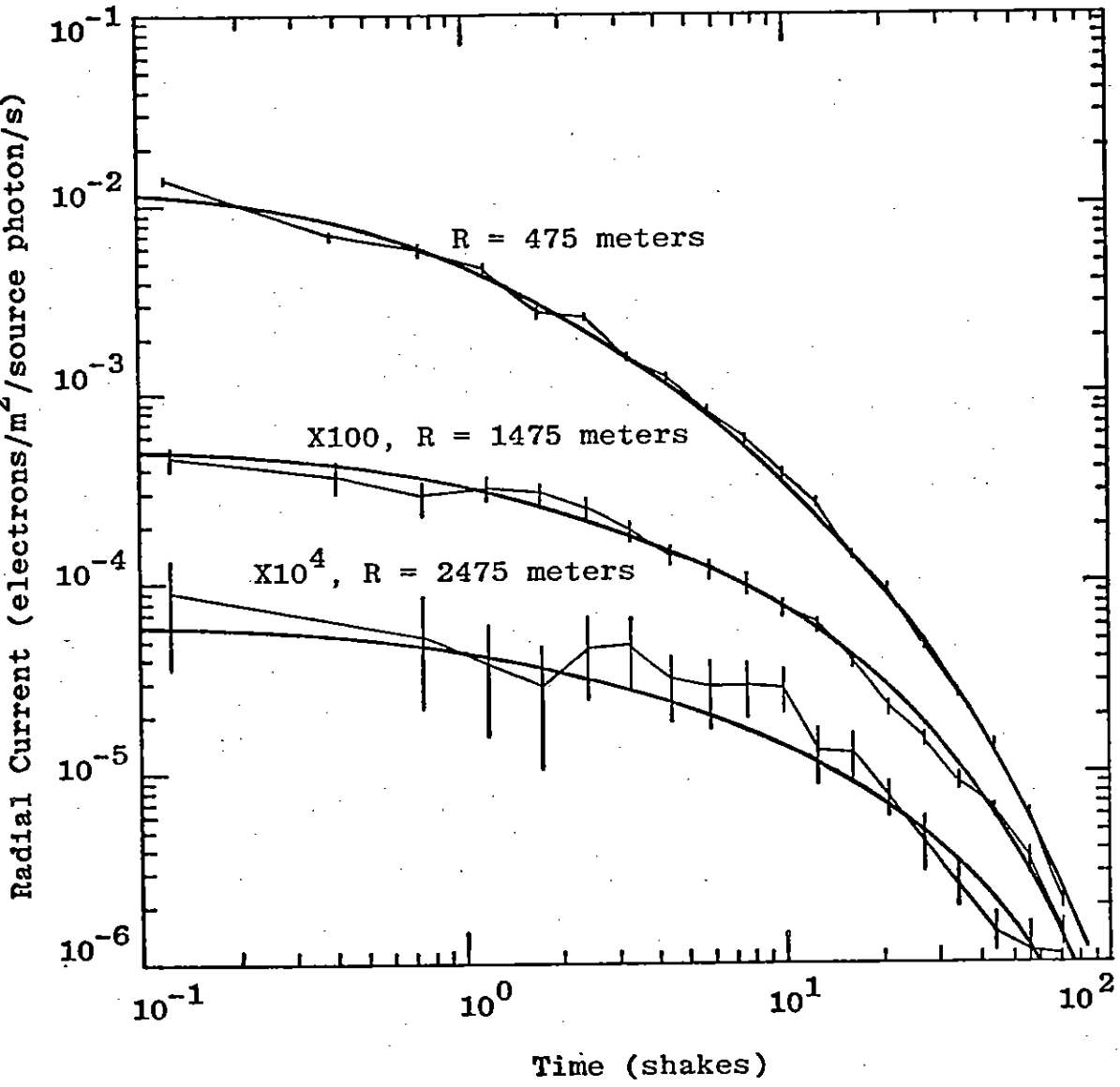

Figure 6. Scattered Gamma Radial Current vs. Time, E_γ = 2 MeV, Bin 2.87° Above Ground, TIG2 Data and Fit of Reference 4

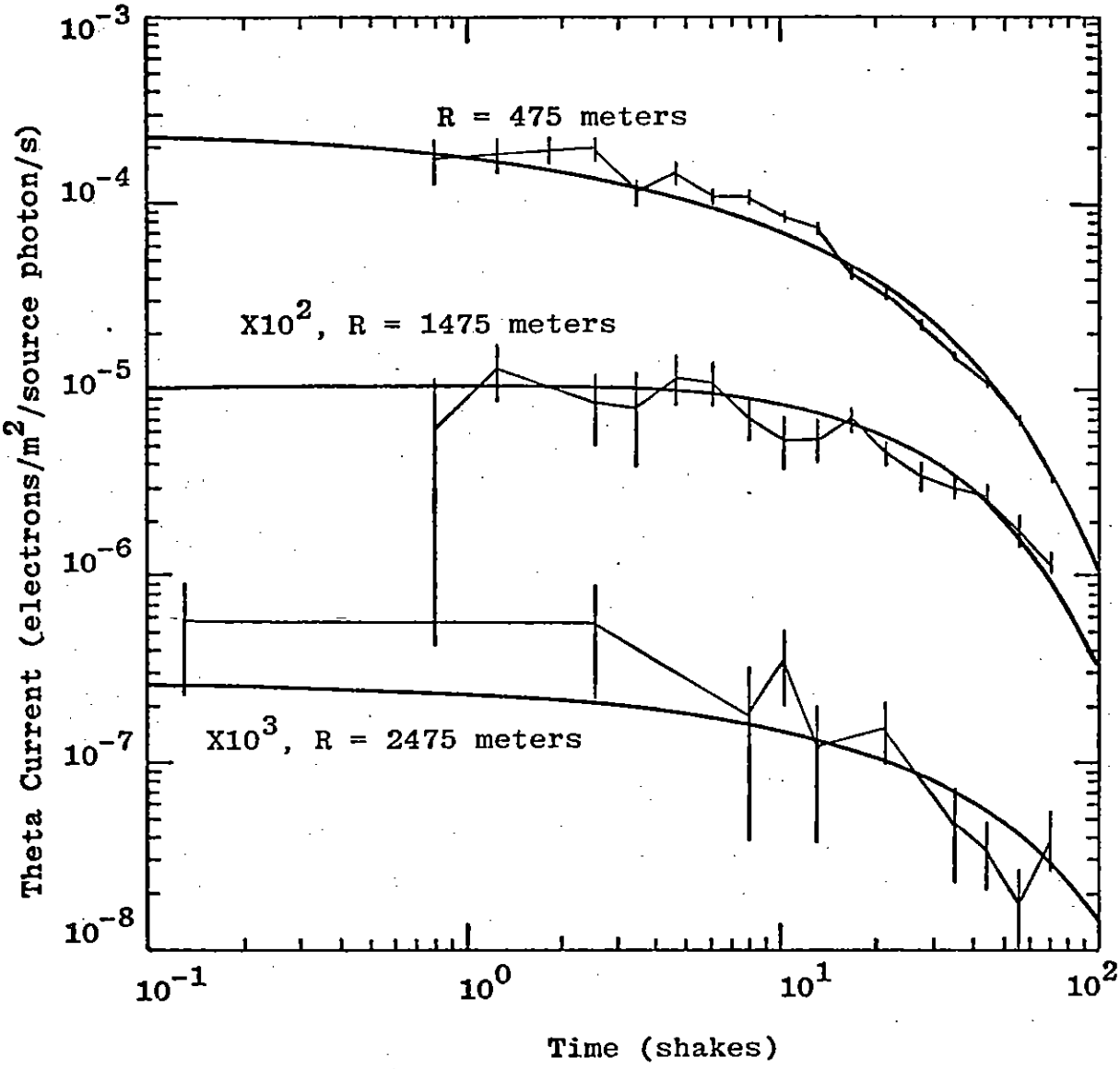

Figure 7. Scattered Gamma Theta Current vs. Time, E_γ = 2 MeV, Bin 2.87° Above Ground, TIG2 Data and Fit of Reference 4

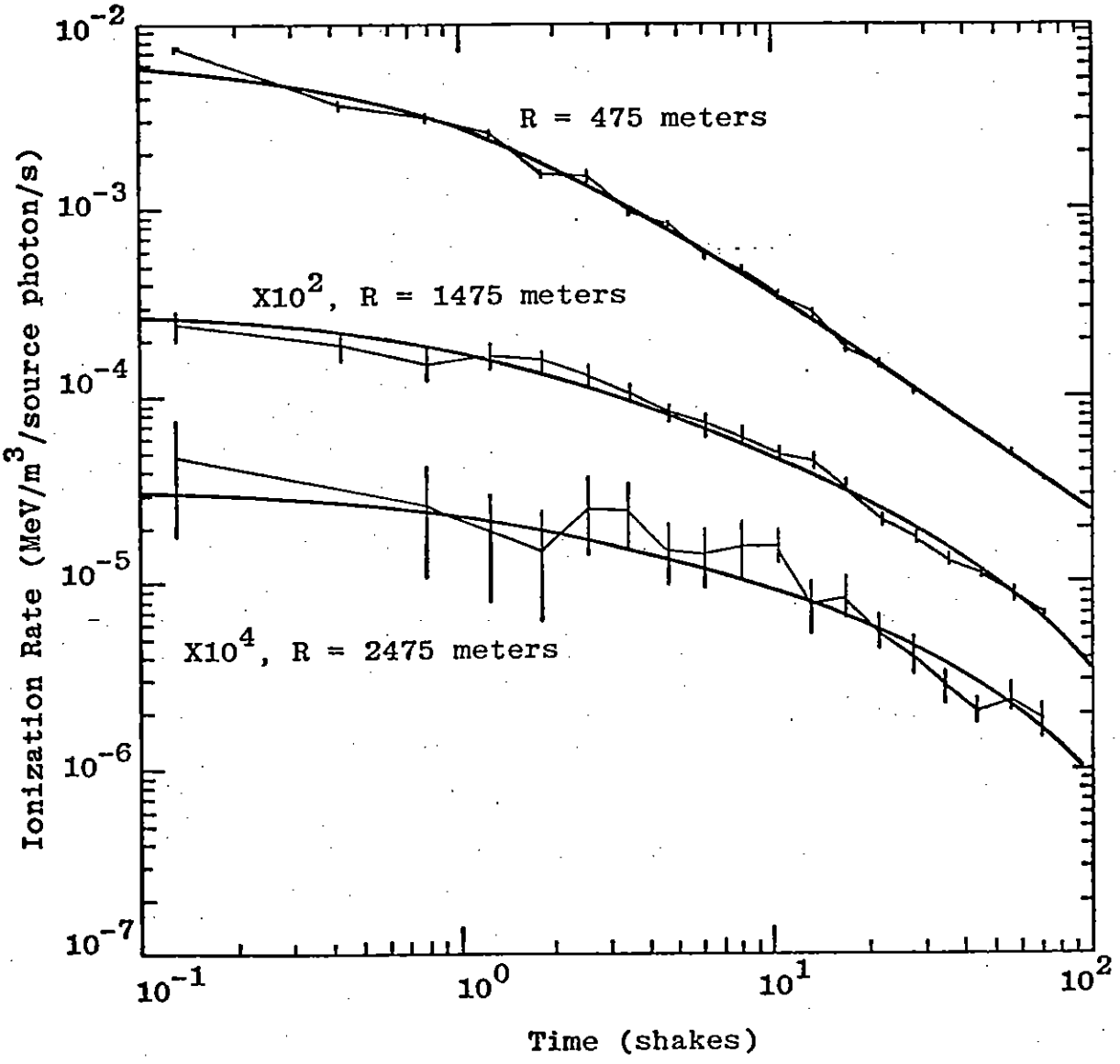

Figure 8. Scattered Gamma Ionization rate vs. Time, E_γ = 2 MeV, Bin 2.87° Above Ground, TIG2 Data and Fit of Reference 4

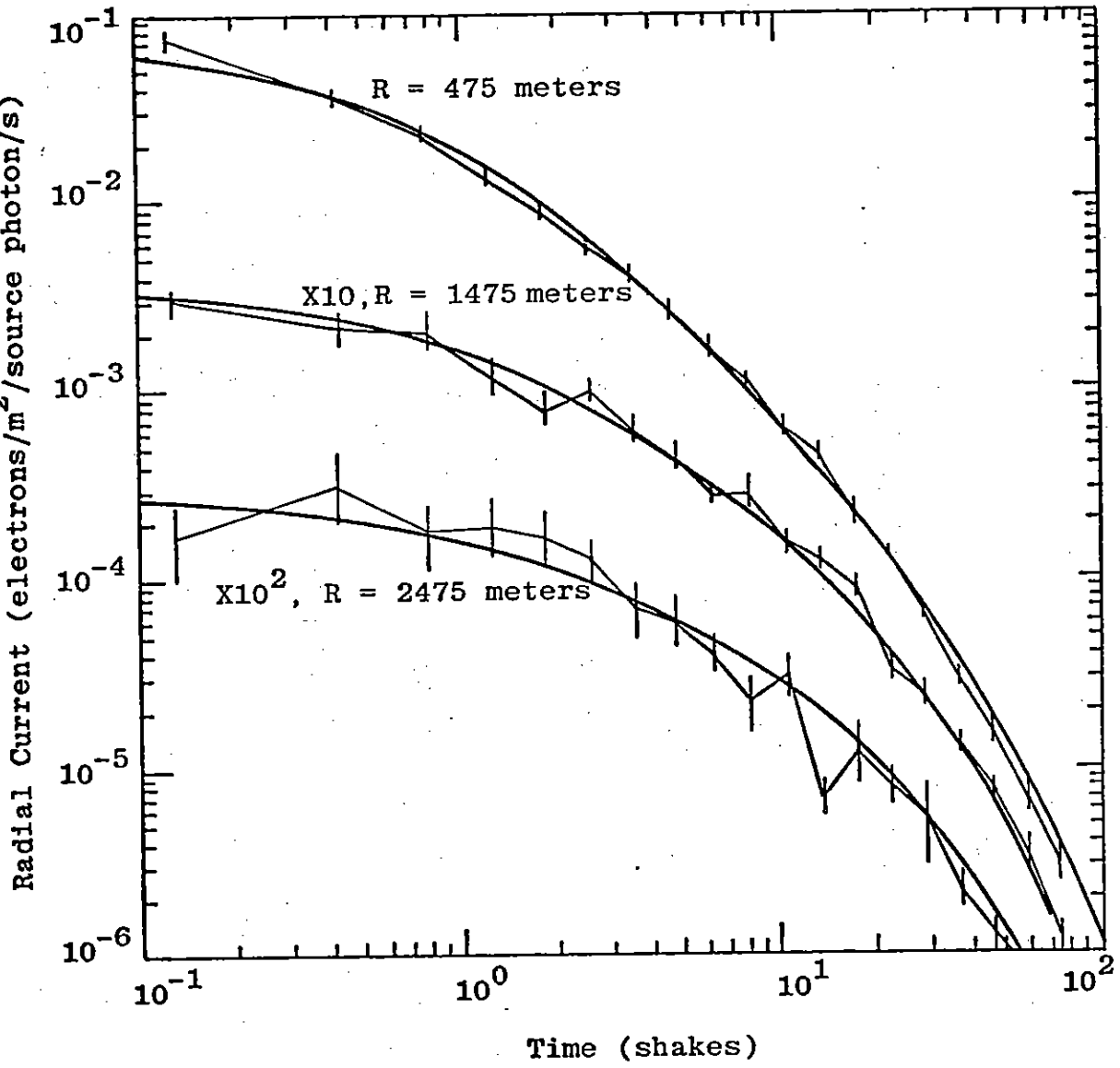

Figure 9. Scattered Gamma Radial Current vs. Time, E_γ = 5 MeV, Bin 2.87° Above Ground, TIG2 Data and Fit of Reference 4

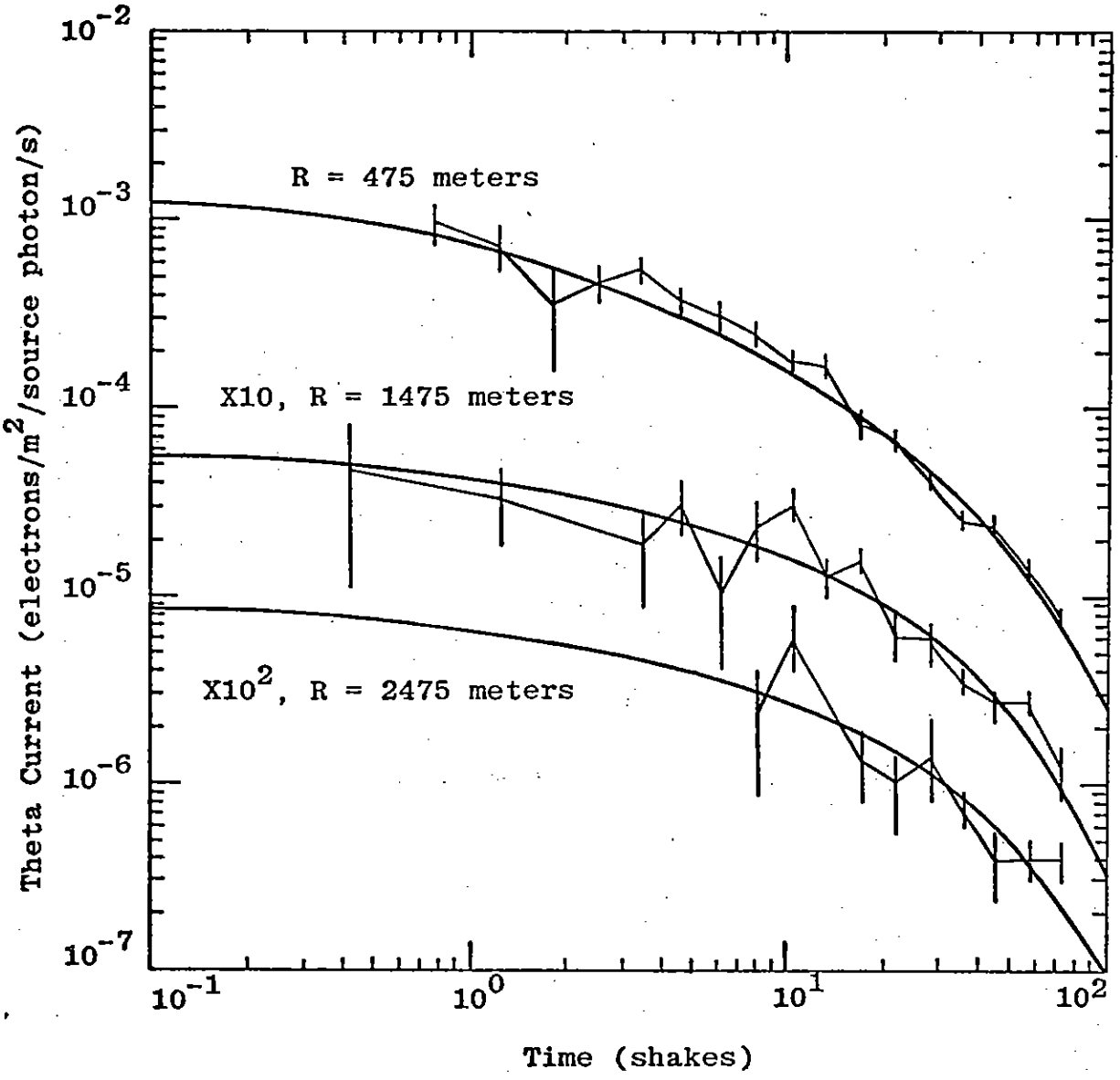

Figure 10. Scattered Gamma Theta Current vs. Time, E_γ = 5 MeV, Bin 2.87° Above Ground, TIG2 Data and Fit of Reference 4

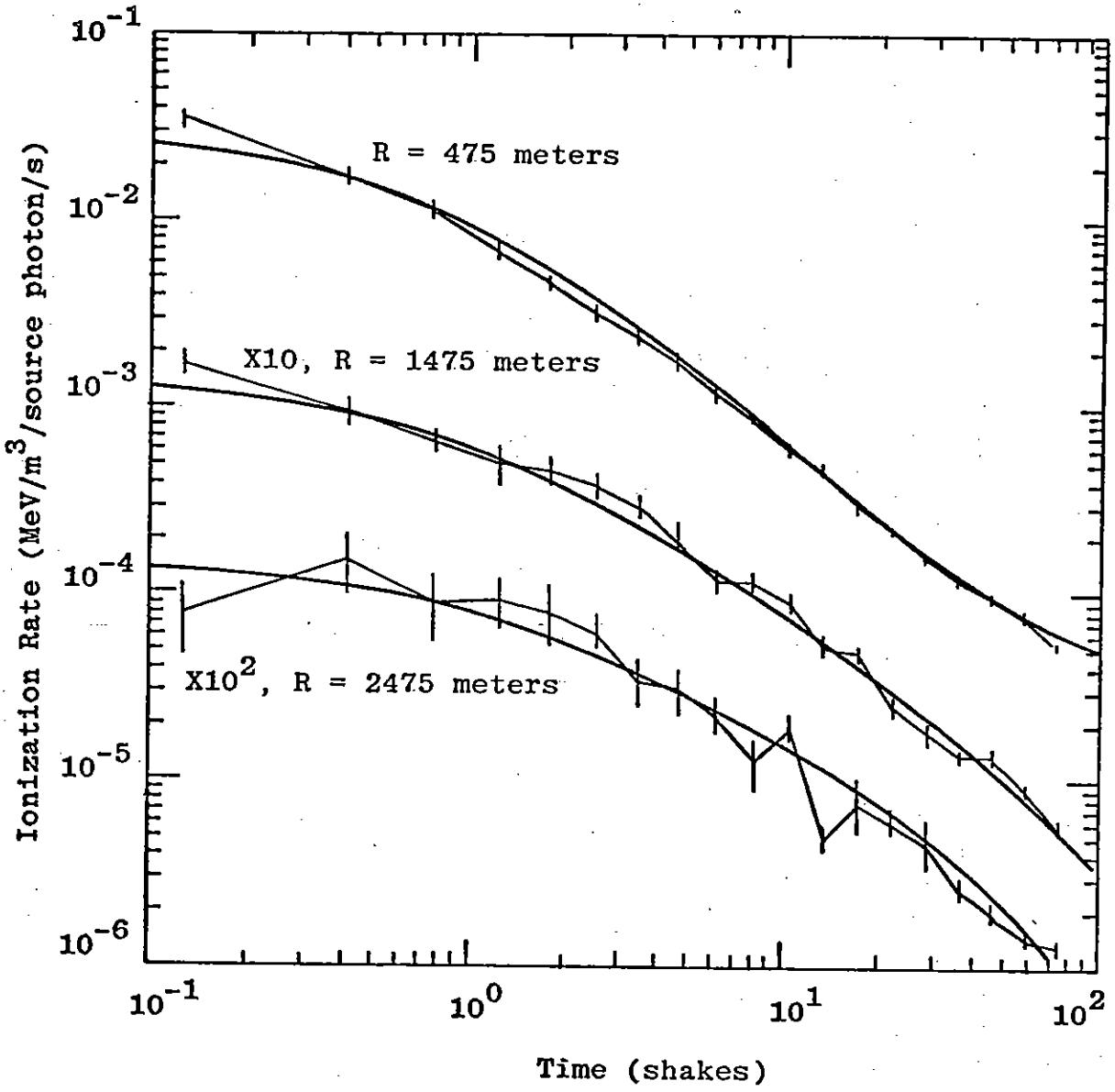

Figure 11. Scattered Gamma Ionization Rate vs. Time, E_γ = 5 MeV, Bin 2.87° Above Ground, TIG2 Data and Fit of Reference 4

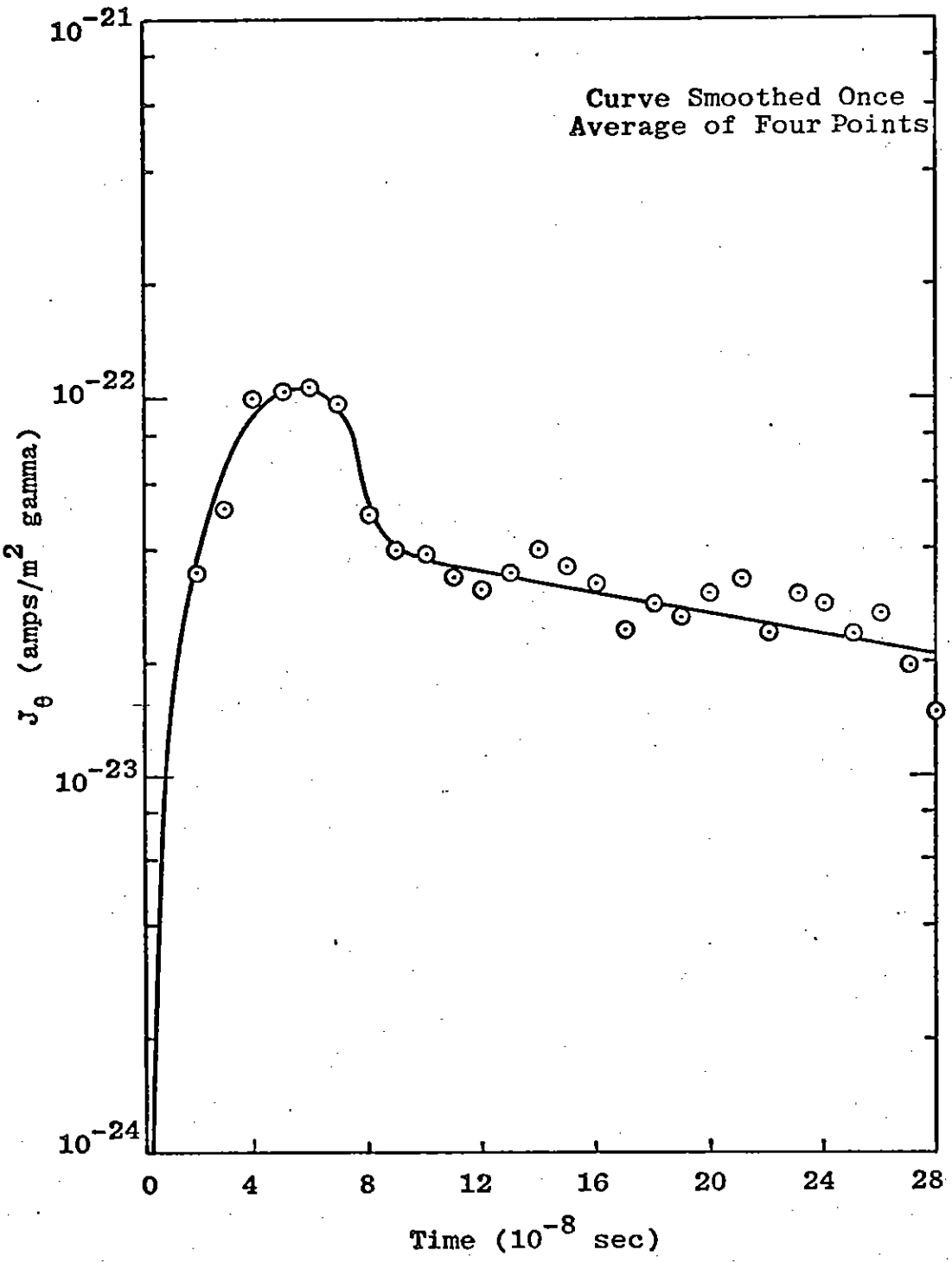

Figure 12. Theta Current vs. Time at 300 Meters for an Initial Gamma Ray at 2 MeV (Ref. 12)

sources would be improved if the curve fit form of equations (3) through (10) were modified to give values of J_θ at t = 0 which decrease for angles above the ground. Since this dependence is connected with the angular dependence discussed below, both topics are covered in the appendix.

2. LEMP-2 SCATTERED GAMMA SOURCES

The scattered gamma response in LEMP-2 is based on the data of Chilton (ref. 6) and LeLevier (ref. 7). The LeLevier Monte Carlo treated the Compton and photoelectric effects, but ignored pair-production. Responses to a delta function of gamma rays at the source are expressed in reference 3 as:

$$J_{s_r}(\tau,r) = \frac{q\mu_e R_i e^{-\mu_{ti}\rho r}\, a_i \mu_{ti}\rho r e^{b_i \mu_{ti}\rho r}}{4\pi r^2}\left(1 - \frac{\bar{a}_i \mu_{ti}\rho r}{\bar{b}_i + \mu_{ti}\rho r}\right) g(\tau) \qquad (11)$$

$$Q_s(\tau,r) = \frac{\mu_{ai} e^{-\mu_{ti}\rho r}\, a_i \mu_{ti}\, \rho r e^{b_i \mu_{ti}\rho r}\, \bar{g}(\tau)}{4\pi r^2} \qquad (12)$$

where r is in centimeters. The time dependences are given by:

$$g(\tau) = \left[\frac{1}{\alpha_1} + \frac{B}{\alpha_2}\right]\left(e^{-\alpha_1 \tau} + Be^{-\alpha_2 \tau}\right) \qquad (13)$$

$$\bar{g}(\tau) = \left[\frac{1}{\bar{\alpha}_1} + \frac{\bar{B}}{\bar{\alpha}_2}\right]\left(e^{-\bar{\alpha}_1 \tau} + \bar{B}e^{-\bar{\alpha}_2 \tau}\right) \qquad (14)$$

The coefficients of equations (13) and (14) are energy and range independent in LEMP-2 and, for τ in shakes, give the following time functions

$$g(\tau) = 3.47\left(e^{-0.445\tau} + 0.08\ e^{-0.0652\tau}\right) \quad (15)$$

$$\bar{g}(\tau) = 8.795\left(e^{-0.331\tau} + 0.22\ e^{-0.0381\tau}\right) \quad (16)$$

which are normalized to unit area. These response functions are based on the data of reference 7.

The scattered flux build-up, f_B, is characterized as in reference 6 by Chilton as

$$f_B = a_i \mu_{ti} \rho r\ e^{b_i \mu_{ti} \rho r} \quad (17)$$

The parameters a_i and b_i (i is the energy index) are those for water in reference 6. The variation of a_i and b_i with atomic number is very well behaved, and it seems that the use of values for water instead of air should result in uncertainties less than a factor of 3 (probably less than 2) out to ranges of 10 mean-free-paths for energies greater than 1 MeV. The uncertainty for the 0.5 MeV bin is larger and the use of a_i and b_i for H_2O at 0.5 MeV instead of parameters for air may result in an overestimate of the scattered flux, based on the data of Chilton.

LEMP-2 also includes a correction term for the Compton current build-up factor

$$f_{j_{c_i}} = 1 - \frac{\bar{a}_i \mu_{ti} \rho r}{\bar{b}_i + \mu_{ti} \rho r} \quad (18)$$

This factor was fitted from the data of LeLevier, which extended to a range of 1 kilometer.

It should be noted that Schaefer (ref. 13) and Pine (ref. 14) also completed Monte Carlo calculations for gamma rays in homogeneous air. Results of these calculations agreed very well with those of LeLevier.

3. LASL MONTE CARLO SCATTERED GAMMA SOURCES

Scattered gamma source fits based on Monte Carlo data were recently reported by Malik, Cashwell, and Schrandt at LASL (ref. 10). Calculations were completed using the MCNP Monte Carlo code for a homogeneous air geometry. Results were scored for gamma energies of 1, 1.5, 2, 3, 4 and 6 MeV at radii of 400, 800, 1200 and 1600 meters. The outer cutoff radius of the calculation was 2000 meters and the time cutoff was 6.33 micro-seconds. Gamma rays were followed until their energy was below 5 percent of the source gamma energy.

Analytic curve fits to the resulting data were also reported in reference 10. These fits are functions of the gamma energy, the range, and the observer time.

$$J(E,r,t) = \frac{\mu_c R_e \; e^{-X} \; B_J A_J \; e^{-S_J t^{N_J}}}{4\pi r^2} \quad \left(\frac{\text{electrons}}{\text{cm}^2\text{-shake-source photon}}\right) \tag{19}$$

$$Q(E,r,t) = \frac{\rho \mu_a E \; e^{-X} \; B_W A_W \; e^{-S_W t^{N_W}}}{4\pi r^2} \quad \left(\frac{\text{MeV}}{\text{cm}^2\text{-shake-source photon}}\right) \tag{20}$$

where E is in MeV, r is in centimeters, and t is in shakes. ρ is the air density (g/cm^3) and

$$X = \mu_t \rho r$$

$$\mu_a E = 0.0283E^{0.703}$$

$$\mu_c R_e = \frac{0.00656E}{1.0 + 0.0013E^3}$$

$$\mu_t = 0.0635E^{-0.52}$$

$$S_W = 2.0E^{0.2}\ X^{-0.73}$$

$$S_J = 2.6\ X^{-0.85}$$

$$N_W = 0.5 - 0.3\ e^{-0.36X}$$

$$N_J = 0.6 - 0.3\ e^{-0.3X}$$

$$B_W = 0.80E^{-0.37}\ X$$

$$B_J = 0.40E^{-0.033}\ X^{1.25E^{-0.15}}$$

$$A_W = \frac{N_W S_W^{1/N_W}}{\Gamma\left(\frac{1}{N_W}\right)}$$

$$A_J = \frac{N_J S_J^{1/N_J}}{\Gamma\left(\frac{1}{N_J}\right)}$$

where Γ is the normal gamma function. The factors B_W and B_J are the time integrated build-up factors for Q and J, respectively. These factors are different for current and ionization and are lower than the build-up factors used in LEMP-2, as would be expected (section III.2. and ref. 10).

4. ANGULAR VARIATION

It is probable that a large portion of the difference between the various scattered-gamma EMP source specifications can be accounted for by the angular dependence of the source.

The LEMP-2 and LASL sources are based on homogeneous air Monte Carlo and are thus most appropriate at angles near vertical (farthest from the ground). SCX curve fits are to TIG2 Monte Carlo data, which treated the air-ground interface. The fit actually used in SCX is for the bin nearest the ground (2.87 degrees). This bin is quite large at the far ranges (2.87 degrees corresponds to a height of 50 meters at 1 kilometer range). Figures 13 and 14 show the variations in J_r, J_θ, and Q versus angle (θ measured from vertical). These data points are taken from the TIG2 Monte Carlo data for 1 MeV at a range of 0.475 kilometers and 4 MeV at ranges of 0.5 and 2 kilometers. The points are for times of 10 and 50 shakes. It would be useful to also have points at earlier times and time-integrated values, but these are not obtainable with acceptable resolution from the available Monte Carlo data plots.

The solid curves of figure 13 show the angular variation of time-integrated data reported by Schaefer (ref. 13) for a 2 MeV source at a range of 312.5 meters. From figure 13, it would be expected that the LEMP-2 scattered sources are almost a factor of 2 larger than those from SCX. Since this is one of the larger uncertainties in the scattered-gamma source terms, both SCX and LEMP-2 should include this angular variation, which

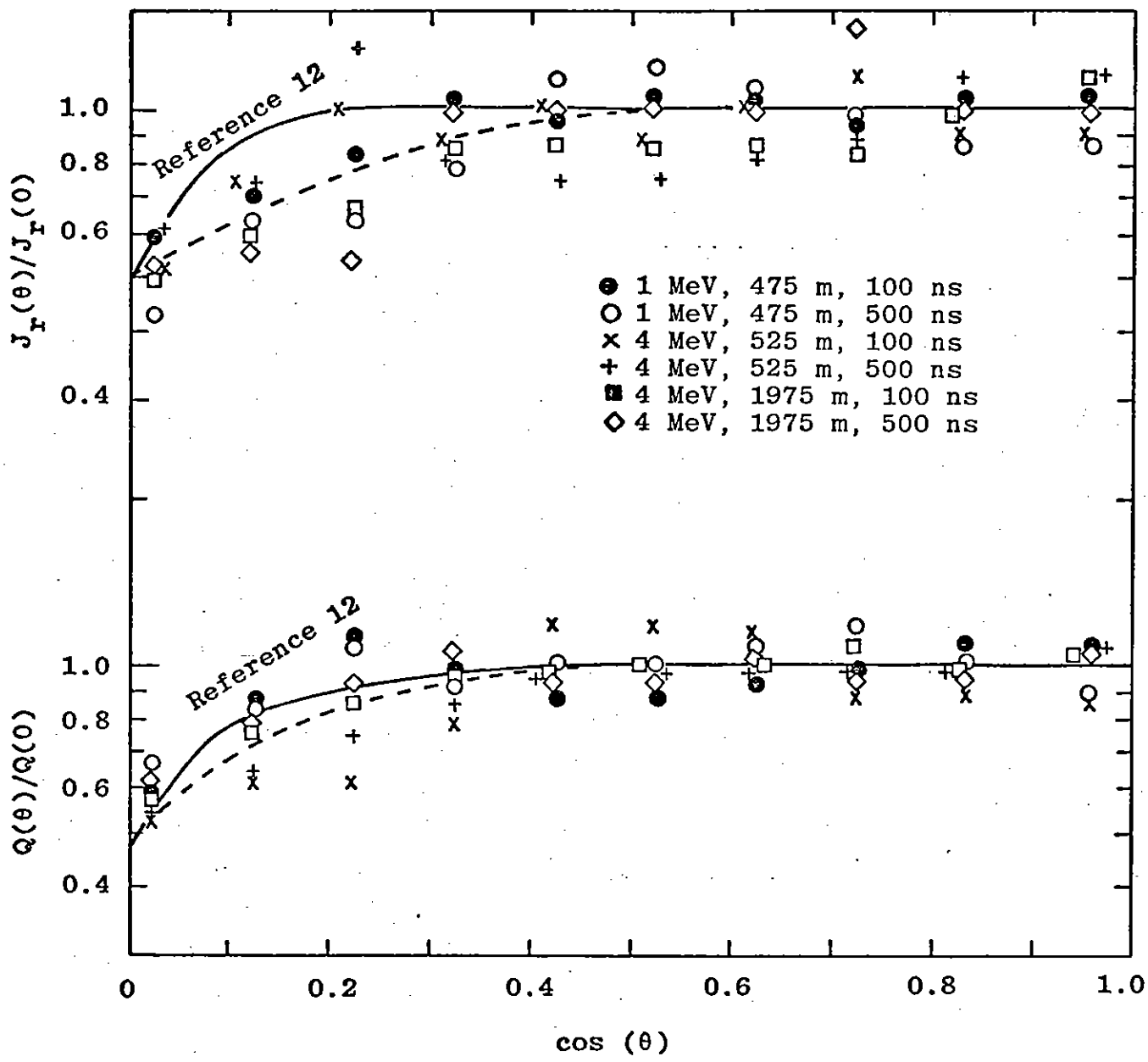

Figure 13. Scattered Gamma Radial Compton Current and Ionization Rate Variation with Angle, Data Points are from TIG2 Results

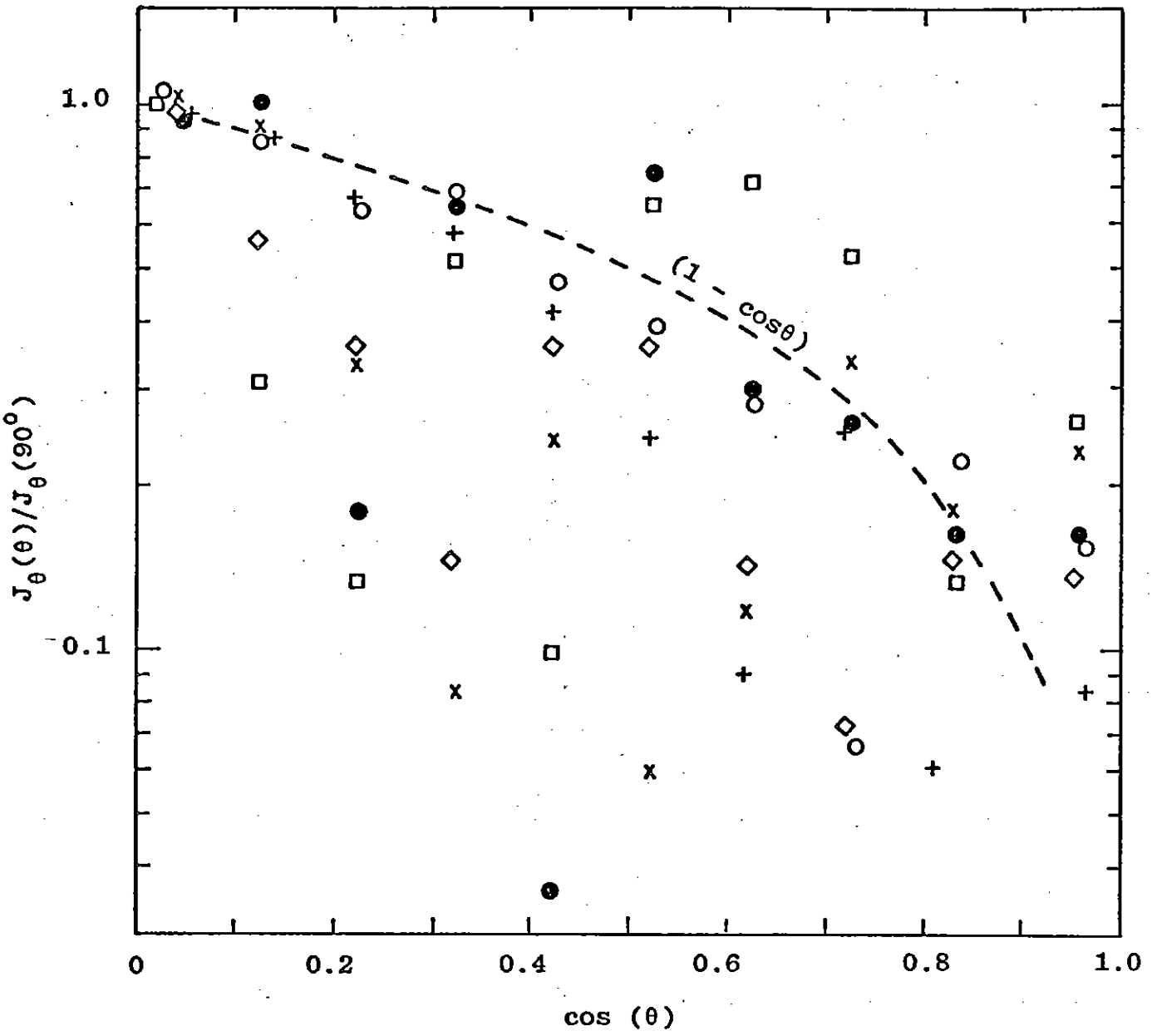

Figure 14. Scattered Gamma Theta Compton Current Variation with Angle, Data Points are from TIG2 Results (legend for data points is given on Figure 13)

neither treats at the present time. In general, this will be height and gamma energy dependent, with possibly a weaker time dependence (very early times).

The J_θ angular dependence previously used in SCX is $(1 - \cos\theta)$, which is plotted as the dashed line of figure 14. This variation gives larger values of J_θ at greater heights above the ground than might be expected from the TIG2 data or reference 13.

Addition of the proper angular dependence to SCX and LEMP-2 will result in improved agreement in the two scattered-gamma specifications and improve the overall accuracy.

Due to the lack of very detailed Monte Carlo data, especially at early times for small angular bins near the ground, a study of the once scattered gamma flux at various ranges and angles was completed analytically/numerically. This was done in order to provide indications of the behavior of the multiply scattered gamma source as a function of angle and time (for J_θ). This work is described in the appendix. The results of this study are not inconsistent with those of figures 13 and 14, if the times which the data points represent are considered. Results in the appendix also show early time behavior, which may be more important than the later times for some problems. Recommended angular variations are presented. These variations are used to scale the SCX data from 2.87 degrees above the ground to 90 degrees above the ground for the following comparisons. The single-scatter approximation of the appendix also indicates that the TIG2 results are not scored on a mesh fine

enough to resolve the J_θ behavior near the surface. SCX curve fits for J_θ probably underestimate the J_θ at the surface by 20 to 50 percent.

5. SOURCE COMPARISONS

The following paragraphs compare the SCX, LEMP-2, and LASL scattered-gamma sources, both delta function and convoluted results, and discuss the relative effects of the scattered sources on the total gamma-induced currents and ionization rates. All SCX results are based on data for the observer near the ground (section III.1.) which has been scaled to 90 degrees (vertical) using the relationships given in the appendix. As illustrated below for a particular case, code-code comparisons can be useful for pointing out certain aspects of source calculations and for increasing the confidence in the results. These comparisons teach little concerning absolute accuracies, however.

Figures 15 through 18 give comparisons of the SCX, LEMP-2, and LASL delta-function scattered-gamma responses at ranges of 0.5 and 2.0 kilometers. The number of source photons is held constant as the energy changes. The SCX and LASL 1, 2 and 5 MeV responses and the LEMP-2 0.5, 1.5 and 5 MeV responses are shown. Agreement is generally a factor of 3 or better. The LEMP-2 5 MeV values are smaller than the SCX and LASL results at early times at 500 meters, but larger at a range of 2 kilometers. The LEMP-2 0.5 and 1.5 MeV responses appear larger than would be expected in relation to the 1.0 and 2.0 MeV SCX and LASL results.

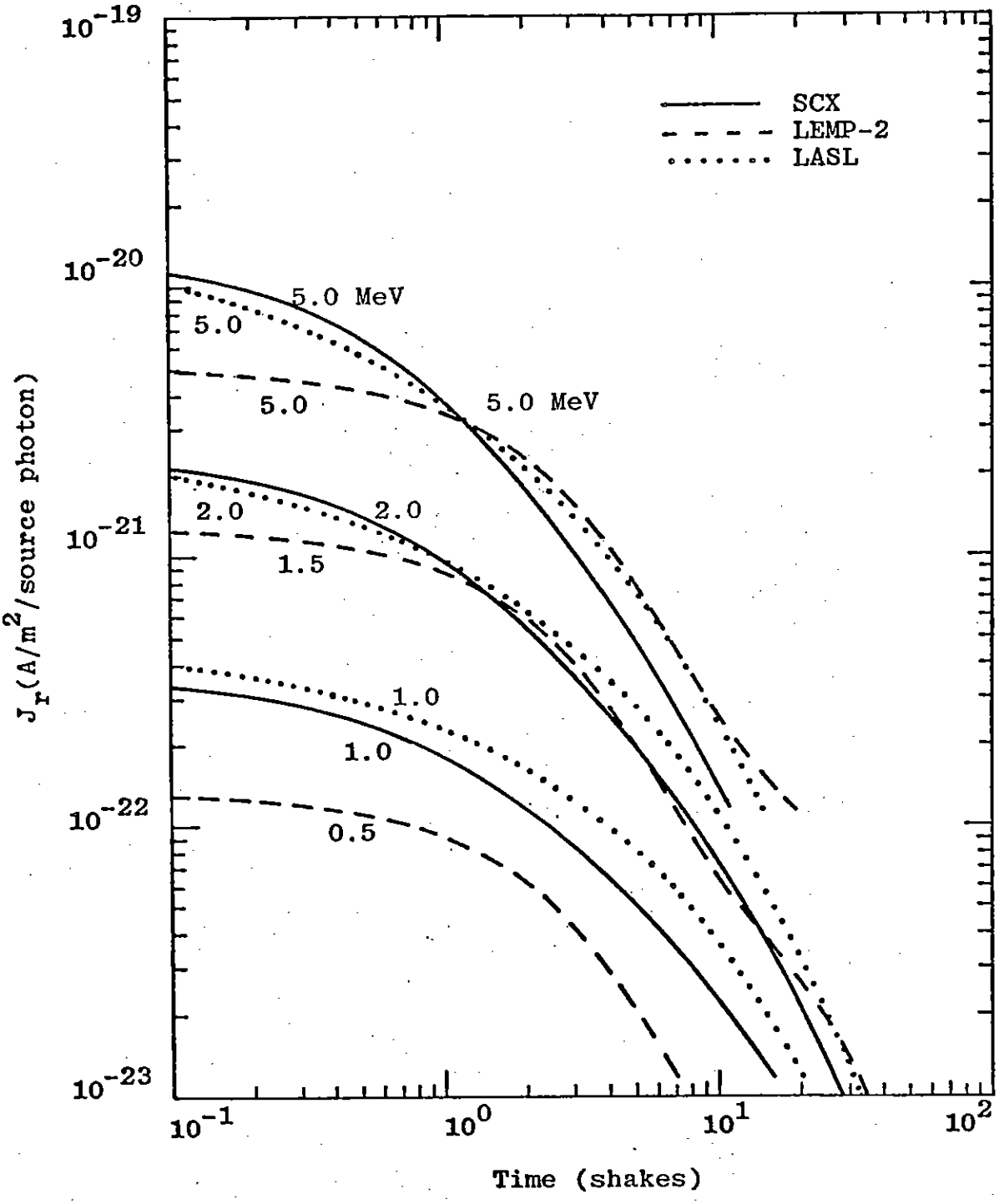

Figure 15. Scattered Gamma Radial Current Delta Function Response Comparison, Range = 500 Meters

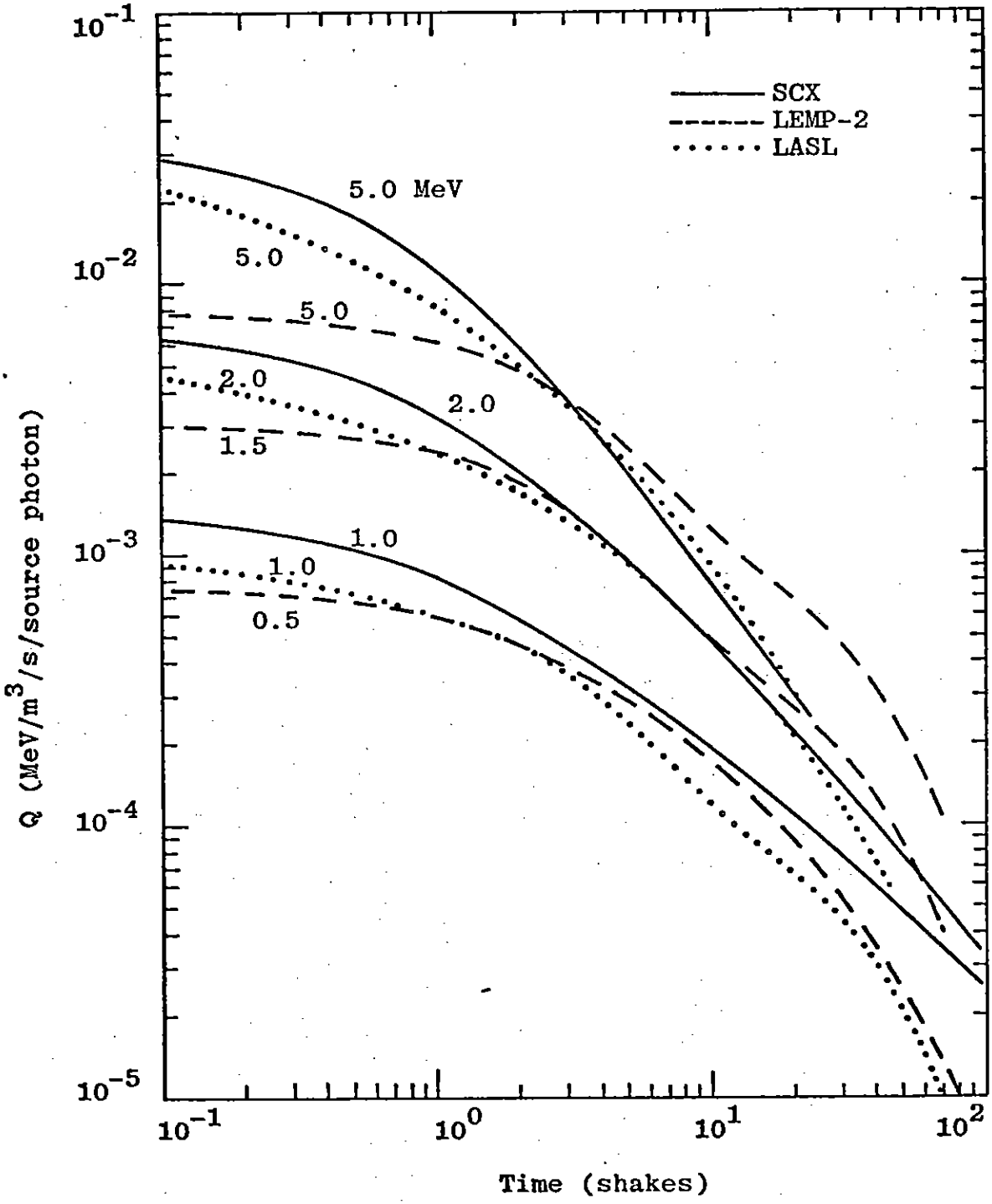

Figure 16. Scattered Gamma Ionization Rate Delta Function Response Comparison, Range = 500 Meters

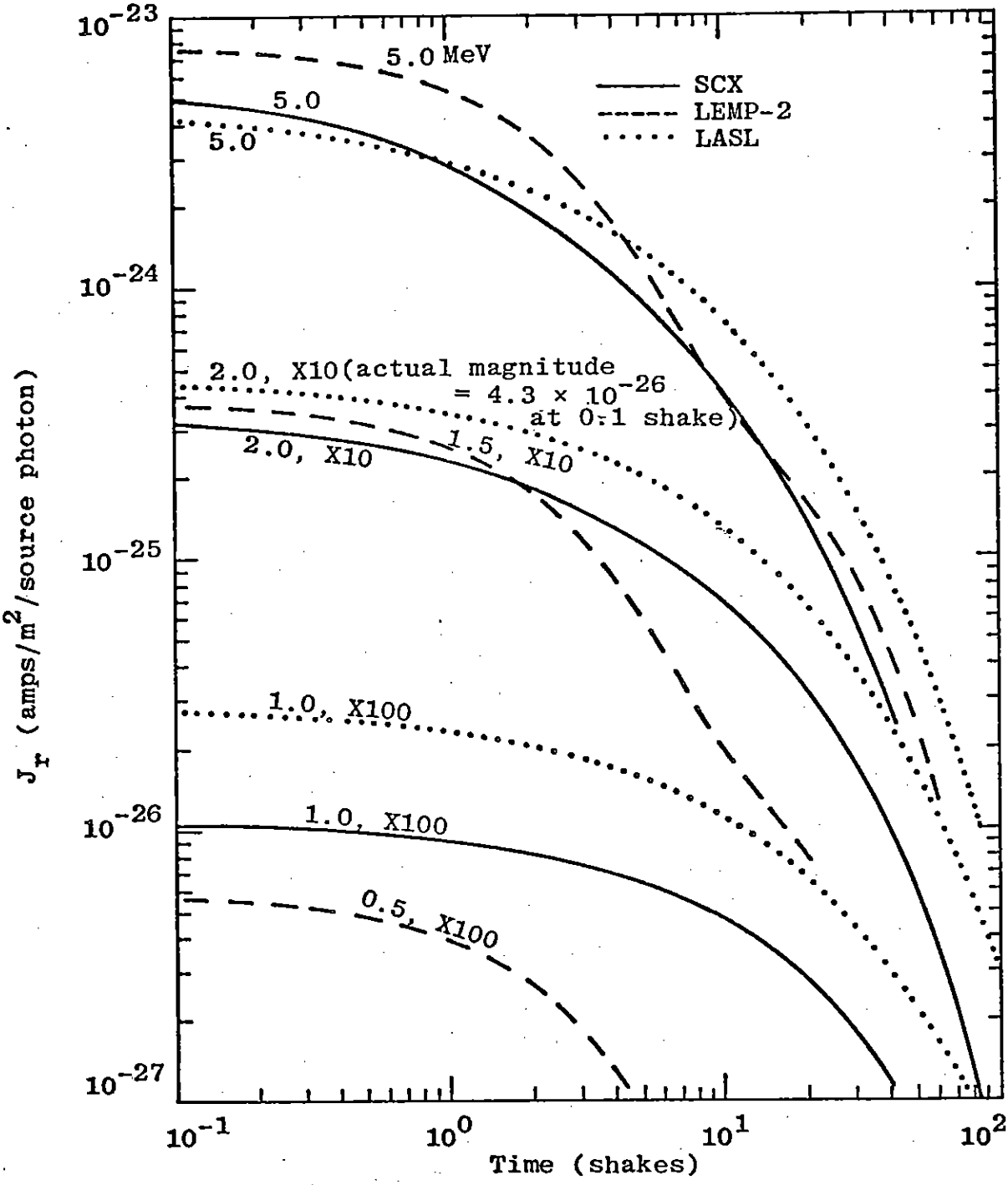

Figure 17. Scattered Gamma Radial Current Delta Function Response Comparison, Range = 2.0 Kilometers

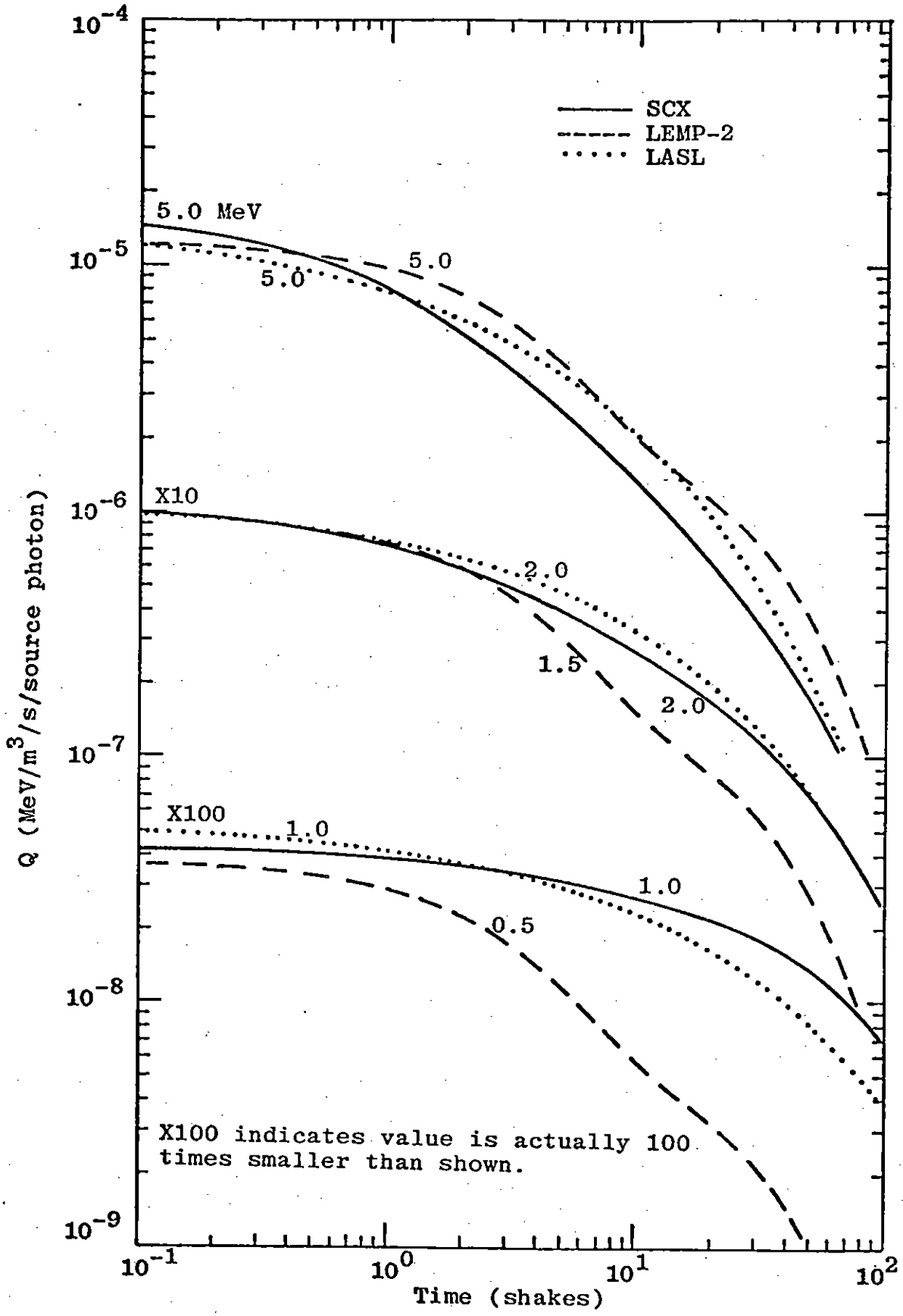

Figure 18. Scattered Gamma Ionization Rate Delta Function Response Comparison, Range = 2.0 Kilometers

This is probably due to the build-up factor used, as previously discussed. Other differences in the time waveforms appear to be almost random. There are considerable differences in the lower energy responses at 2.0 kilometers. However, the high energies dominate at large ranges so that these differences are usually not of great importance. This illustrates the need for treating a spectrum of gamma energies and not just a single average energy.

Time integrated values of J and Q for various gamma energies and ranges are given by tables 6 and 7. For the gamma energies of greatest interest at a given range, the differences in the three specifications are usually a factor 2 or less. For the 2 and 3 kilometer observers, the integrated SCX 5 MeV results for J and Q are less than the LEMP-2 and LASL 5 MeV results. These differences are mainly at later times and may be due to the neglect of the photoelectric effect in TIG2 and the increased absorption by the ground of photons which would contribute at later times at these far ranges.

It is useful to note that approximately 15 to 25 percent of the integrated current is generated on the time interval 0.1-1 shake and 40-50 percent on the interval 1-10 shakes, with the remainder at later times. Thus, even though the later time magnitudes are small, the energy content is appreciable. The importance of this content will be determined by the observer location, relative device gamma and neutron yields, neutron spectrum, etc.

Table 6

$\int J_r dt$ ($10^{-9} \leq t \leq 10^{-6}$ s)

	SCX	LEMP-2	LASL
R = 500 m:			
E_γ = 0.5 MeV		4.22×10^{-30}	2.73×10^{-30}
1.0 MeV	1.00×10^{-29}		1.44×10^{-29}
1.5 MeV		4.04×10^{-29}	3.13×10^{-29}
2.0 MeV	4.23×10^{-29}		5.05×10^{-29}
5.0 MeV	1.38×10^{-28}	1.59×10^{-28}	1.56×10^{-28}
R = 1000 m:			
E_γ = 0.5 MeV		2.44×10^{-32}	6.66×10^{-33}
1.0 MeV	1.01×10^{-31}		1.77×10^{-31}
1.5 MeV		9.72×10^{-31}	7.67×10^{-31}
2.0 MeV	1.33×10^{-30}		1.86×10^{-30}
5.0 MeV	1.18×10^{-29}	1.45×10^{-29}	1.49×10^{-29}
R = 2000 m:			
E_γ = 0.5 MeV		1.83×10^{-36}	5.46×10^{-38}
1.0 MeV	1.62×10^{-35}		4.17×10^{-35}
1.5 MeV		1.20×10^{-33}	7.77×10^{-34}
2.0 MeV	2.29×10^{-33}		4.43×10^{-33}
5.0 MeV	1.65×10^{-31}	2.47×10^{-31}	2.56×10^{-31}
R = 3000 m:			
E_γ = 0.5 MeV		1.88×10^{-40}	5.06×10^{-43}
1.0 MeV	3.01×10^{-39}		1.15×10^{-38}
1.5 MeV		2.00×10^{-36}	9.51×10^{-37}
2.0 MeV	4.71×10^{-36}		1.30×10^{-35}
5.0 MeV	2.93×10^{-33}	5.63×10^{-33}	5.79×10^{-33}

Table 7

$\int Qdt$ ($10^{-9} \leq t \leq 10^{-6}$ s)

	SCX	LEMP-2	LASL
R = 500 m:			
E_γ = 0.5 MeV		5.35×10^{-11}	1.30×10^{-11}
1.0 MeV	9.19×10^{-11}		6.52×10^{-11}
1.5 MeV		2.16×10^{-10}	1.28×10^{-10}
2.0 MeV	2.28×10^{-10}		1.89×10^{-10}
5.0 MeV	5.29×10^{-10}	5.54×10^{-10}	4.39×10^{-10}
R = 1000 m:			
E_γ = 0.5 MeV		3.35×10^{-13}	2.15×10^{-14}
1.0 MeV	8.98×10^{-13}		6.41×10^{-13}
1.5 MeV		5.43×10^{-12}	2.72×10^{-12}
2.0 MeV	6.70×10^{-12}		6.28×10^{-12}
5.0 MeV	4.21×10^{-11}	5.13×10^{-11}	4.18×10^{-11}
R = 2000 m:			
E_γ = 0.5 MeV		2.62×10^{-17}	1.05×10^{-19}
1.0 MeV	1.53×10^{-16}		1.10×10^{-16}
1.5 MeV		6.87×10^{-15}	2.23×10^{-15}
2.0 MeV	1.16×10^{-14}		1.29×10^{-14}
5.0 MeV	5.71×10^{-13}	8.79×10^{-13}	7.22×10^{-13}
R = 3000 m:			
E_γ = 0.5 MeV		2.74×10^{-21}	7.23×10^{-25}
1.0 MeV	3.25×10^{-20}		2.44×10^{-20}
1.5 MeV		1.16×10^{-17}	2.32×10^{-18}
2.0 MeV	2.68×10^{-17}		3.37×10^{-17}
5.0 MeV	1.08×10^{-14}	2.01×10^{-14}	1.62×10^{-14}

Variations of these delta-function responses at specific times as a function of range are given by figures 19 through 26. These figures also illustrate the faster fall-off of the SCX 5 MeV responses at later times (50 shakes).

It should be remembered that the data on which the LEMP-2 fits are based extended to approximately 1 kilometer (LeLevier, ref. 7) and 10 mean-free-paths (Chilton, ref. 6). The LASL data base extended to 1.6 kilometers and the SCX data to a range of 3 kilometers. For many calculations (e.g., smaller yields), the differences in gamma sources at the larger ranges (~2-3 km) would not be of great importance.

Since some of the differences in time of the delta functions are smoothed when these responses are folded with the weapon output time history, folded responses for SCX and LEMP-2 are compared in figures 27 through 30. The only direct comparison in figure 27 (0.5 km) is for 5 MeV, with the LEMP-2 curve not quite a factor of 2 smaller and with a slightly wider pulse width. To illustrate variations with energy, SCX values at 1, 2, 3, 5 and 8 MeV for a range of 0.5 kilometer and at 3, 4, 5, 6 and 8 MeV for a range of 2 kilometers are shown by figures 28 and 29. The lower energies, for most spectra of interest, are negligible at large ranges. This illustrates the importance of treating the higher energy portions of the spectrum instead of just using a single average value. Figure 30 shows that the LEMP-2 5 MeV response is over a factor of 2 larger than that of SCX at 2 kilometers. Variations of the peaks of these folded functions with range are shown by figure 31.

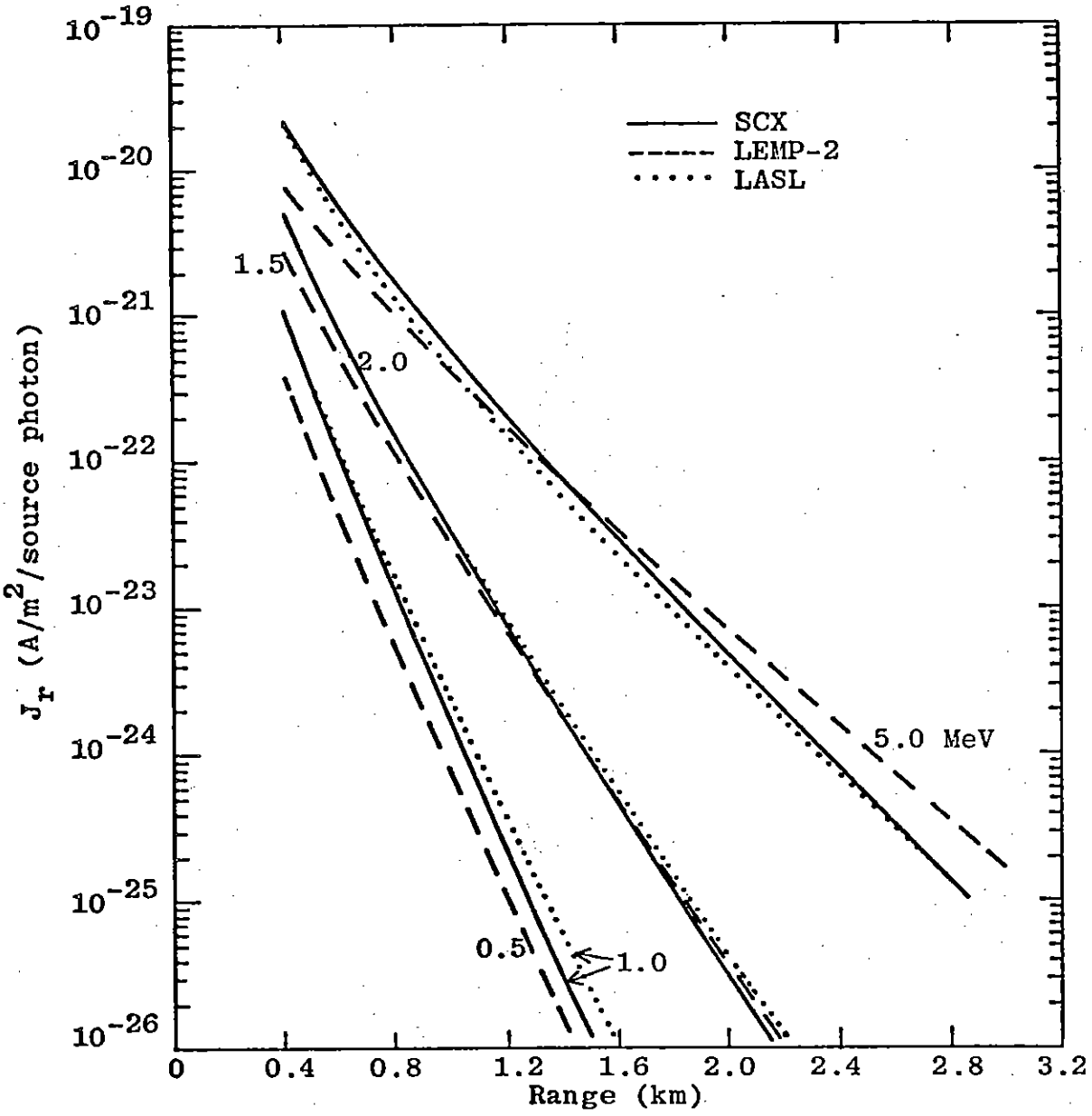

Figure 19. Scattered Gamma Radial Current Delta Function Response Comparison, Time = 0.1 Shake

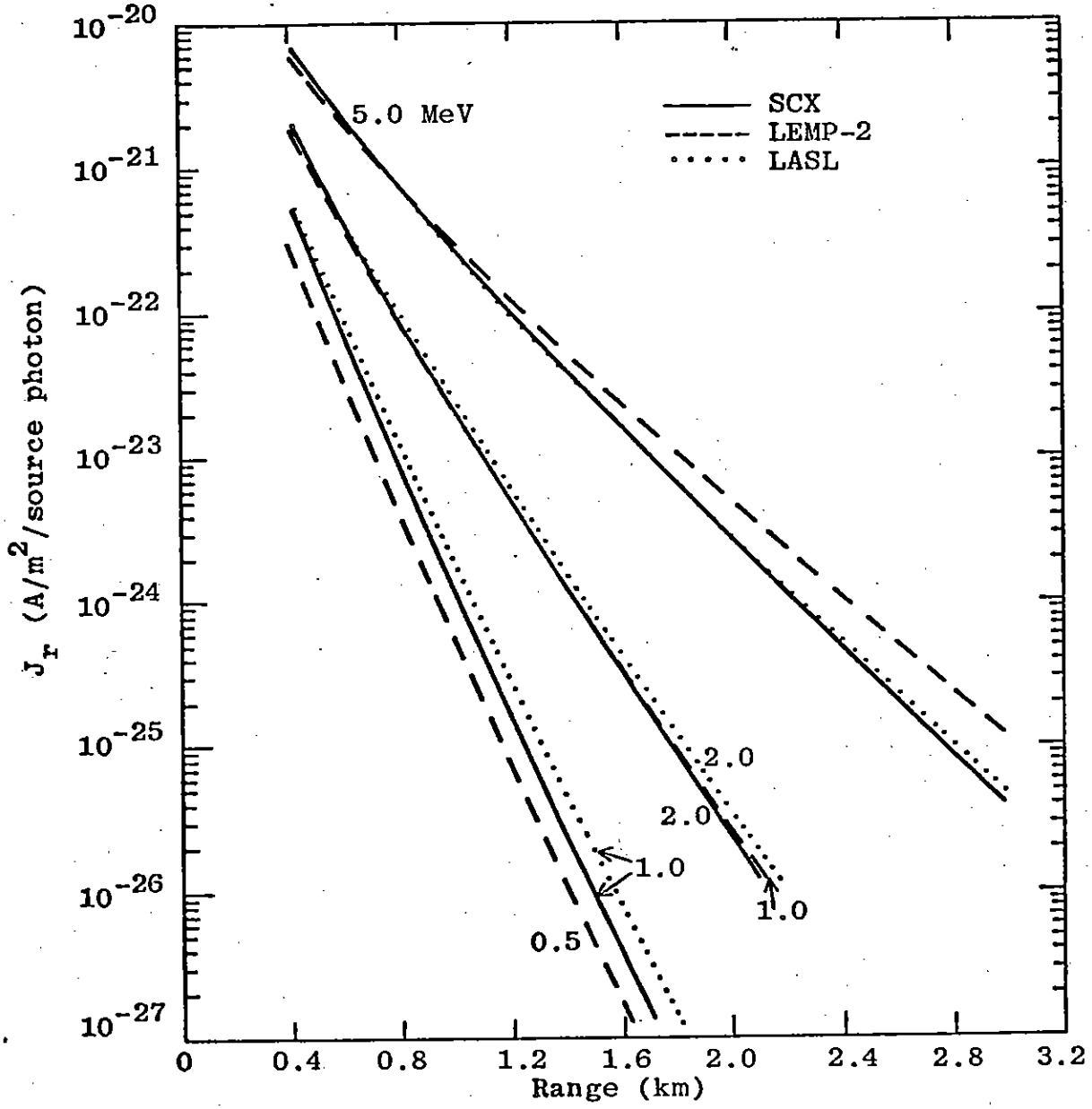

Figure 20. Scattered Gamma Radial Current Delta Function Response Comparison, Time = 1.0 Shake

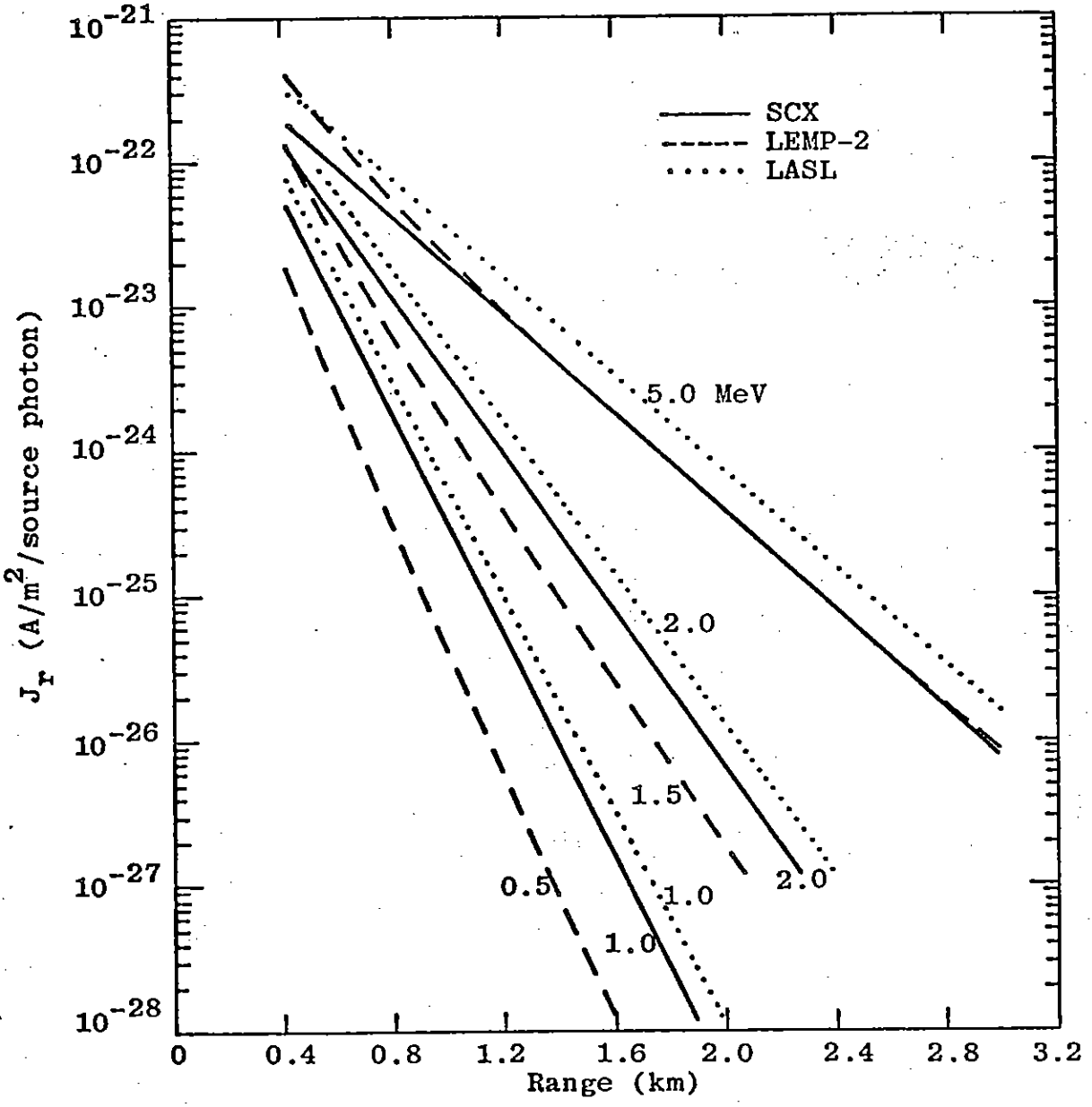

Figure 21. Scattered Gamma Radial Current Delta Function Response Comparison, Time = 10 Shakes

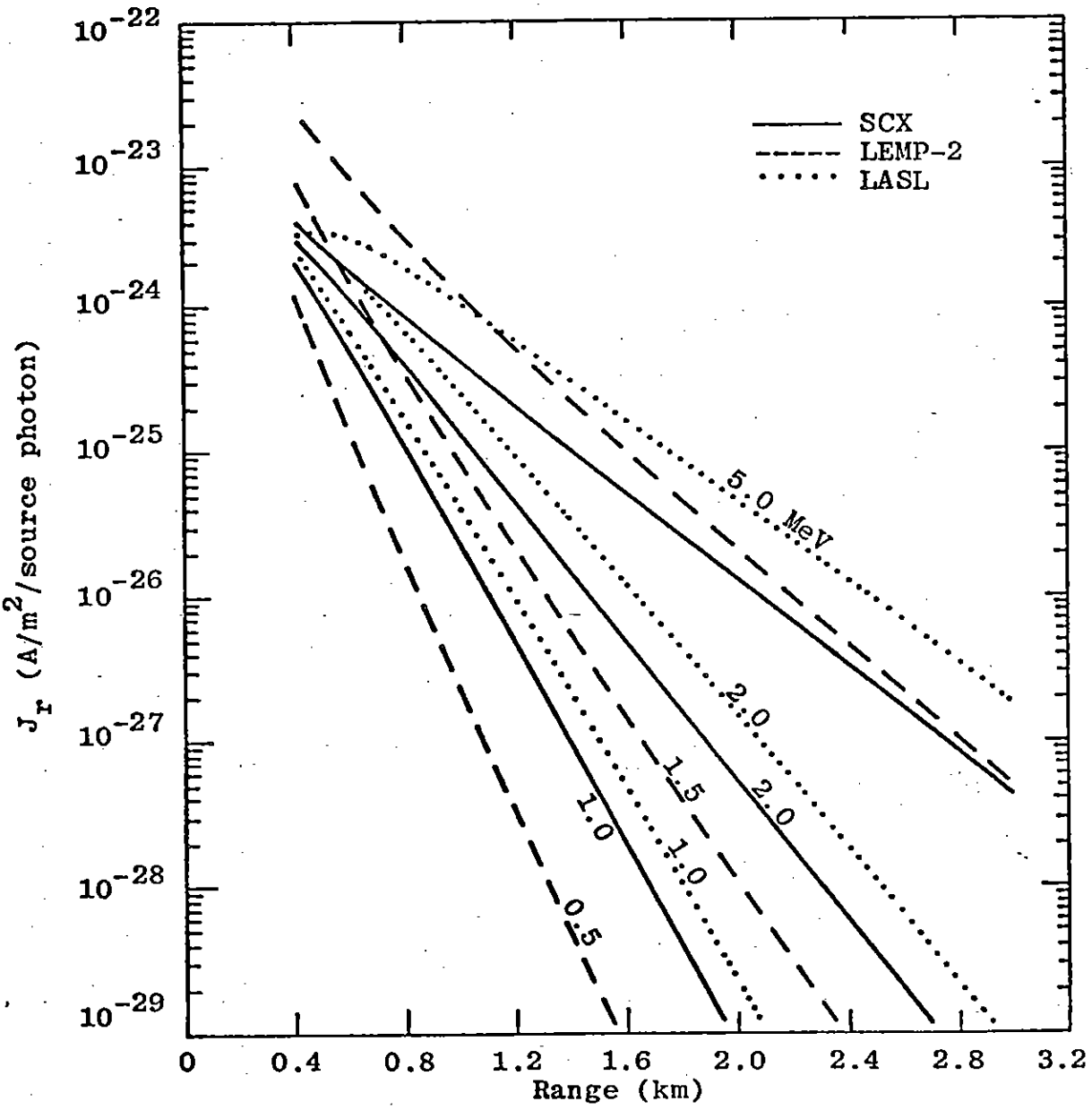

Figure 22. Scattered Gamma Radial Current Delta Function Response Comparison, Time = 50 Shakes

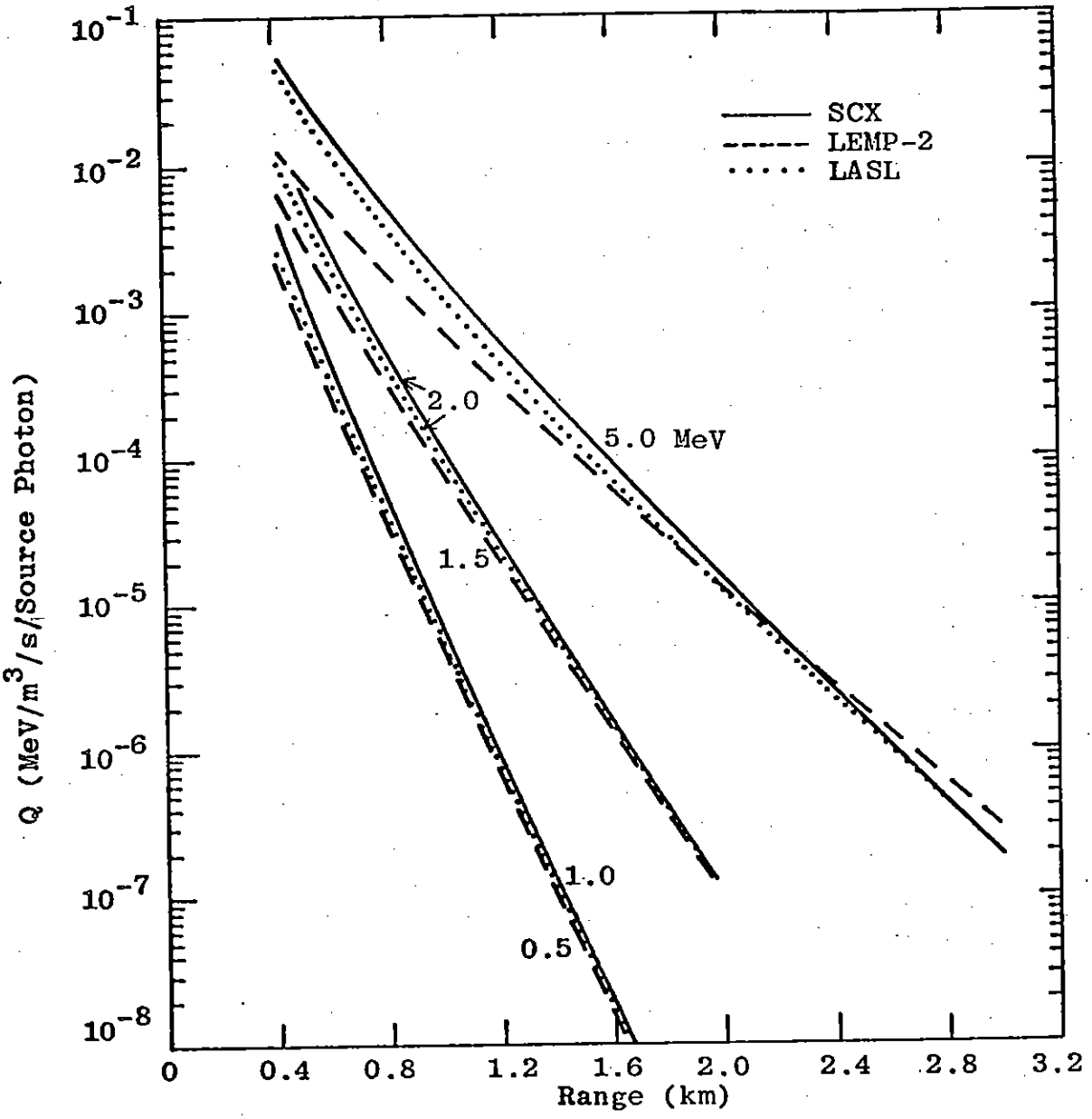

Figure 23. Scattered Gamma Ionization Rate Delta Function Response Comparison, Time = 0.1 Shake

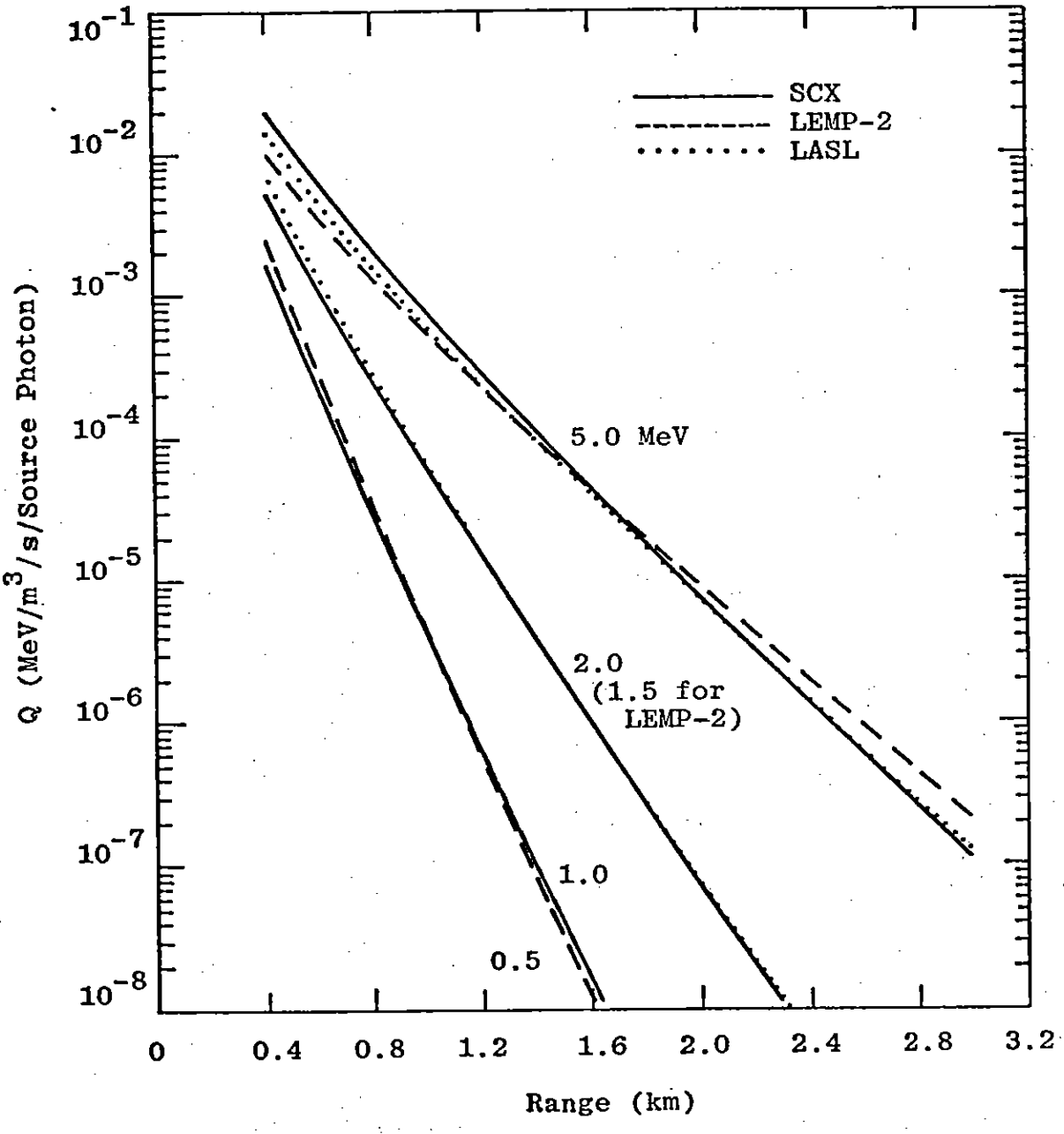

Figure 24. Scattered Gamma Ionization Rate Delta Function Response Comparison. Time = 1.0 Shake

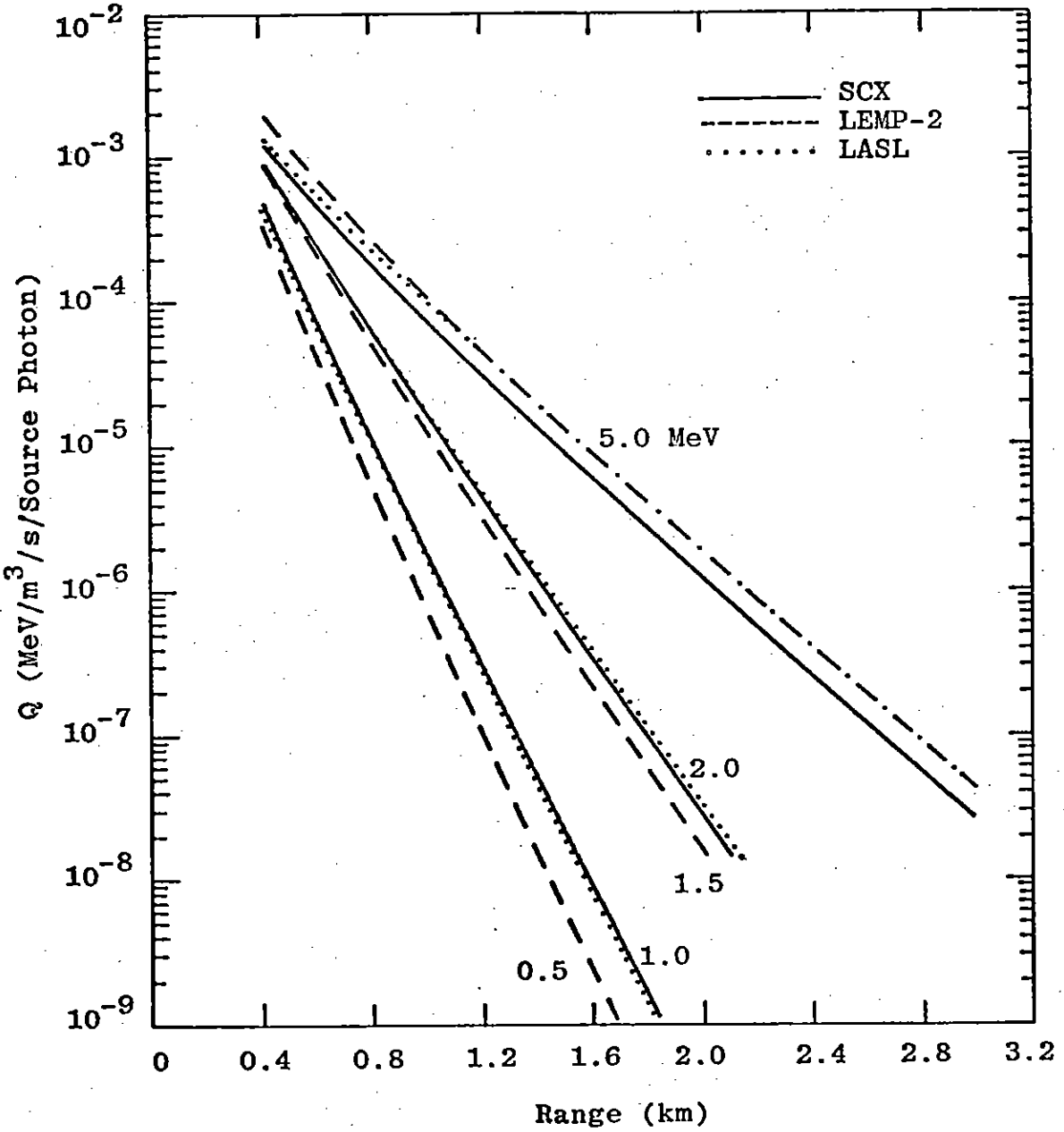

Figure 25. Scattered Gamma Ionization Rate Delta Function Response Comparison, Time = 10 Shakes

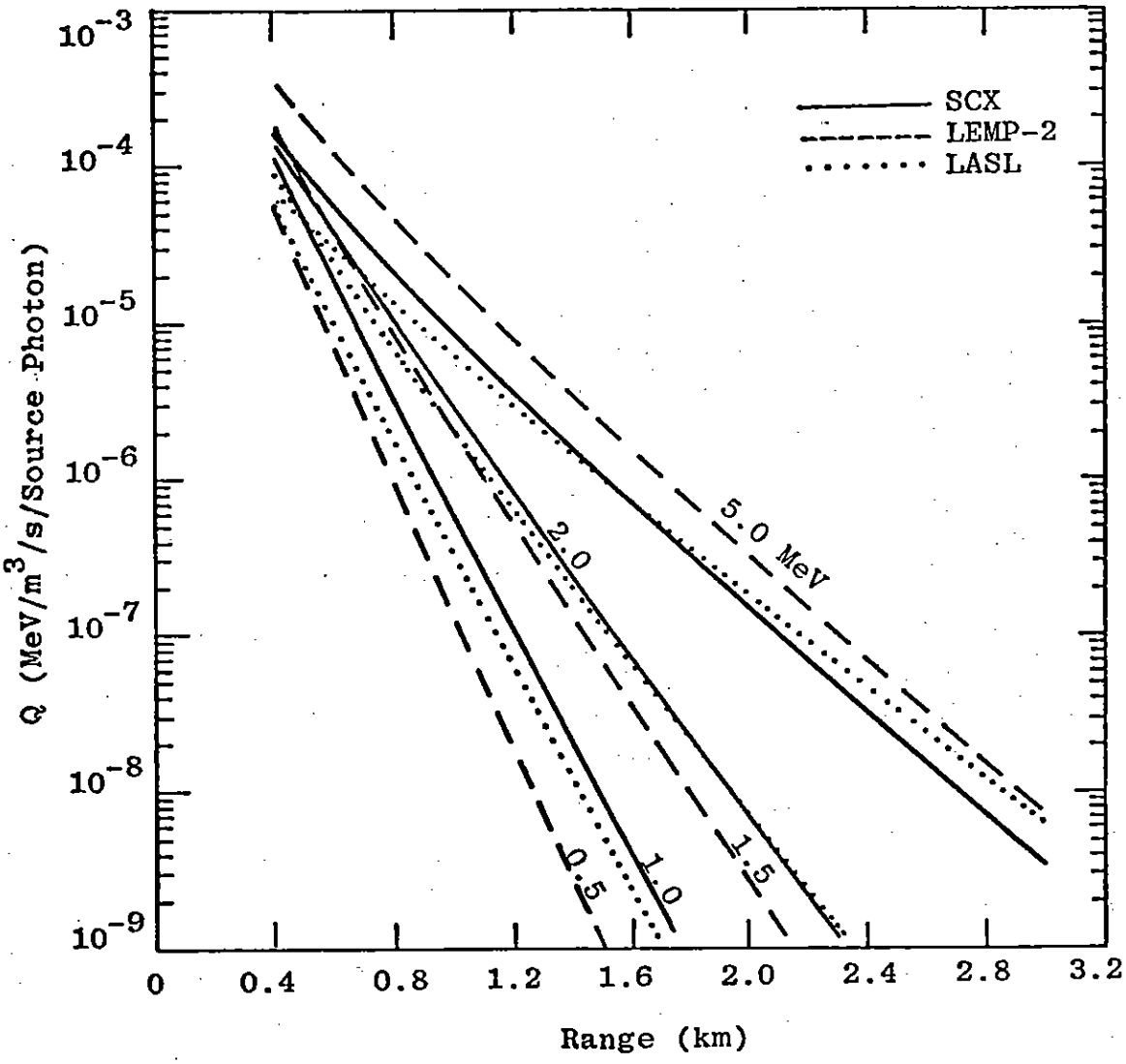

Figure 26. Scattered Gamma Ionization Rate Delta Function Response Comparison, Time = 50 Shakes

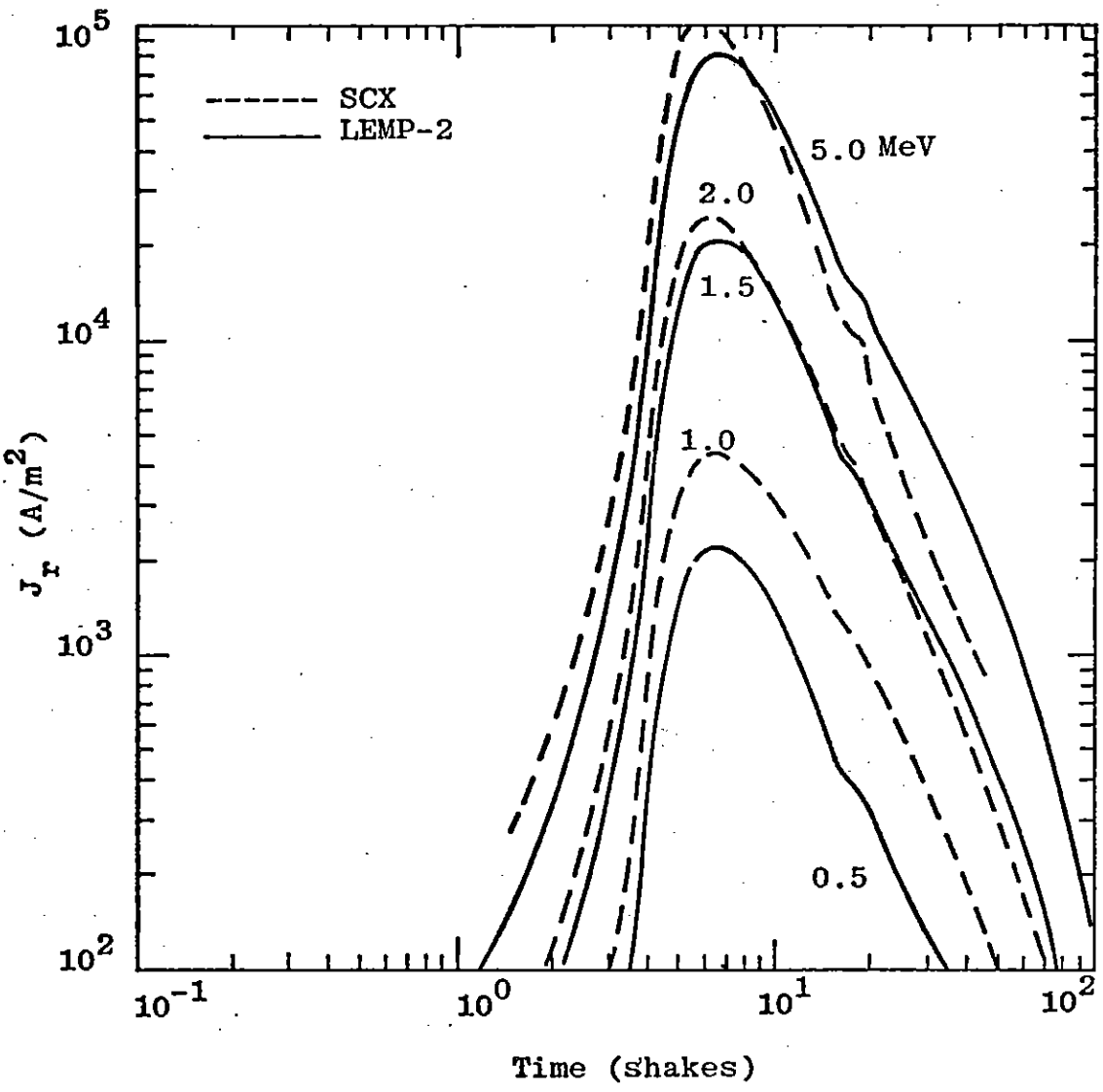

Figure 27. Convoluted Scattered-Gamma Radial Current vs. Time, SCX-LEMP-2 Comparison, Range = 500 Meters

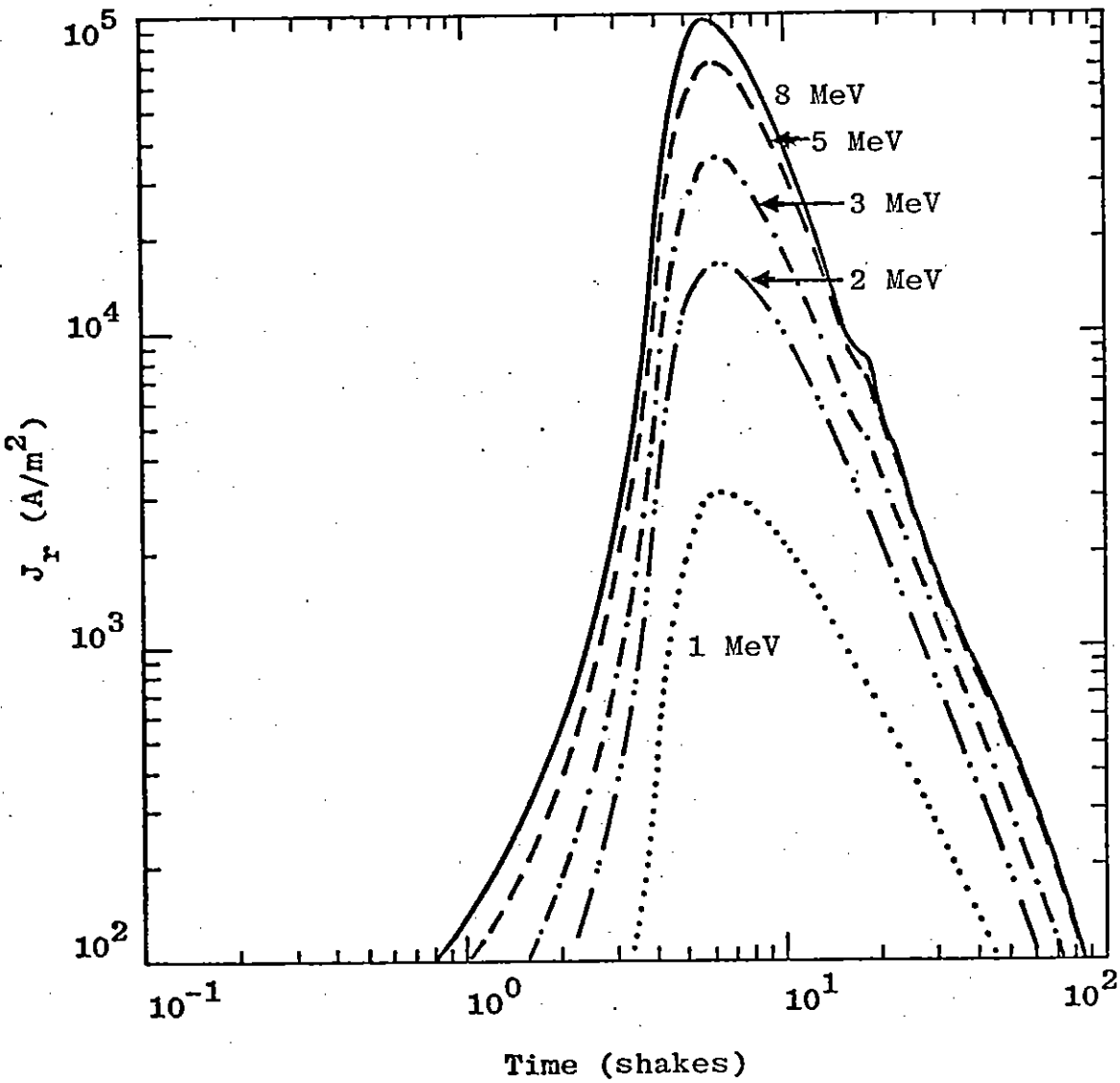

Figure 28. Convoluted Scattered-Gamma Radial Current vs. Time, SCX Energy Variation, Range = 500 Meters

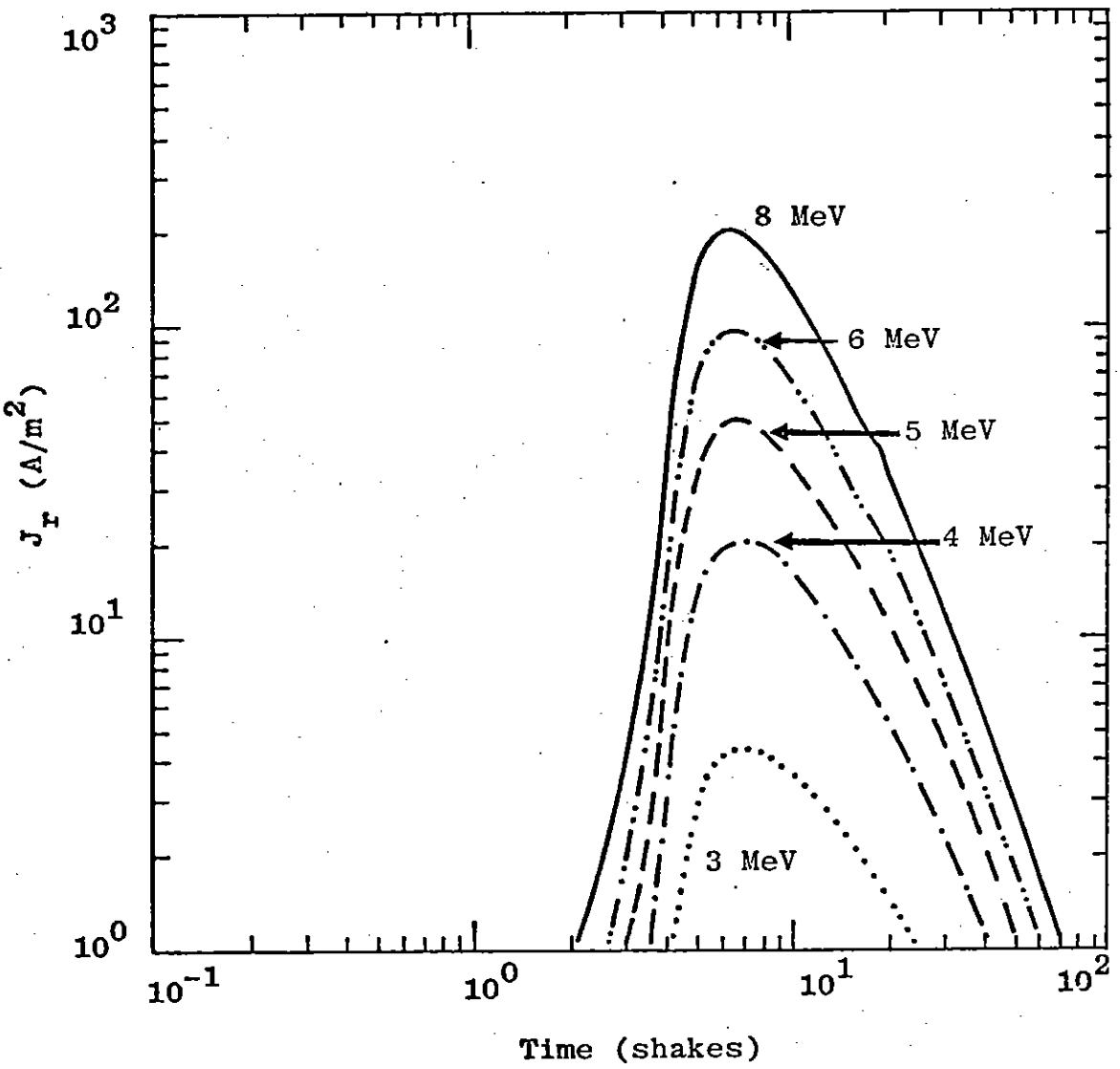

Figure 29. Convoluted Scattered-Gamma Radial Current vs. Time, SCX Energy Variation, Range = 2 Kilometers

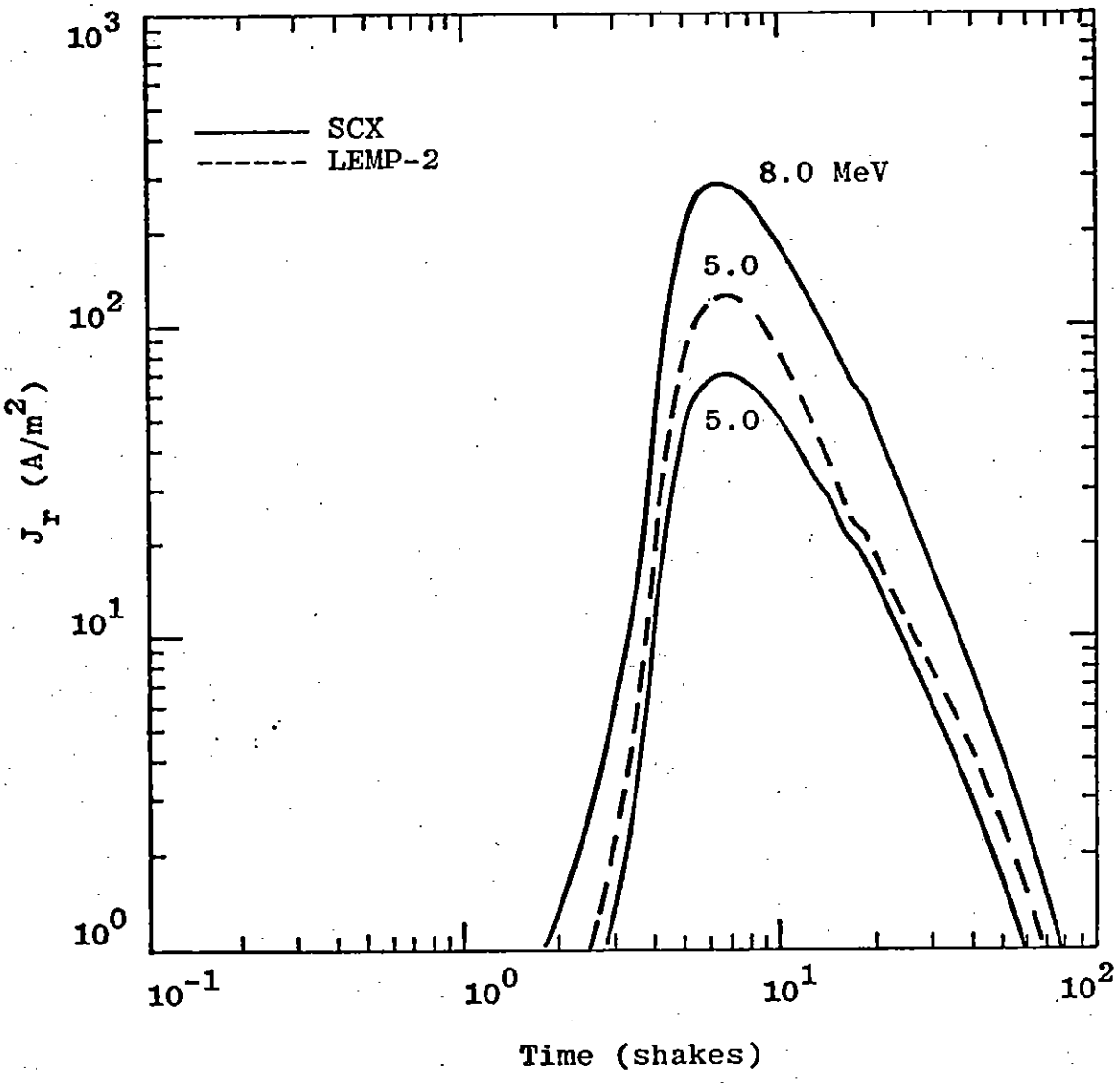

Figure 30. Convoluted Scattered-Gamma Radial Current vs. Time, SCX-LEMP-2 Comparison, Range = 2 Kilometers

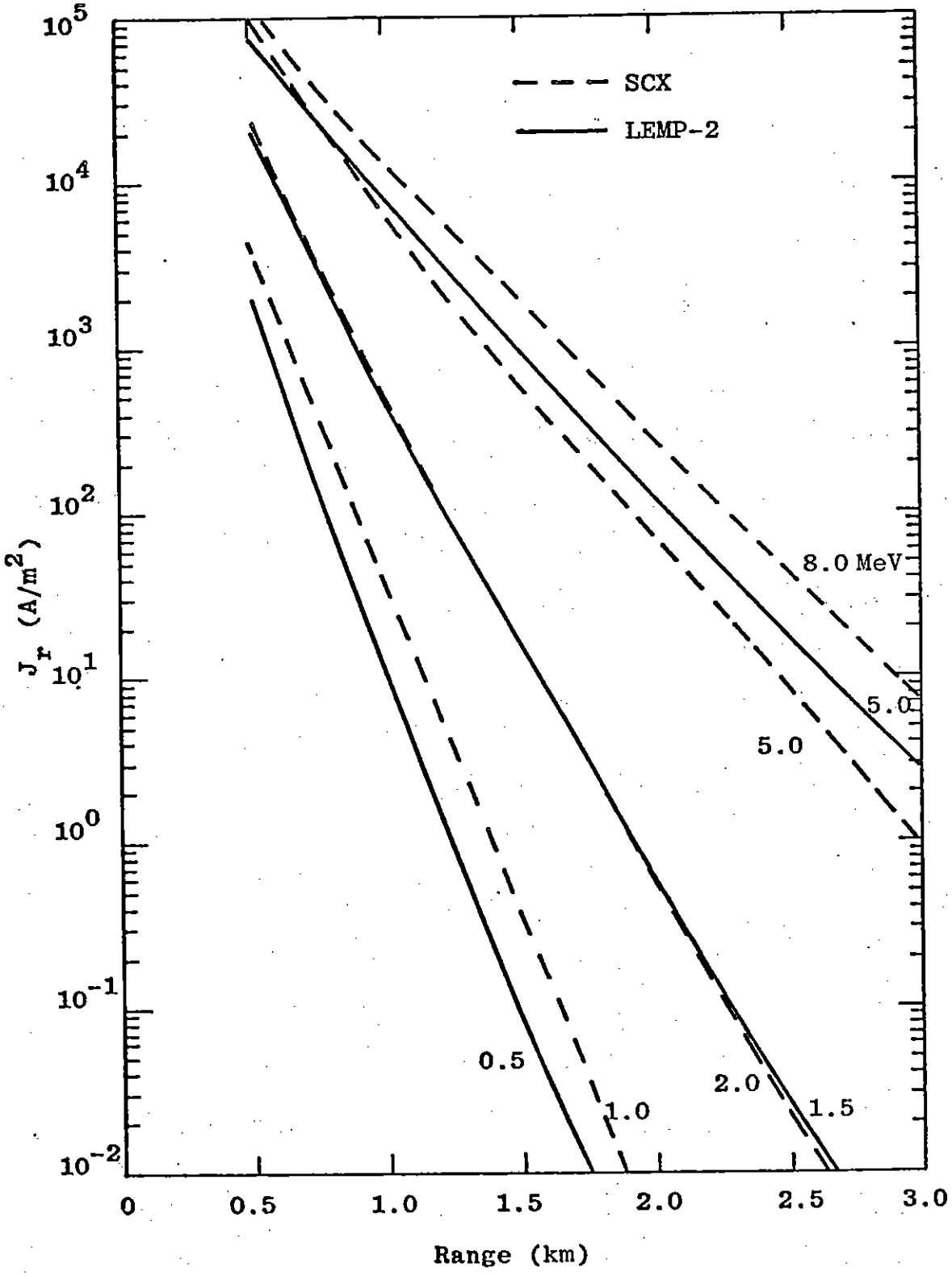

Figure 31. Peak Convoluted Scattered-Gamma Radial Current vs. Range, SCX-LEMP-2 Comparison

When the prompt (direct) sources of section II (which were in good agreement) are added to the scattered sources, the differences due to the scattered sources become less apparent. Figures 32, 33, and 34 give comparisons at 0.5 and 2 kilometers. At 0.5 kilometer (figure 32), the LEMP-2 curves show the greater importance of the scattered sources by the way they smooth the sharp peak in the source curve. This is also seen in figure 33 for the 2 kilometer, 5 MeV curve, which is nearly a factor of 50 percent larger for LEMP-2, almost entirely because of the scattered source. Even for the lower energies at 2 kilometers (figure 34), the SCX currents do not show this smoothing at the peak, but do have a much wider pulse width. The LEMP-2 results do not have a pulse width that is range dependent. SCX values of J_θ are not given here since the homogeneous air models on which the LEMP-2 and LASL results are based cannot produce this component.

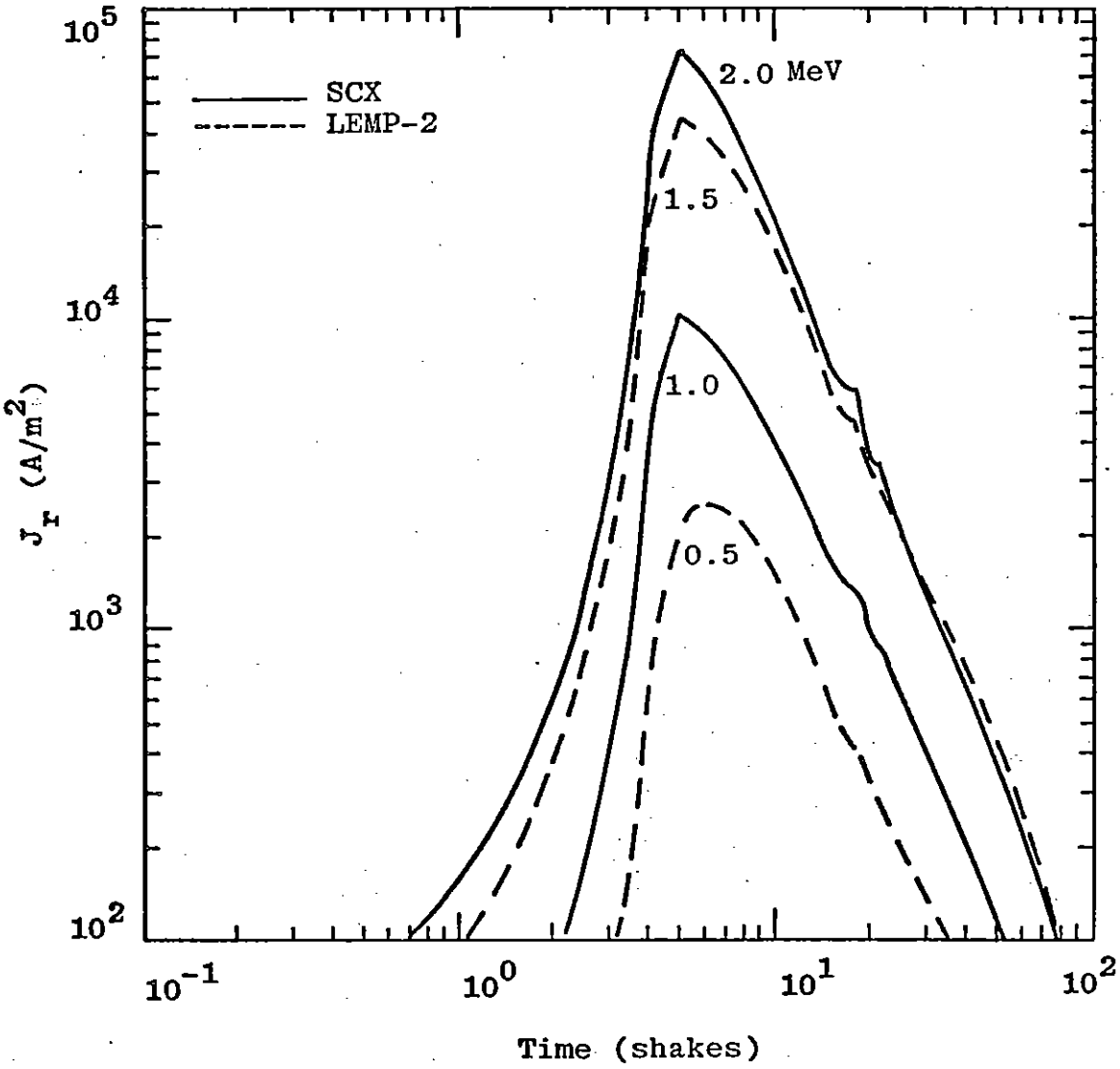

Figure 32. Total Convoluted Prompt Gamma Radial Current vs. Time, SCX-LEMP-2 Comparison, Range = 500 Meters

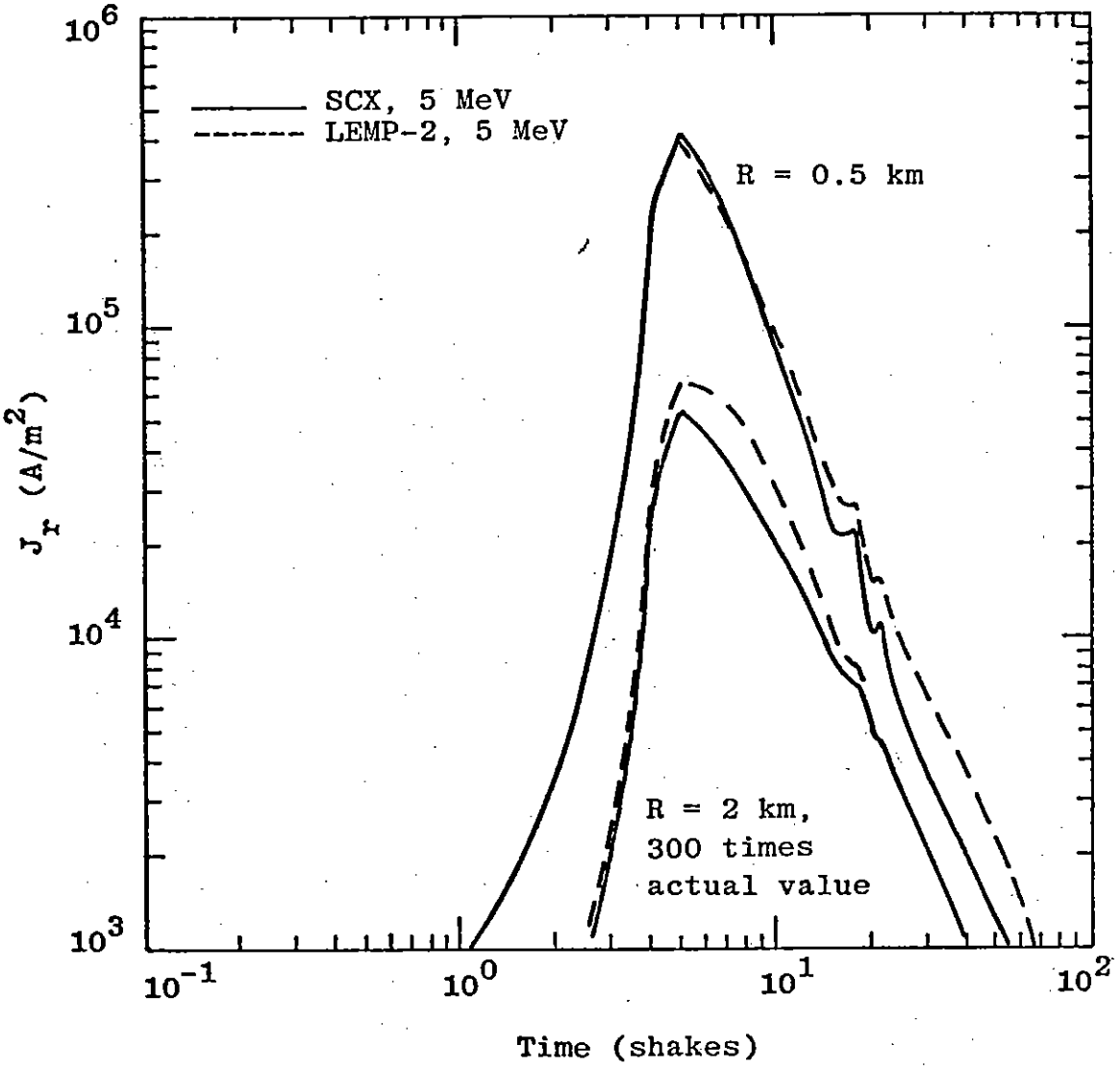

Figure 33. Total Convoluted Prompt Gamma Radial Current vs. Time, SCX-LEMP-2 Comparison

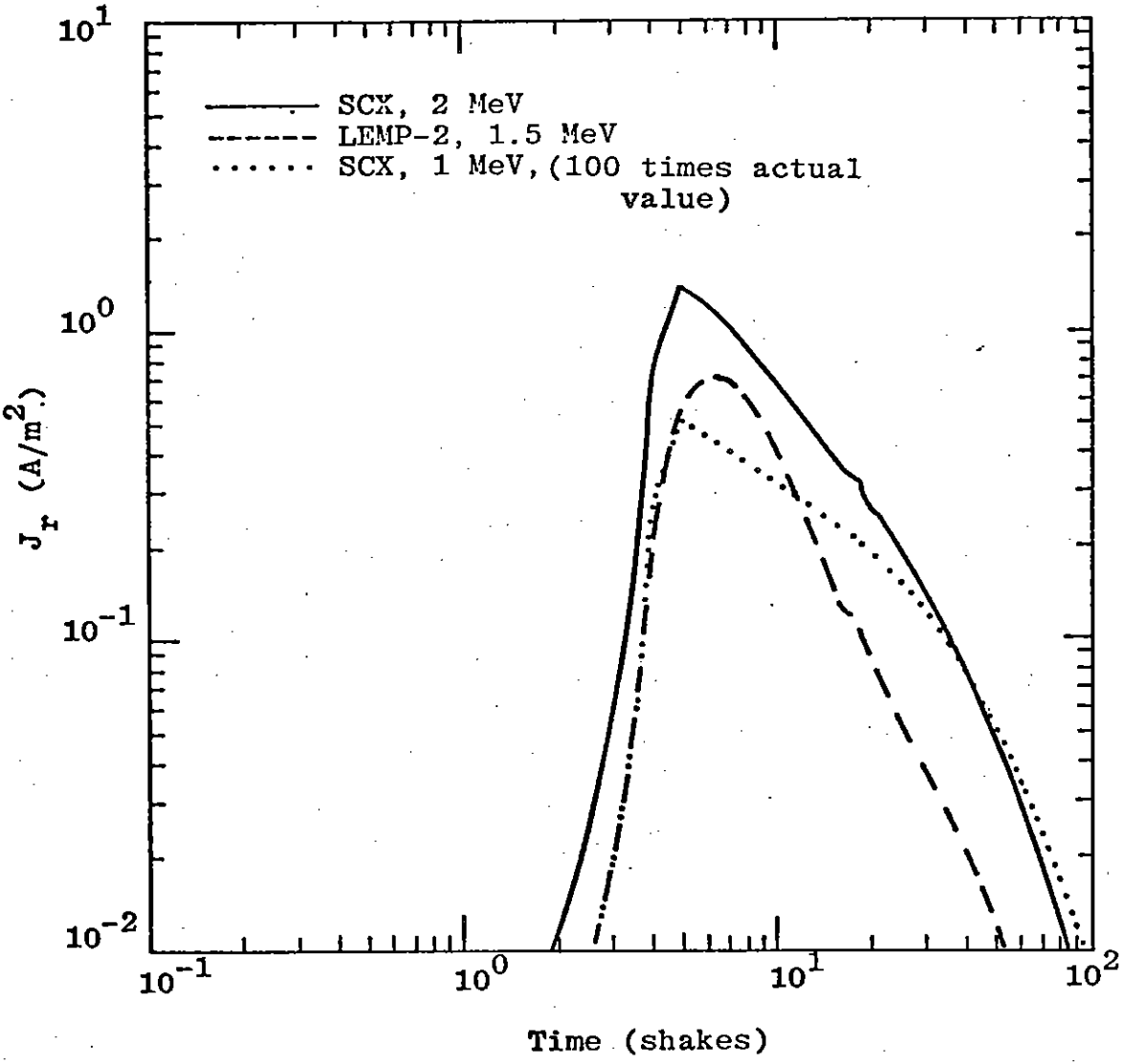

Figure 34. Total Convoluted Prompt Gamma Radial Current vs. Time, SCX-LEMP-2 Comparison, Range = 2 Kilometers

SECTION IV

NEUTRON-INDUCED SOURCES

Neutron-induced EMP sources are implemented in both SCX and LEMP-2 by the use of analytic fits. The following subsections describe the data on which the fits are based for each code and also comparisons of the sources computed by each code.

1. NEUTRON MONTE CARLO DATA

Curve fits for both codes are predominantly based on the Monte Carlo results of Sargis, et al. (ref. 8). These calculations were completed using a late-time version of the Monte Carlo code O5RNIES in 1972 using the latest available ENDF/B cross section data. Results are available for 0, 200 and 300 meter heights-of-burst to local times of 1 second. Observer Compton current and ionization rate data for locations in the air and ground, out to ranges of 5 kilometers, are on tape, although the data for ranges greater than 3 kilometers have large statistical uncertainties.

The interactions treated by the Monte Carlo included air and ground inelastic scatters, air and ground captures, and neutron recoil ionization.

A comparison of results using new and previously available neutron and gamma cross sections is given in reference 8. Changes in cross sections, particularly those for oxygen, caused the predicted sources to increase approximately a factor of 2 (at 1 and 100 microseconds) at a range of 480 meters. At farther

ranges, a similar change in cross sections may result in an even larger effect. Statistical uncertainties are usually on the order of ±50 percent, although they may be much larger (a factor of 2 or more).

2. SCX NEUTRON SOURCES

Neutron-induced sources in SCX are computed using curve fits to the data of reference 8 which were developed by Wood and Fishbine (ref. 15). These curve fits were developed for use in two-dimensional surface-burst EMP codes, with emphasis being placed on smoothness in time and range. This resulted in the sacrifice of some accuracy with respect to the data.

Figures 35 through 40, from reference 15, compare the curve fits with the Monte Carlo at ranges of 0.5 and 2 kilometers for the angular bin nearest the ground. This data is for the spectrum of table 8. Different curve-fit coefficients must be used in order to treat a different spectrum. Current work for AFWL is providing coefficients for just the 14 MeV group so that the contribution of this group may be easily varied (ref. 16).

Curve-fit values sometimes deviate a factor of 3 or more from the data, especially between 10^2 and 10^3 microseconds, but probably provide a better representation of the source. It should be remembered that the smoothing of the data in range may provide a better representation of the actual values than the Monte Carlo results at a given spatial point due to the reduction of statistical deviations.

Also shown on these figures are the curve-fit values for bins centered at 81.4 and 41.4 degrees from the vertical.

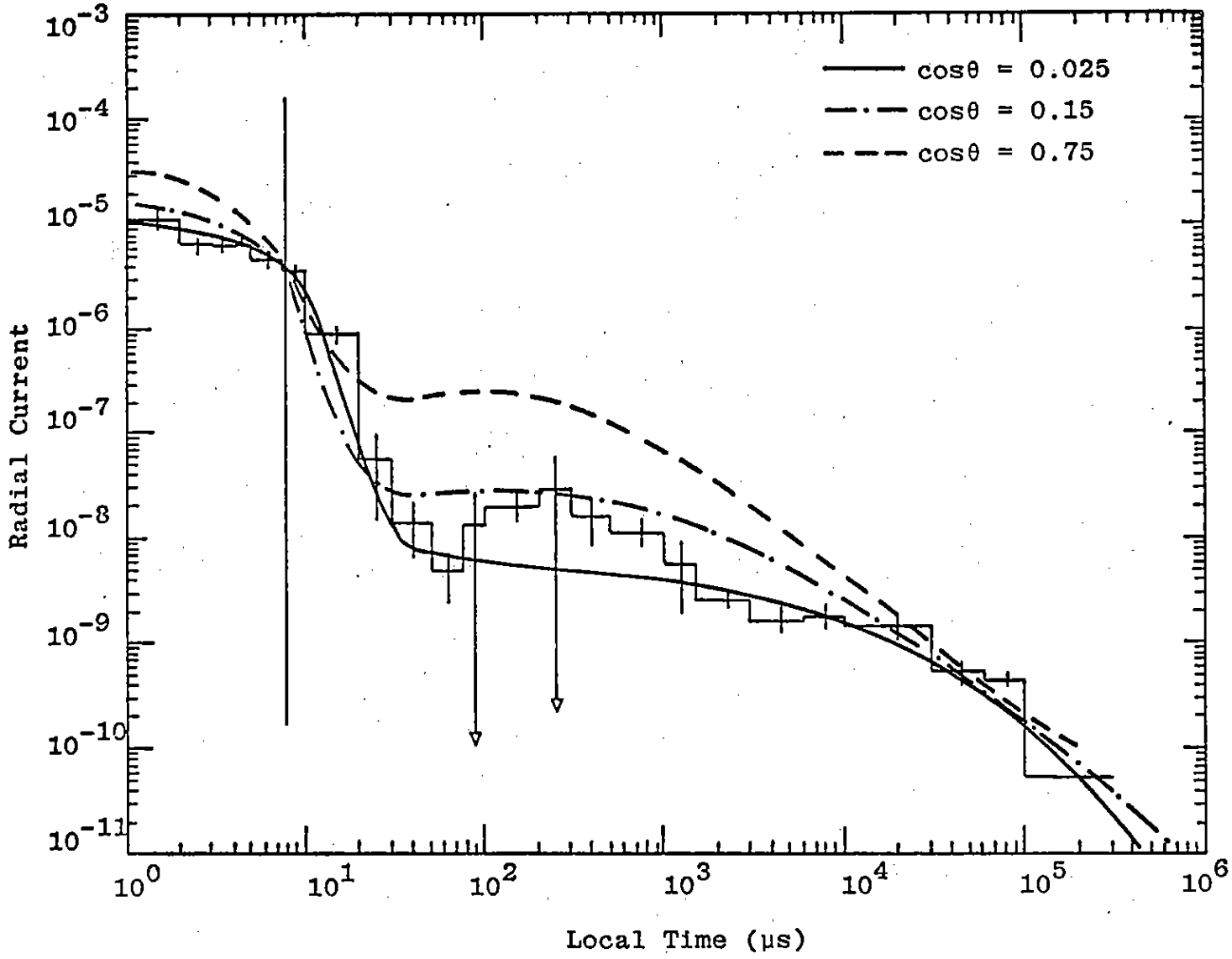

Figure 35. Radial Current vs. Time for the Radius Bin Centered at 500 Meters, Monte Carlo for Bin Centered at cosθ = 0.025 (Ref. 8), SCX Neutron Fits (Ref. 15)

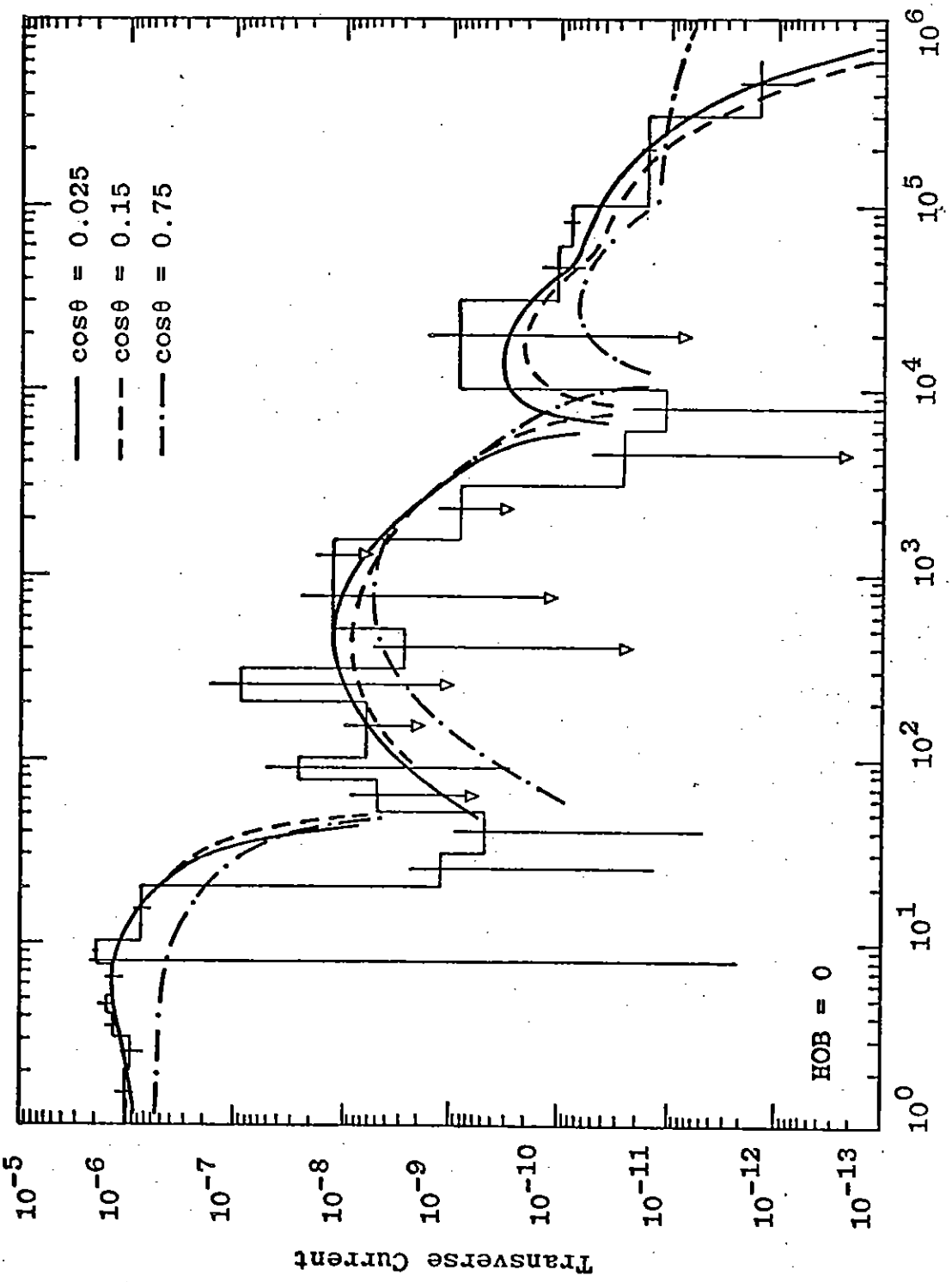

Figure 36. Transverse Current vs. Time for the Radius Bin Centered at 500 Meters, Monte Carlo for Bin Centered at cosθ = 0.025 (Ref. 8), SCX Neutron Fits (Ref. 15)

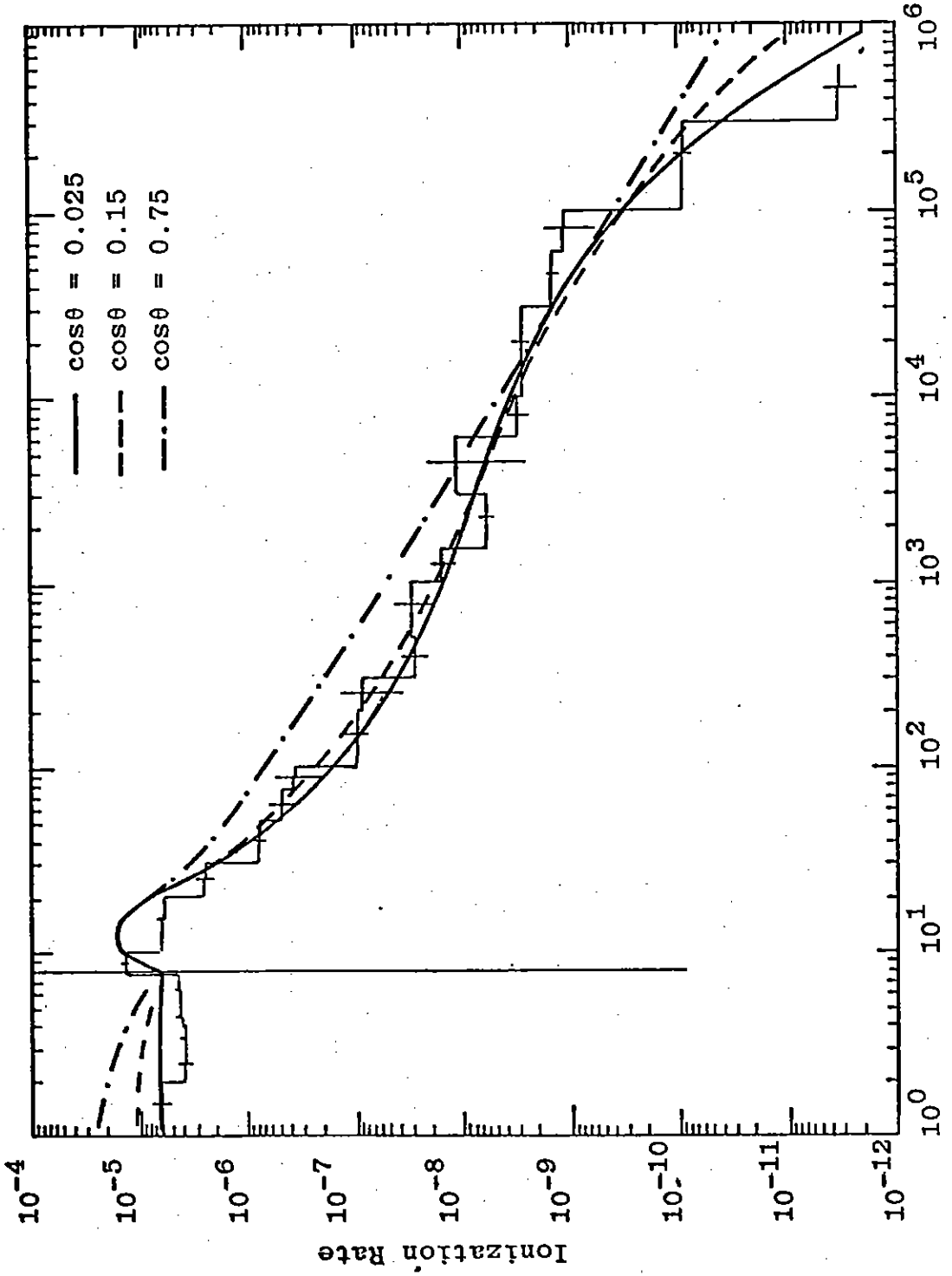

Figure 37. Ionization Rate vs. Time for the Radius Bin Centered at 500 Meters, Monte Carlo for Bin Centered at cosθ = 0.025 (Ref. 8), SCX Neutron Fits (Ref. 9)

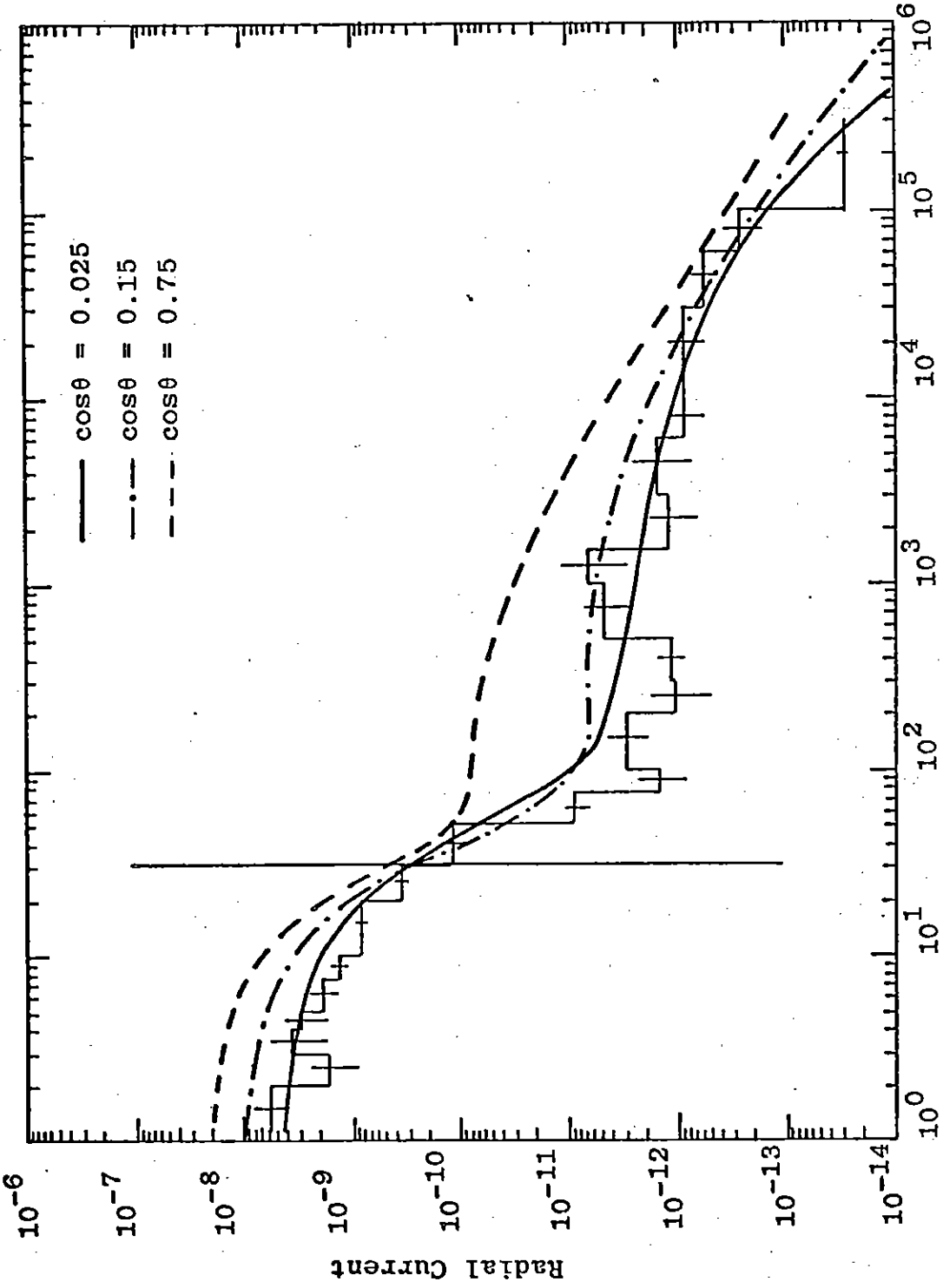

Figure 38. Radial Current vs. Time for the Radius Bin Centered at 2000 Meters, Monte Carlo for Bin Centered at cosθ = 0.025 (Ref. 8), SCX Neutron Fits (Ref. 15)

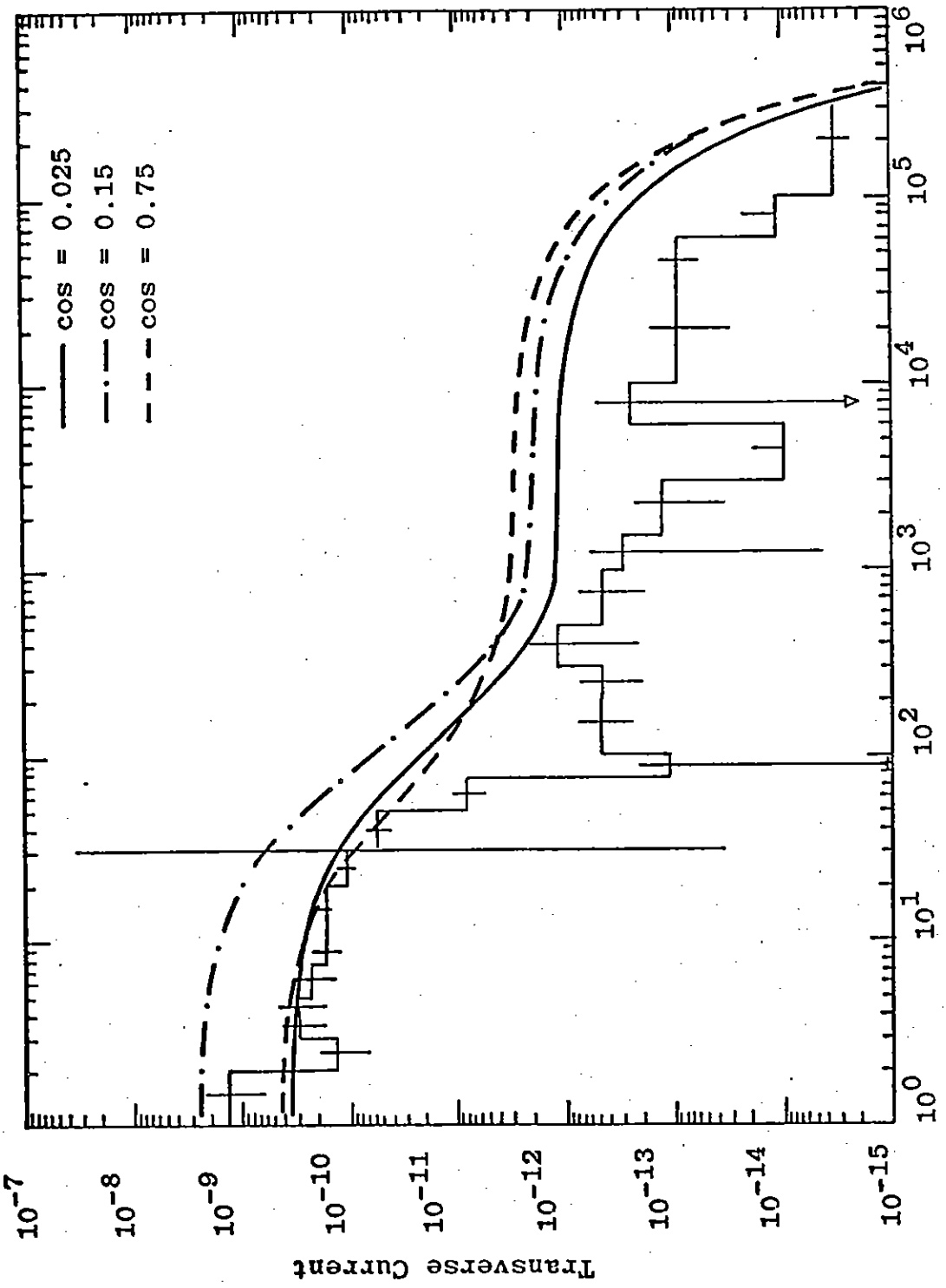

Figure 39. Transverse Current vs. Time for the Radius Bin Centered at 2000 Meters, Monte Carlo for Bin Centered at cosθ = 0.025 (Ref. 8), SCX Neutron Fits (Ref. 15)

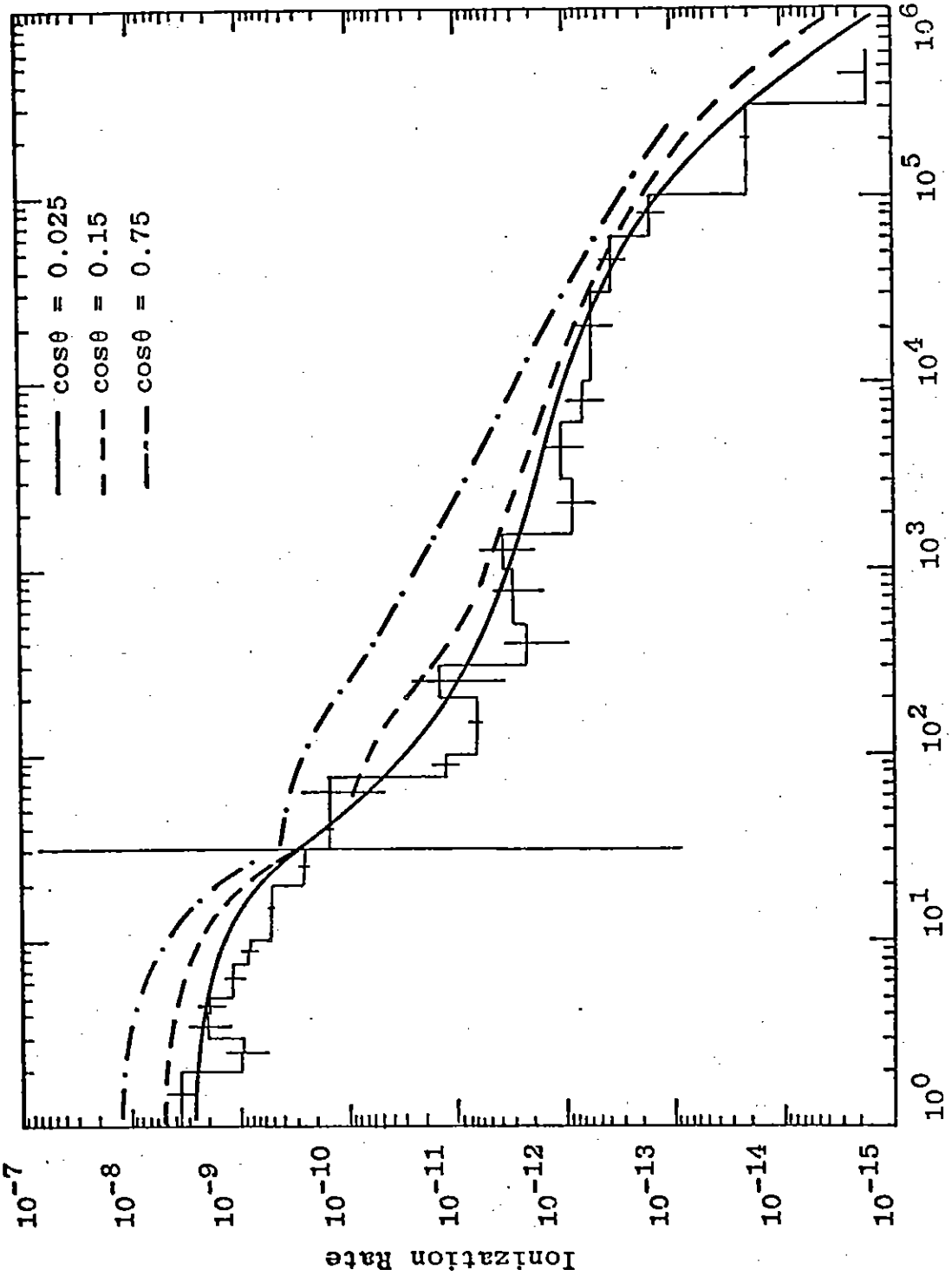

Figure 40. Ionization Rate vs. Time for the Radius Bin Centered at 2000 Meters, Monte Carlo for Bin Centered at cosθ = 0.025 (Ref. 8), SCX Neutron Fits (Ref. 15)

Table 8

ENERGY DISTRIBUTION OF NEUTRONS FOR A GENERAL THERMONUCLEAR SOURCE

Energy	Fractional Number	Energy/Source Neutron (MeV)
<.0290 keV	0.0	0.0
0.290 - .10. keV	.002	1.3×10^{-7}
.101 - .583 keV	.024	8.2×10^{-6}
.583 - 3.35 keV	.122	2.4×10^{-4}
3.35 - 110 keV	.365	.02069
110 - 550 keV	.102	.03366
0.55 - 1.11 MeV	.085	.0706
1.11 - 1.83 MeV	.062	.09114
1.83 - 2.35 MeV	.028	.0585
2.35 - 2.46 MeV	.005	.012
2.46 - 3.01 MeV	.019	.0520
3.01 - 4.07 MeV	.0260	.092
4.07 - 4.97 MeV	.0170	.0768
4.97 - 6.36 MeV	.0180	.102
6.36 - 8.19 MeV	.0147	.107
8.19 - 10.0 MeV	.0141	.128
10.0 - 12.2 MeV	.0256	.284
12.2 - 15 MeV	.0706	.960
	$\Sigma n = 1.0$	$\Sigma E = 2.09$ MeV

Variations in the fits over this angular range (41.4 to 88.6 degrees) can be over an order of magnitude. Variations in the ionization are often less than those for the radial current. Figure 41 shows the time integrated variations at a range of 500 meters, with approximately a factor of 2 variation from 90 to 0 degrees. Only the values for the bin nearest the ground have been used in SCX, with an angular dependence of $(1 - \cos\theta)$ for the transverse current component, J_θ. This introduces a large uncertainty in the source values, usually providing an underestimate for sources at angles above the ground. Since most SCX calculations do not continue past 10^2 microseconds, this problem may not be of as great an importance as it would for later times. Any extension of the problem time would probably warrant the addition of the angular dependence to SCX. These comparisons do not include data at times less than 1 microsecond which are discussed below. A neutron source routine does exist which treats the neutron source angular dependence and this is being added to SCX at the present time. This routine was used to generate the curves of figures 35 through 40 for angles above the ground.

3. LEMP-2 NEUTRON SOURCES

The LEMP-2 neutron sources are described by curve fits to each of the major source production mechanisms: air and ground inelastics, air and ground captures, and neutron recoil (ionization). By separating the treatment of various effects, portions of the curve fits may be more easily understood in terms of the

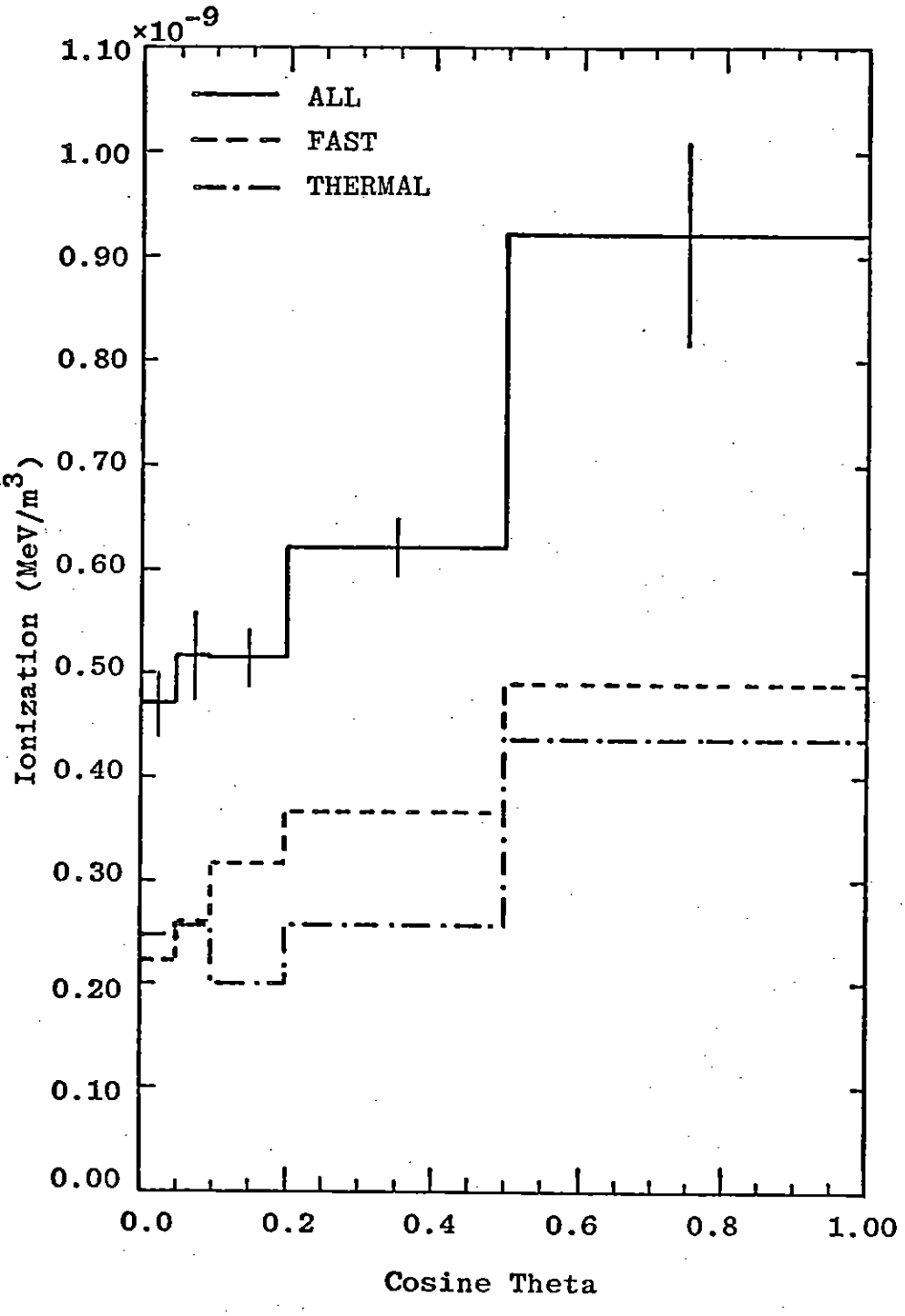

Figure 41. Polar Angle Variation of Neutron-Induced Total Ionization at Radius 450 through 440 Meters, Due to Thermonuclear Source on Ground (Ref. 8)

problem physics and also may be easily modified if better data becomes available. J_θ is not treated in LEMP-2.

Curve fits were based on the data of reference 8, with consideration given to previous fits and analytic studies (refs. 17 and 18). Sample comparisons of the curve fits with the Monte Carlo are given by figures 42 and 43 which are taken from reference 3. Variations in the fits and data are typically on the order of a factor of 2 or less for observers near the surface at intermediate ranges.

4. CODE-CODE COMPARISONS

Figures 44 through 47 compare the SCX and LEMP-2 neutron fits at ranges of 0.5 and 2 kilometers. Angular variations are included in the LEMP-2 fits and LEMP-2 values at $\theta = 0$ (vertical) and 90 degrees are presented. For the 90 degree case (that for which the original SCX fits are valid), the SCX and LEMP-2 values usually agree to within a factor of 2 or better. However, these plots illustrated the need for adding the angular dependence to SCX.

In LEMP-2, one of the input quantities is the fraction of neutrons which have energies above approximately 6 MeV. If this fraction is taken to be the number above 12 MeV (table 8), the comparisons with the SCX fits are improved for the surface observer.

For times less than 100 microseconds, the main change in SCX due to the angular variation will be the addition of the ground inelastic effects at early times. This effect can be quite large (e.g., figure 44).

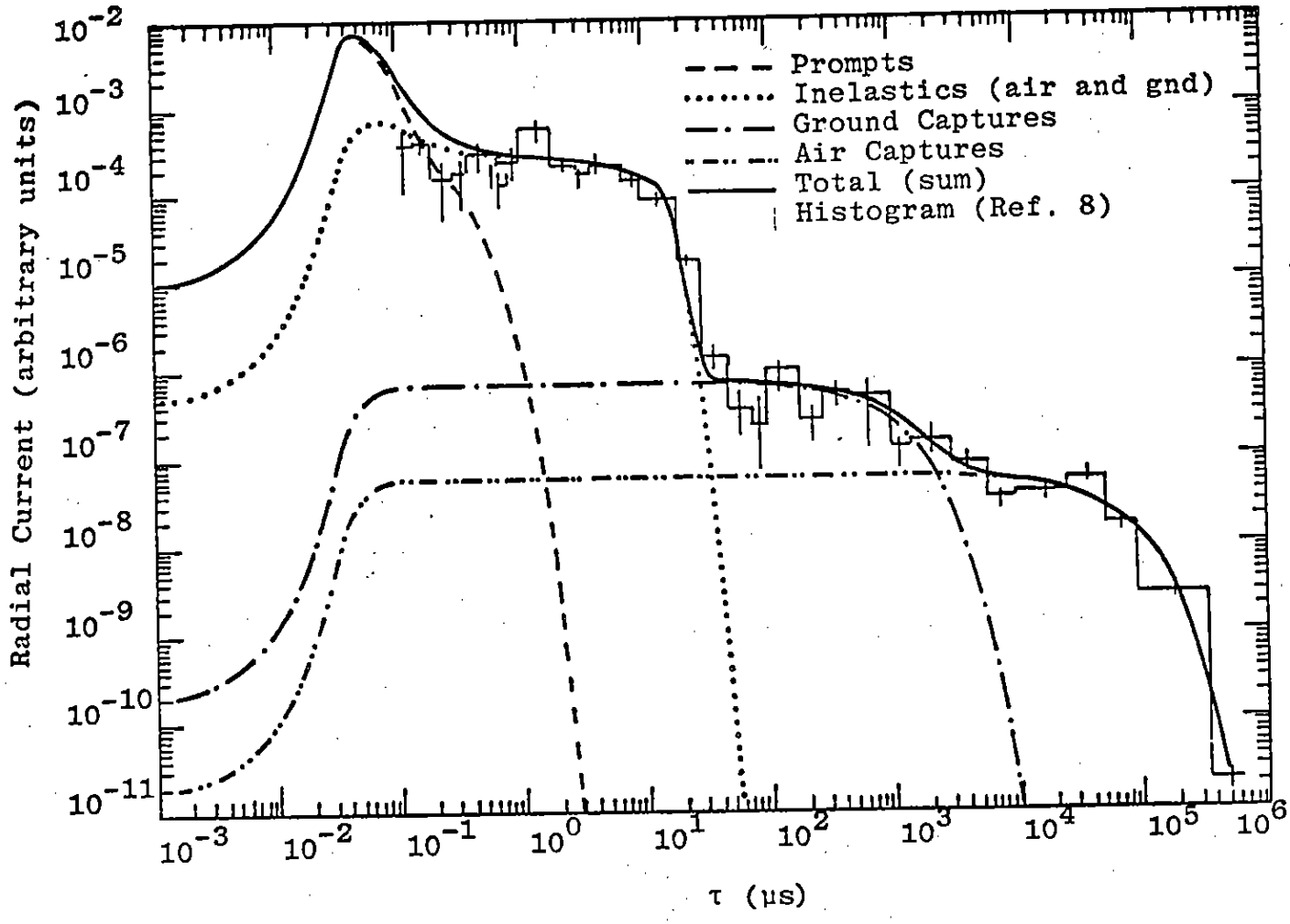

Figure 42. LEMP-2 Radial Current vs. Retarded Time (μs). An example of the source fits and a comparison of the neutron fits with the neutron Monte Carlo data (Ref. 8)

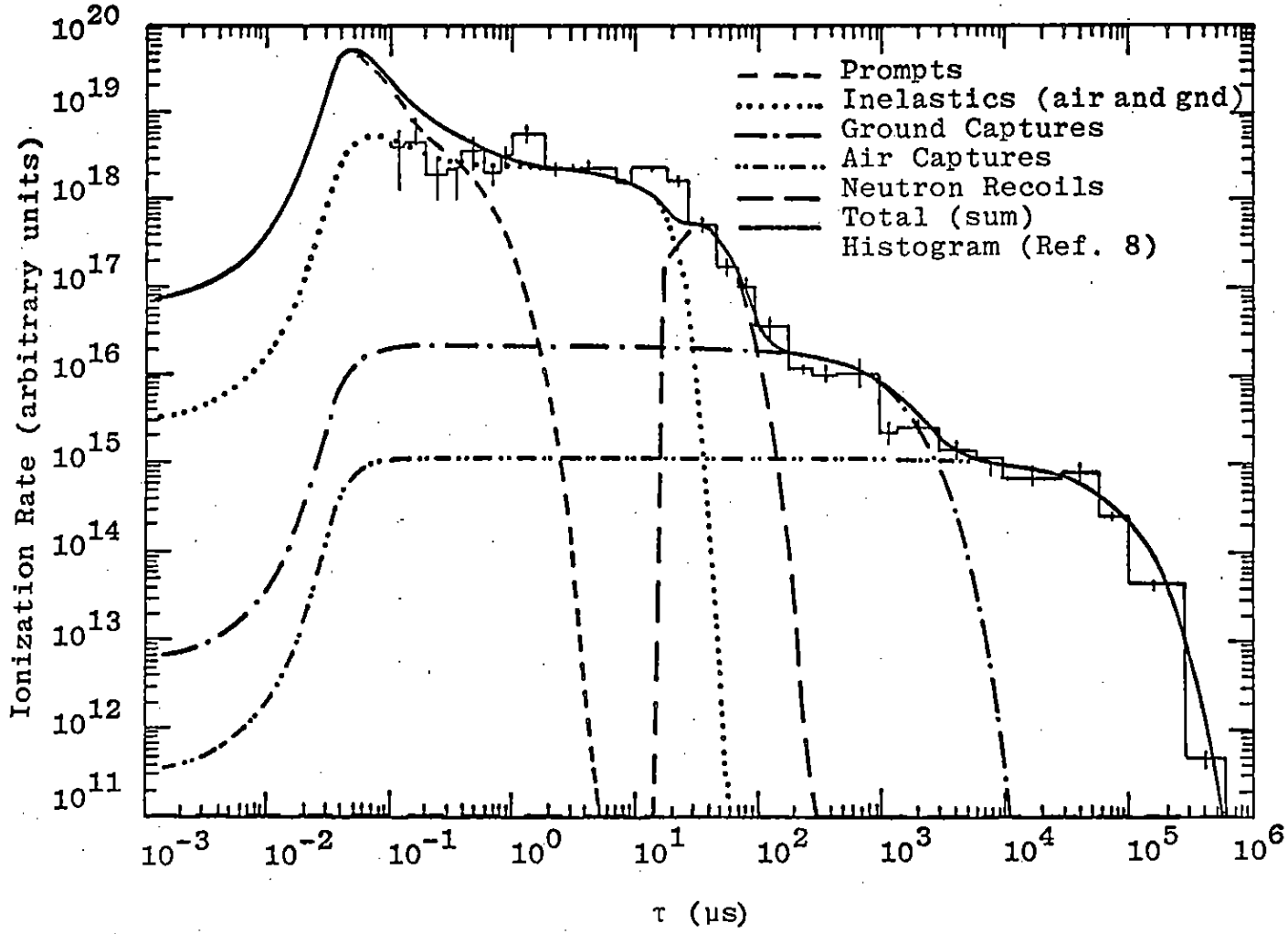

Figure 43. LEMP-2 Ionization Rate vs. Retarded Time (μs). An Example of the Fits and a Comparison of the Neutron Fits with the Neutron Monte Carlo Data (Ref. 8)

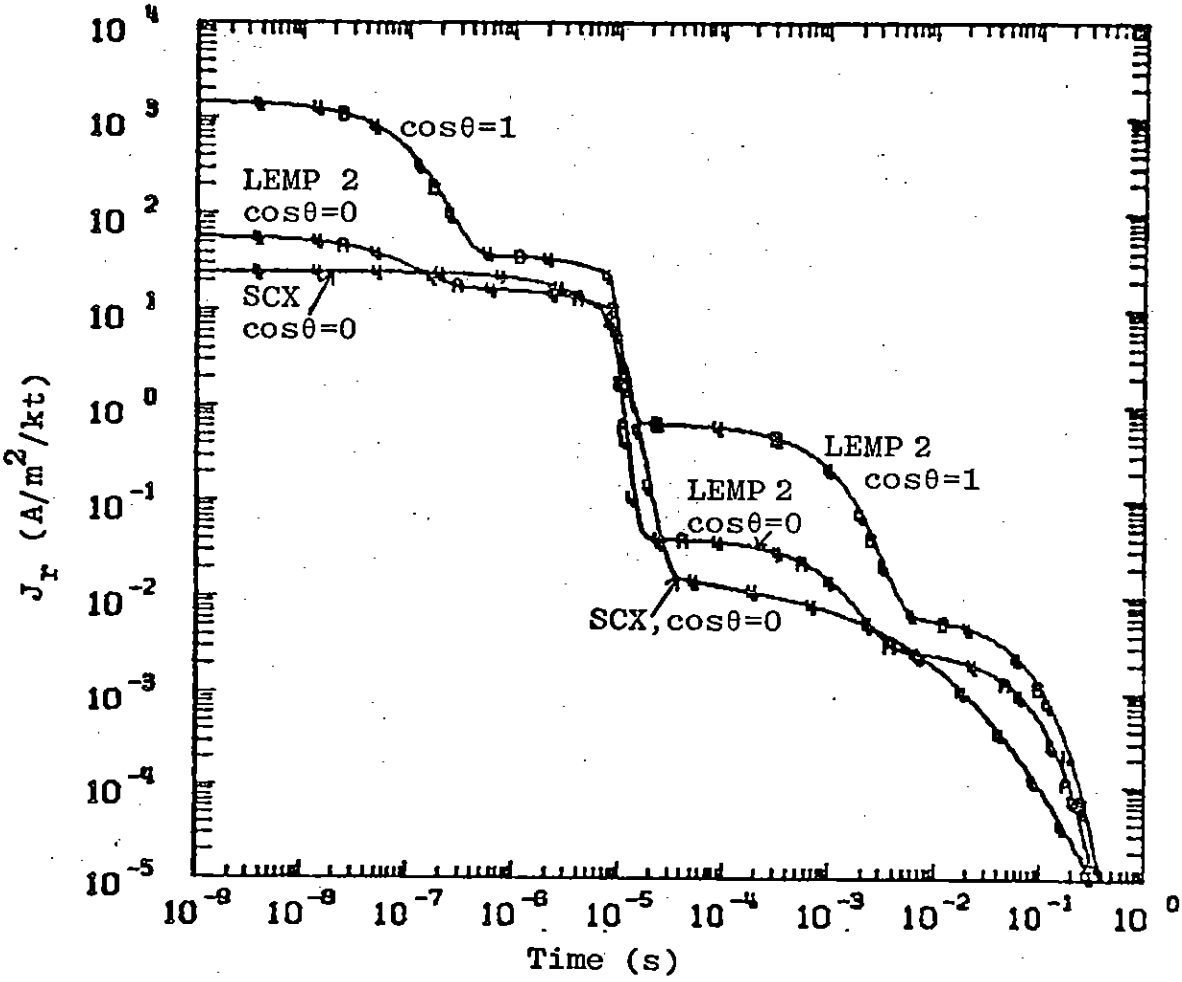

Figure 44. Neutron-Induced Radial Current vs. Time, SCX-LEMP 2 Comparison, Range = 500 Meters

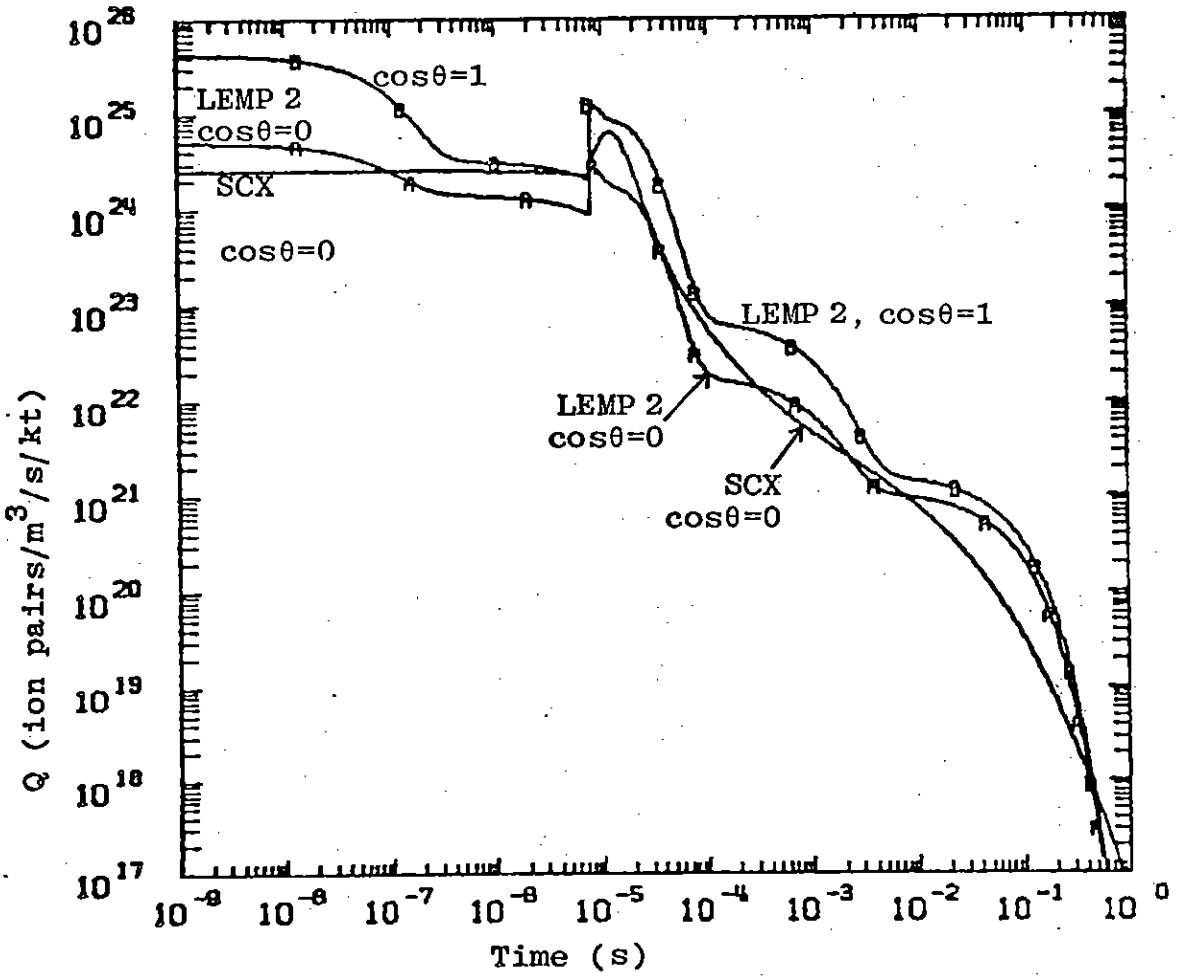

Figure 45. Neutron-Induced Ionization Rate vs. Time, SCX-LEMP 2 Comparison, Range = 500 Meters

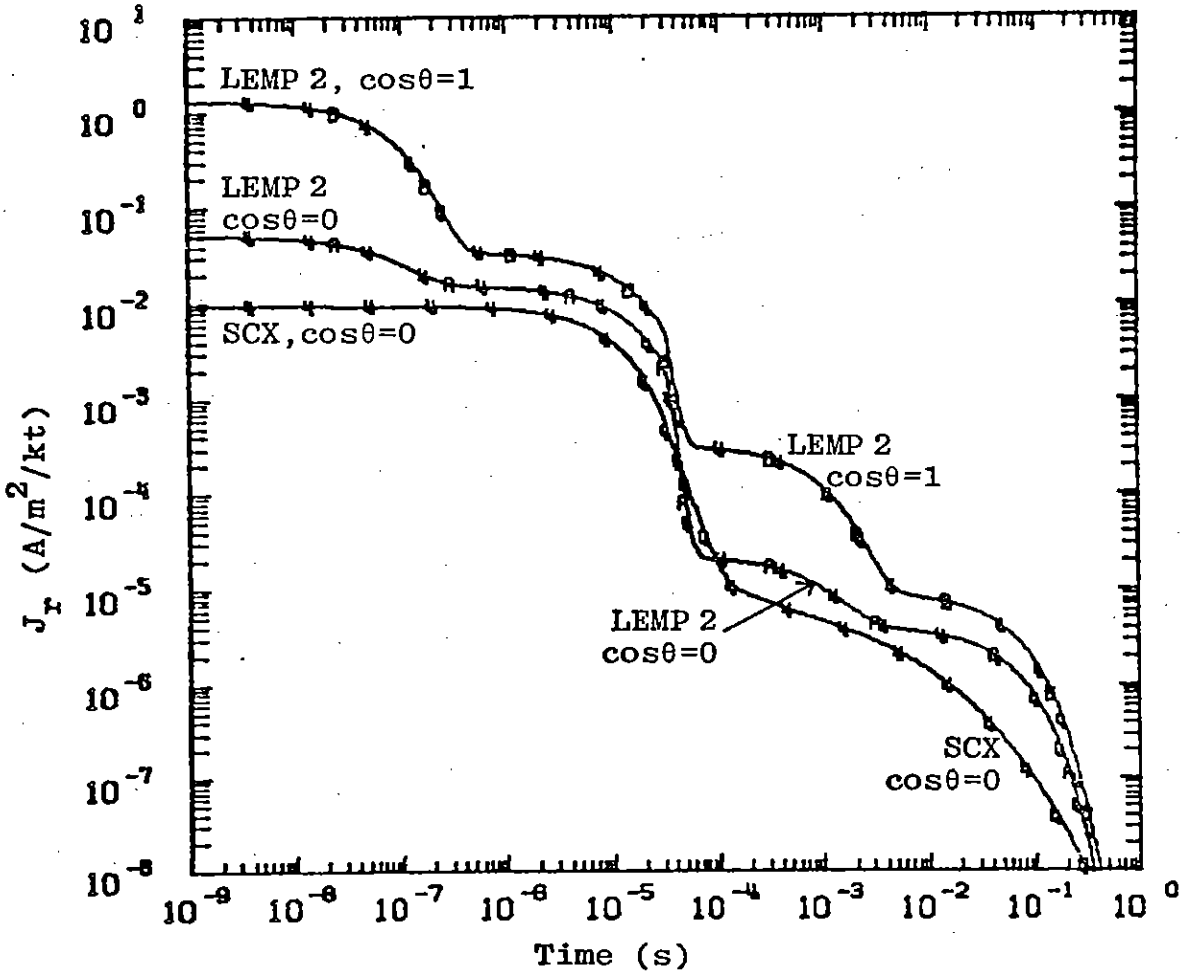

Figure 46. Neutron-Induced Radial Current vs. Time, SCX-LEMP 2 Comparison, Range = 2 Kilometers

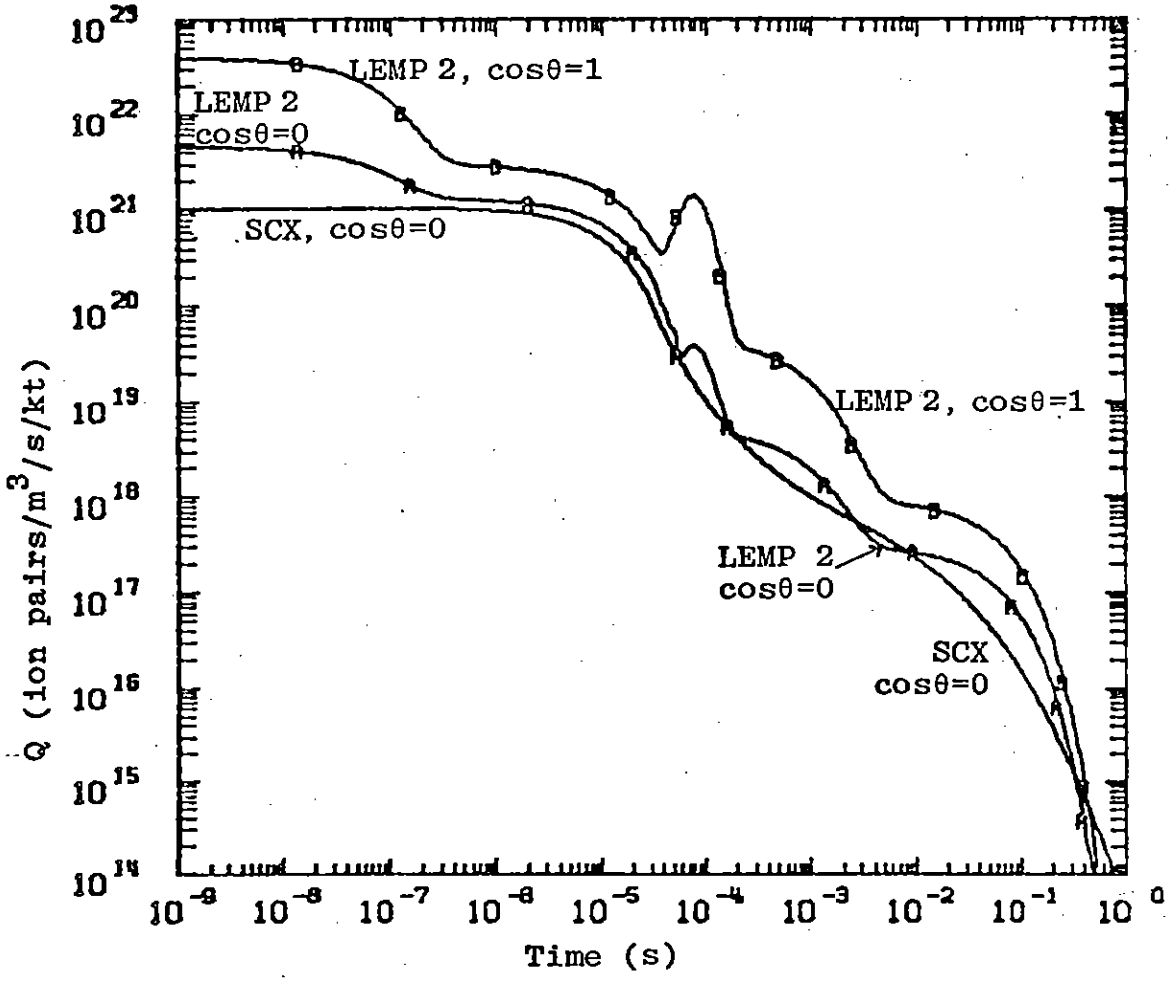

Figure 47. Neutron-Induced Ionization Rate vs. Time, SCX-LEMP 2 Comparison, Range = 2 Kilometers

5. NEUTRON RECOIL CURRENTS

A source term not treated by the Monte Carlo of reference 8 or by SCX or LEMP-2 is the current generated by the scattering of the neutrons by air atoms. This mechanism was noted by Longmire (ref. 19) and was called to the attention of the authors by Gilbert* in connection with underground nuclear test analysis.

For dry air, the dominant mechanism will be the production of positively charged nitrogen atoms (probably with an average charge greater than one) by the elastic scattering of the neutrons. Other processes, such as (n,α), (n,p) reactions may also contribute and should be studied in greater detail.

If the air is humid, there will be (n,p) scattering from the hydrogen in the water. For 100 percent relative humidity at $75^{\circ}F$, there will be 3 percent water vapor. The scattering of 14 MeV neutrons will produce a current of approximately 10^{-23} amps/(neutron/s) which is larger (by about a factor of 5) than those presently computed for the scattering in N_2 and O_2.

Using energy dependent cross sections for 3 percent H_2O, the radial current due to neutron scattering (not (n,γ)) shown by figure 48 is obtained (ref. 20). These values are compared with Monte Carlo results (same data as figure 35). These currents are about a factor of 2 less than those given by reference 19 and are significantly less for the case of a surface burst than the (n,γ) produced currents. The two currents do have opposite signs so that neglect of this effect only tends to

---

*Gilbert, J., private communication, July 12, 1978.

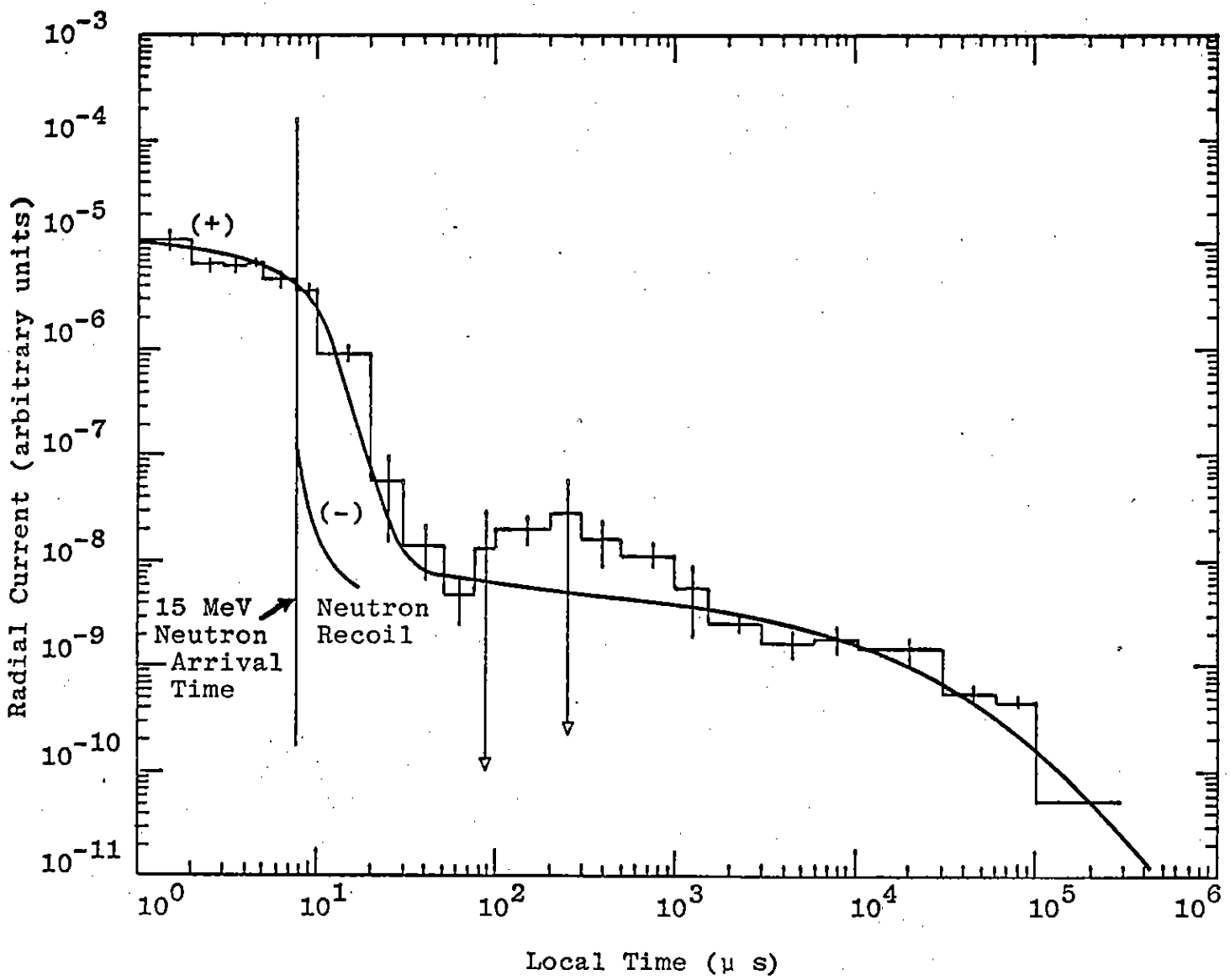

Figure 48. Comparison with Neutron Recoil Currents. Radial Current vs. Time for the Radius Bin Centered at 500 Meters, Cosine θ Centered at 0.025, of an On-the-Ground Spectrum Burst.

provide a small overestimate of the currents. These values may be in error by factors of approximately 2 to 5 but are not likely to impact surface burst results. As noted in reference 19, these sources may be important for other geometries.

SECTION V

CONCLUSIONS

From the data of the previous sections, the following summary can be made:

1. Direct gamma currents and ionization rates are probably correct to within a factor of 2 or better for most ranges of interest. For the early times where these sources are important, the accuracy for fast pulses could be improved by treating finite electron lifetime effects. This uncertainty is not so important for slower pulses and is range independent.

2. Scattered gamma sources are probably accurate to within a factor of 2 or 3. SCX, LEMP-2, and LASL curve fits generally agree to within a factor of 2 or better even at ranges of a few kilometers (for energies of importance there). The main discrepancy appears to be the lack of a treatment of angular variations in either SCX or LEMP-2. This results in LEMP-2 overestimating the scattered gamma flux near the ground by approximately a factor of 2, and SCX underestimating the sources at significant distances above the ground by the same factor. The TIG2 data used in SCX treats the presence of the ground and the resulting transverse currents, which may be important for some problems.

3. Neutron sources are typically accurate to within factors of 3 or better near the ground, although larger errors may be present. The lack of a treatment of the angular dependence in SCX probably results in the underestimation of sources

by one to two orders of magnitude for observers high in the air. One of the effects which is underestimated by not treating the angular variation is the effect of ground capture sources at early time.

The gamma source variations can be implemented in EMP codes in a relatively straightforward manner. Addition of the neutron source angular variation into SCX is being completed using available routines, and comparisons of results with and without the source angular variations are being made.

An effect which potentially applies to all sources is self consistency. This can cause a reduction in peak Compton currents of more than a factor of 2 and is very dependent on the time histories of the electric and magnetic fields. It is not practical to track individual particles in codes such as SCX in order to evaluate this effect. Thus table lookup schemes have been developed for SCX and LEMP-2 in order to include self consistency in the simulations at a reasonable cost. For most applications, these treatments are probably accurate to within 50 percent or better, as shown by comparisons with one-dimensional particle codes in the close-in region. The effects at farther ranges on radiated fields such as E_θ may be larger due to the integration of non-linear effects over a significant range.

This discussion has not included treatments of electron scattering and absorption by the ground. Electron and gamma

scattering by systems which may be in the source region has also been ignored. These are more scenario dependent and therefore more difficult to treat than the sources needed to compute general EMP environments.

The effects of the shock wave are also not included in the results presented here. Increases in density due to the shock wave will cause a local increase in deposition and a decrease in the source strength at more distant ranges. There will be decreased attenuation in the rarefied region behind the shock front. Increases in temperature will also cause an increase in the ionization density, especially at closer ranges. These effects are normally not included in EMP calculations at the present time, although some work is being done in this area.

REFERENCES

1. Dalich, S.J., and K.D. Granzow, Two-Dimensional Ground Burst Electromagnetic Pulse Calculational Method, AFWL-TR-73-286, Vol. III, Air Force Weapons Laboratory, Kirtland AFB, NM, February 1974.

2. Asbury, R.K., SCX Code Description and User's Manual, DC-TN-1290-4 (Draft), Dikewood Industries, Inc., May 5, 1978.

4. Knutson, G.R., "Preliminary Curve-Fit Representations for Gamma Induced Air-Over-Ground EMP Sources," EMP Theoretical Note 175, Air Force Weapons Laboratory, Kirtland AFB, NM, December 1972.

5. Peterson, David H., TIG2 (A Monte Carlo Code for Predicting Electrical Currents and Ionization Rates Resulting from Photon Transport in the Vicinity of a Material Interface), DC-TN-1214-2, The Dikewood Corporation, November 16, 1970.

6. Chilton, A.B., Nucleonics, 23, pp. 119-122, August 1965.

7. LeLevier, R.E., Compton Current and the Energy Deposition Rate from Gamma Quanta - A Monte Carlo Calculation, RM-4151-PR, The RAND Corporation, June 1964. (Also EMP Theoretical Note 37).

8. Sargis, D.A., E.R. Parkinson, J.N. Wood, R.E. Dietz, and C.A. Stevens, Late-Time Sources for Close-In EMP, DNA 3064F, Defense Nuclear Agency, August 1972.

9. Hubbell, J.H., Photon Cross Sections, Attenuation Coefficients, and Energy Absorption Coefficients from 10 keV to 100 GeV, NSRDS-NBS 29, National Bureau of Standards, August 1969.

10. Malik, J.S., E.D. Cashwell, and R.G. Schrandt, The Time Dependence of the Compton Current and Energy Deposition from Scattered Gamma Rays, LA-7386-MS (Informal Report), Los Alamos Scientific Laboratory, July 1978.

11. Jones, C.W., "Compton Electron Range Data for EMP Calculations," EMP Phenomenology Memo No. 10, Dikewood Industries, Inc., June 14, 1977.

12. Jones, C.W., "ODRTS: A One-Dimensional Real Time Source Routine," EMP Phenomenology Memo No. 1, Dikewood Industries, Inc., February 11, 1975.

13. Schaefer, R.R., "Prompt Gamma Effects in the Vicinity of a Ground-Air Interface," EMP Theoretical Note 10, Air Force Weapons Laboratory, Kirtland AFB, NM, May 26, 1965.

14. Pine, V.W., "Prompt Gamma Effects in a Homogeneous Atmosphere," EMP Theoretical Note 66, Air Force Weapons Laboratory, Kirtland AFB, NM, October 6, 1969.

15. Wood, J.N., and B.H. Fishbine, Representation of Late Time Low Altitude Electromagnetic Pulse Sources, AFWL-TR-74-339, Air Force Weapons Laboratory, Kirtland AFB, NM, September 1975.

16. Wood, J., and M. Legan, Enhanced Neutron-Induced Sources for Surface Burst EMP, SAI-78-201-AQ, Science Applications, Inc., June 1978.

17. O'Dell, A.A., C.L. Longmire, and H.J. Longley, The Development of Improved Late-Time Sources for the LEMP Computer Code, MRC-R-104, Mission Research Corp., January 1974.

19. Longmire, C.L., Survey of Neutron Induced EMP, MRC-N-336, Mission Research Corp., March 1978.

20. Jones, C.W., Direct Neutron-Induced Currents for DIABLO HAWK, DC-TN-1298-2 (Draft), Dikewood Industries, Inc., August 11, 1978.

APPENDIX A

ONCE-SCATTERED GAMMA FLUX ANGULAR VARIATIONS

The angular variations of the scattered-gamma sources described in section III have only been approximately described by available Monte Carlo data. Statistical variations in the simulations, especially at early times, and the large scoring bin sizes often tend to mask these variations. While not giving a complete description of the scattered gamma source, the computation of the once-scattered flux described below should provide useful data for scaling laws which may be applied to more accurate Monte Carlo data.

The once-scattered flux reaching an observer at location $\vec{r}$ due to one source gamma ray is

$$F_1(\vec{r},\tau) = \int_V \frac{e^{-\sigma_T \rho r_1}}{4\pi r_1^2} \frac{\rho d\sigma_c(\vec{r}_1,\vec{r}-\vec{r}_1)}{d\Omega|\vec{r}-\vec{r}_1|^2} e^{-\sigma_T' \rho |\vec{r}-\vec{r}_1|} \times \delta(|\vec{r}| + c\tau - |\vec{r}_1| - |\vec{r}-\vec{r}_1|)\, dV \qquad \text{(A1)}$$

where δ is the Dirac delta function, $d\sigma_c/d\Omega(\vec{r}_1,\vec{r}-\vec{r}_1)$ is the differential Compton scattering cross section and $\vec{r}_1$ is the vector from the source to any given location of the first gamma scatter. Primed quantities are for the scattered photon and unprimed quantities are for the unscattered photon from the source. The volume of integration, V, will extend over all space in the air for which a gamma can scatter at an angle for which $d\sigma/d\Omega$ is

non-zero and for which $\{|\vec{r}_1| + |\vec{r} - \vec{r}_1| - |\vec{r}|\}/c$ is less than the maximum time of interest. For a surface burst, scattering locations in the ground need not be considered.

Set

$$G_1(\vec{r}_1) = \frac{e^{-\sigma_T \rho r_1}}{4\pi r_1^2} \tag{A2}$$

$$G_2(\tau, \vec{r} - \vec{r}_1) = \frac{\sigma_T' \rho \; e^{-\sigma_T' \rho |\vec{r} - \vec{r}_1|} \; \delta(|\vec{r}| + c\tau - |\vec{r}_1| - |\vec{r} - \vec{r}_1|)}{|\vec{r} - \vec{r}_1|^2} \tag{A3}$$

The ionization rate and Compton current components due to interaction of the once-scattered gamma flux may then be written as

$$Q(\vec{r}, \tau) = \int_V G_1(\vec{r}_1) G_2(\tau, \vec{r} - \vec{r}_1) \frac{d\sigma(\vec{r}_1, \vec{r} - \vec{r}_1)}{d\Omega} \rho E_e' \, dV \left(\frac{\text{MeV}}{\text{m}^3\text{-sec}}\right) \tag{A4}$$

$$J_r(\vec{r}, \tau) = \int_V G_1(\vec{r}_1) G_2(\tau, \vec{r} - \vec{r}_1) \frac{d\sigma(\vec{r}_1, \vec{r} - \vec{r}_1)}{d\Omega} \frac{(\vec{r} - \vec{r}_1) \cdot \vec{r}}{|\vec{r} - \vec{r}_1| \; |\vec{r}|} R_e' \, dV$$

$$\left(\frac{\text{electrons}}{\text{m}^3\text{-sec}}\right) \tag{A5}$$

$$J_\theta(\vec{r}, \tau) = \int_V G_1(\vec{r}_1) G_2(\tau, \vec{r} - \vec{r}_1) \frac{d\sigma(\vec{r}_1, \vec{r} - \vec{r}_1)}{d} \frac{\hat{\theta} \cdot (\vec{r} - \vec{r}_1)}{|\vec{r} - \vec{r}_1|} R_e' \, dV$$

$$\left(\frac{\text{electrons}}{\text{m}^3\text{-sec}}\right) \tag{A6}$$

where

$$dV = r_1^2 \sin\theta \; dr_1 \; d\theta \; d\phi \tag{A7}$$

and $\hat{\theta}$ is a unit vector perpendicular to $\vec{r}$ and defined to be upward vertical ($\phi = 0$).

The ϕ dependence may be evaluated analytically for each (r,θ) point in the numerical integrations of equations (A4), (A5) and (A6), excluding regions in the ground. This permits the evaluation of these integrals in a short time on the AFWL CDC CYBER 176. The forms for the differential cross section and the relation of electron range and average electron energy as a function of scattered gamma energy make complete analytic solutions almost impractical. Extensions to treat the second-scatter are straightforward and may be performed in the future. The major additional complication in treating the second scatter is the necessity of including scattering locations in the ground. This is conceptually easy but very time consuming numerically.

The results obtained using the relations described above agree to within 40 percent or better with the Monte Carlo for reasonable ranges at early times. Variations in time also agree well with the Monte Carlo to times of a few shakes when higher order scatters would be expected to become important. The numerical results thus appear to have the proper behavior.

Figures A1, A2, and A3 show numerical results at a range of 500 meters for various observer distances above the ground (constant slant range). The behavior at other ranges is very similar with decay rates being faster for closer ranges, and larger for farther ranges, as would be expected.

Using physical arguments, the values of Q and J_r at the air-ground interface ($\theta = 90^o$) would be expected to have a value of 0.5 the value at $\theta = 0^o$ (vertically upward) at early times. The results are consistent with this reasoning. In addition, the

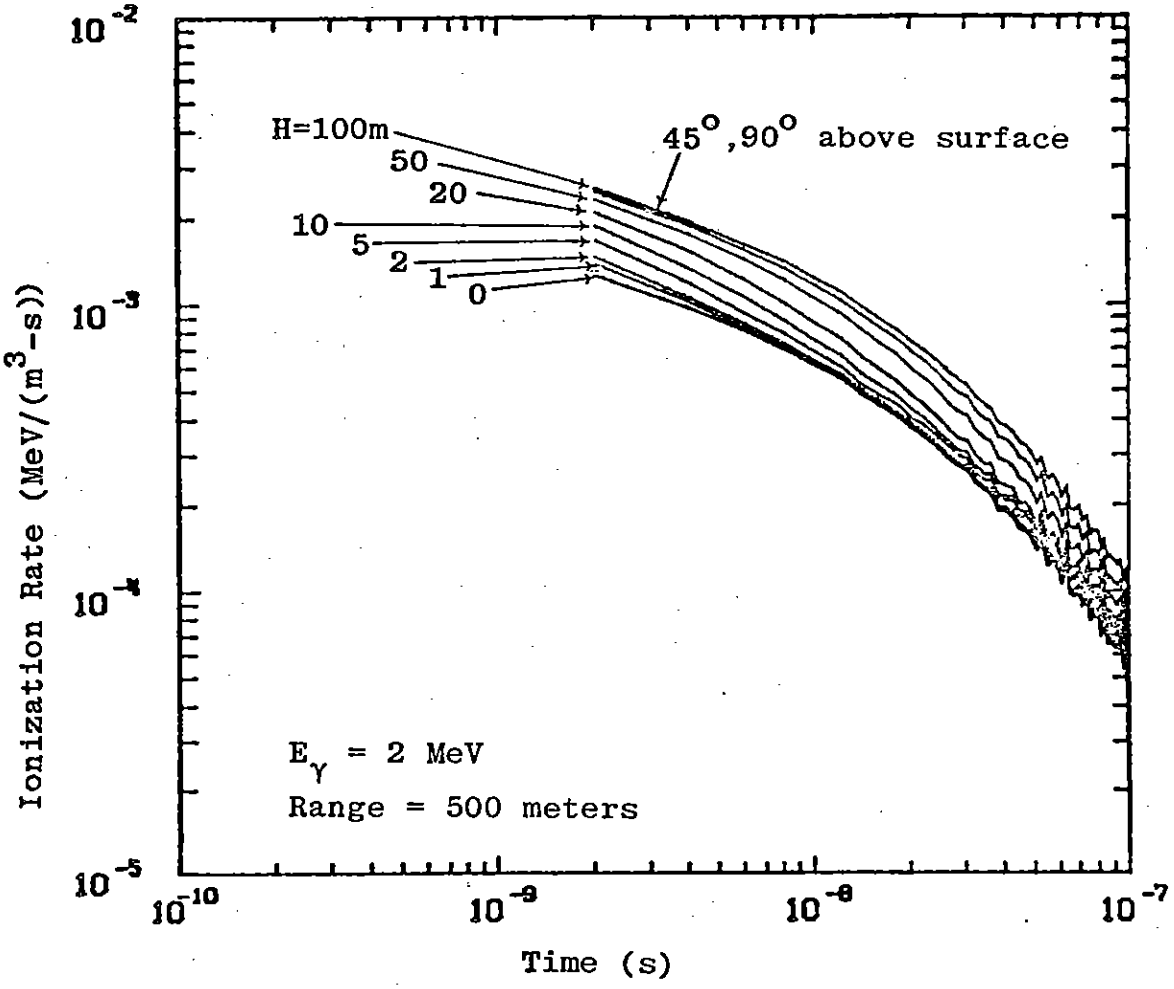

Figure A1. First Scatter Ionization Rate vs. Time and Distance Above Ground

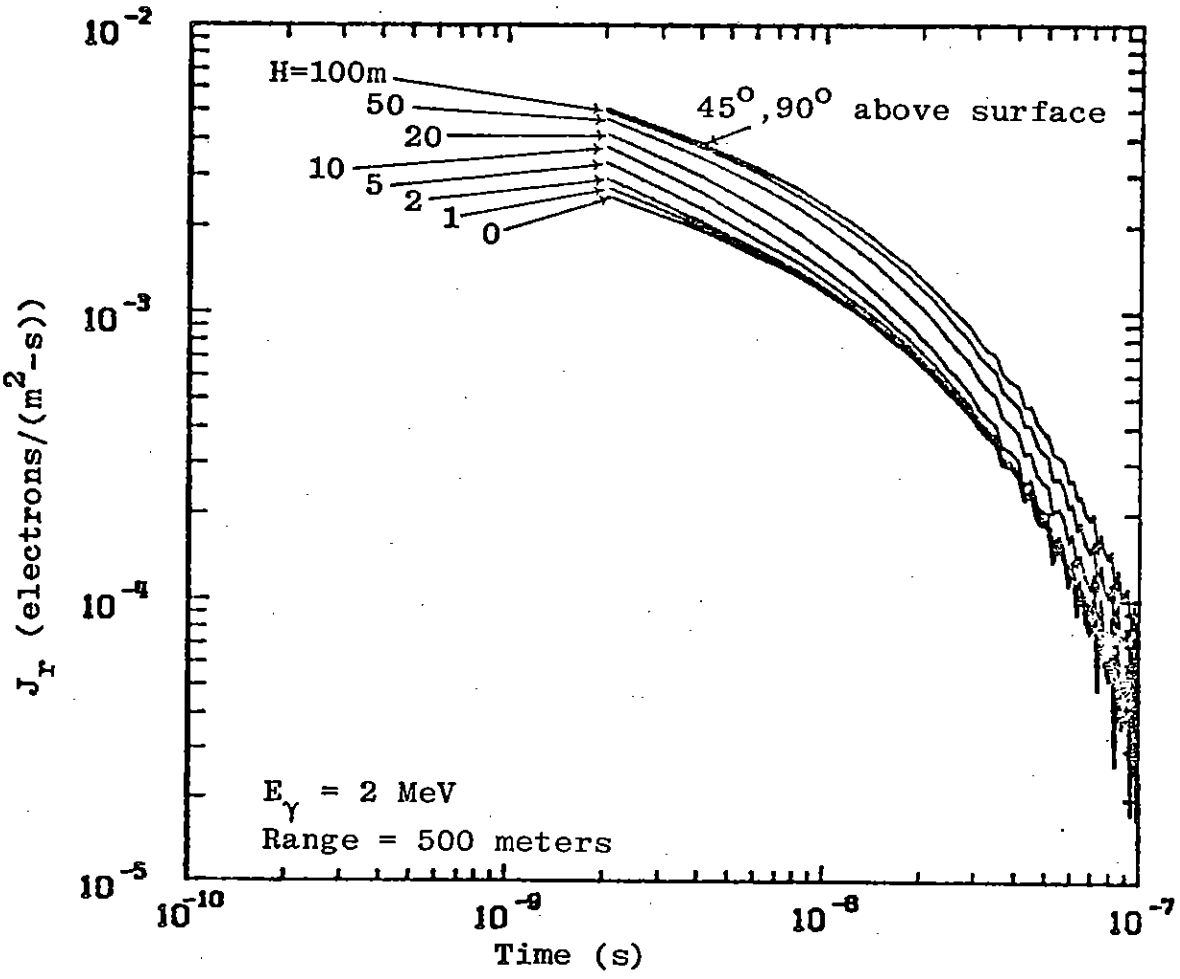

Figure A2. First Scatter Radial Current vs. Time and Distance Above Ground

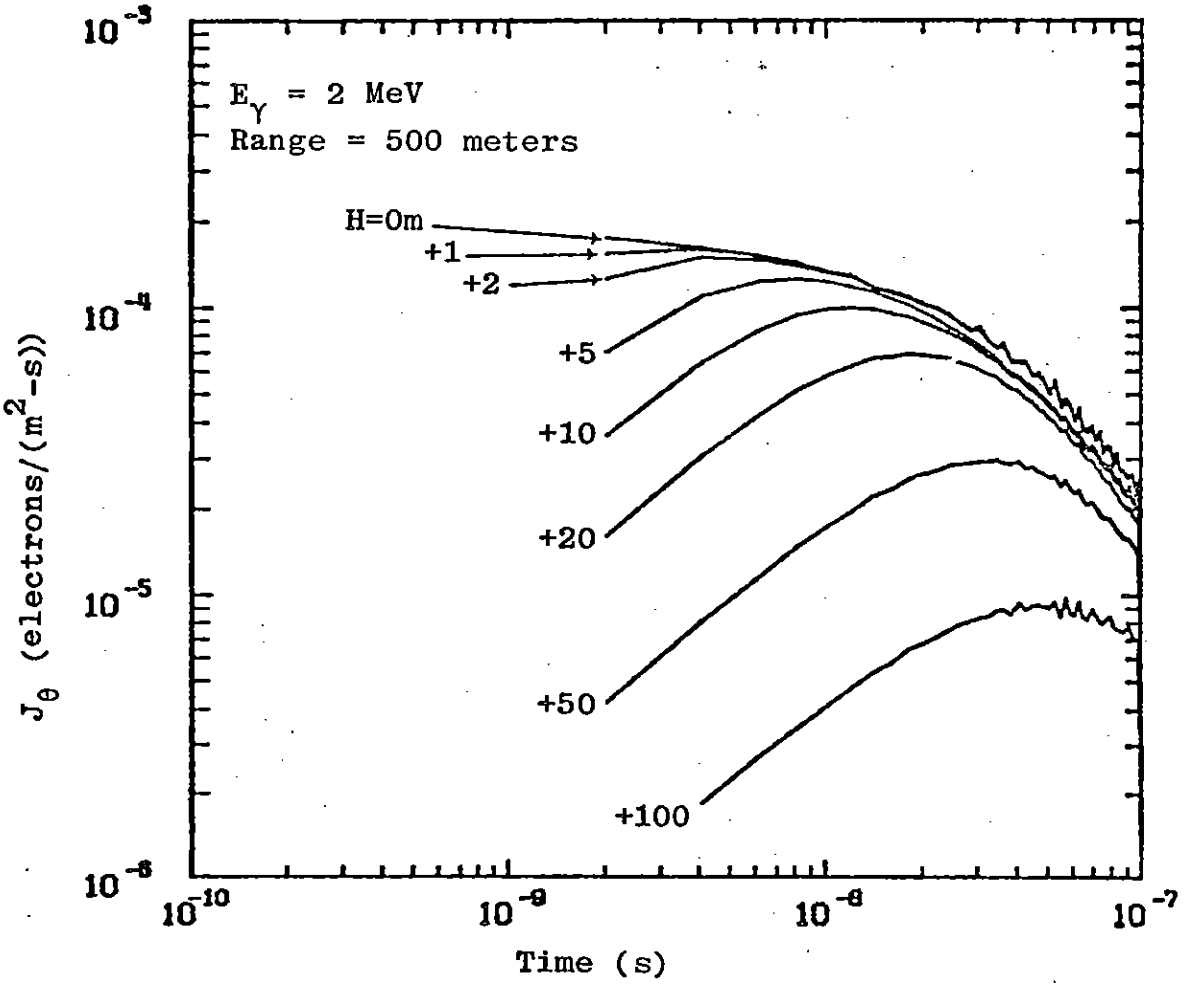

Figure A3. First Scatter Theta Current vs. Time and Distance Above Ground

results for a given height (angle θ above the surface) cannot be affected by the presence of the ground until times governed by causality.

Given the values of the sources at the surface, the values at higher angles may be approximated by using fits to the variations of figures A1, A2 and A3.

$$Q(\theta) = Q(0^{o})[1.01 + 0.644 \tan^{-1} ((\theta + 0.00256)\ 17.45)] \quad \text{(A8)}$$

$$J_r(\theta) = J_r(0^{o})[0.88 + 0.747 \tan^{-1} ((\theta + 0.015)\ 12.25)] \quad \text{(A9)}$$

$$J_\theta(\theta) = J_\theta(0^{o})\left[\frac{B}{(R \sin\theta + B)}\right]^3 e^{-4\theta^{2.5}} \quad \text{(A10)}$$

where θ is in radians, R is in meters, and

$$B = 18\left(1 + 2\ \ell n \frac{T}{2 \times 10^{-9}}\right) \quad \text{(A11)}$$

with T the time in seconds. Comparisons of the behavior of these fits and the first scatter results are given by figures A4, A5 and A6. Considering the uncertainties in this treatment, especially for times greater than a few shakes when the many-scattered contribution dominates, the accuracy of these fits should be sufficient for evaluating these angular variation effects in an EMP fields code such as SCX, in which their implementation will be straightforward.

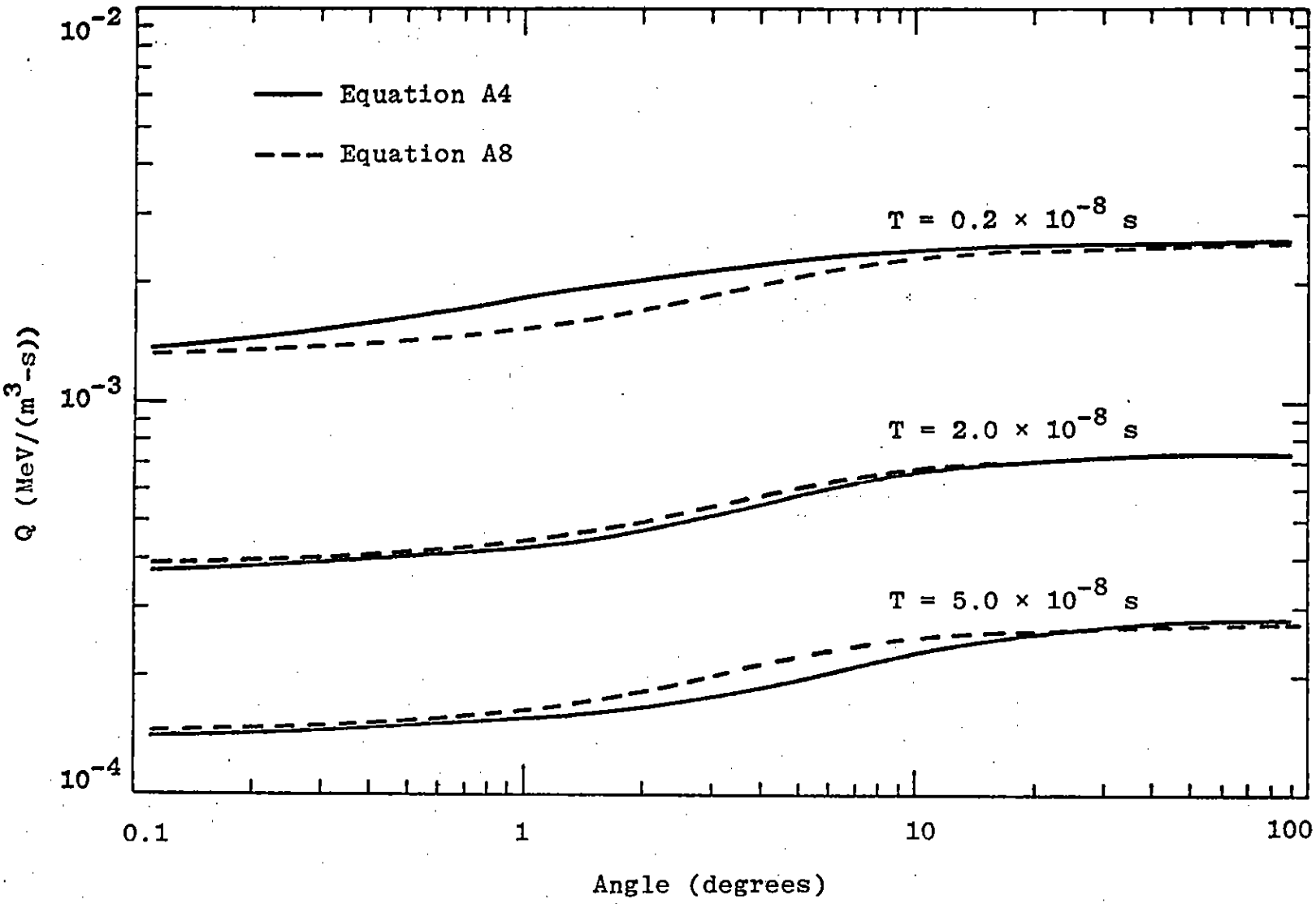

Figure A4. Ionization Rate vs. Angle Above Surface, Range = 500 Meters, E_γ = 2 MeV

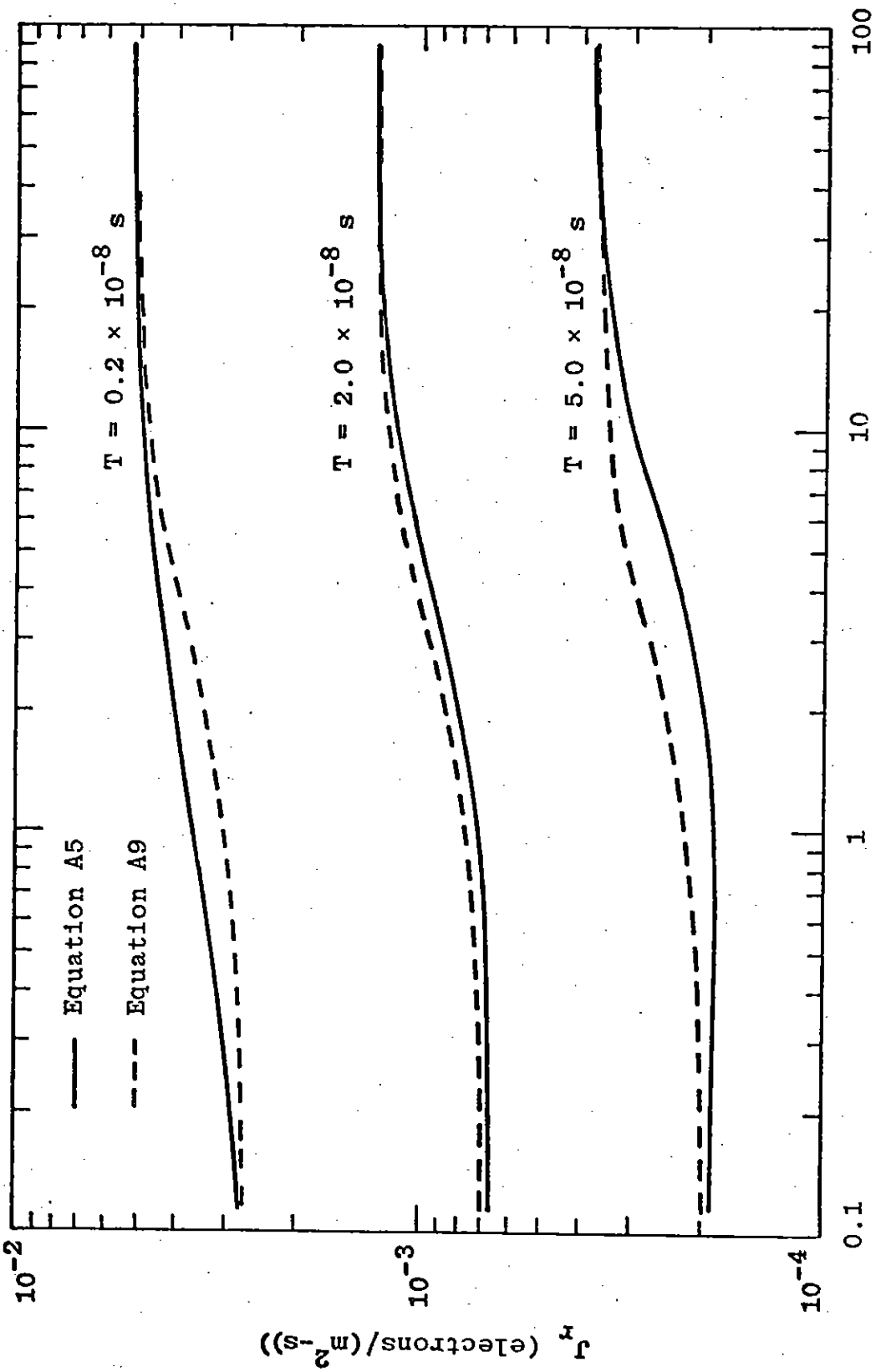

Figure A5. Radial Current vs. Angle Above Surface, Range = 500 Meters, E_γ = 2 MeV

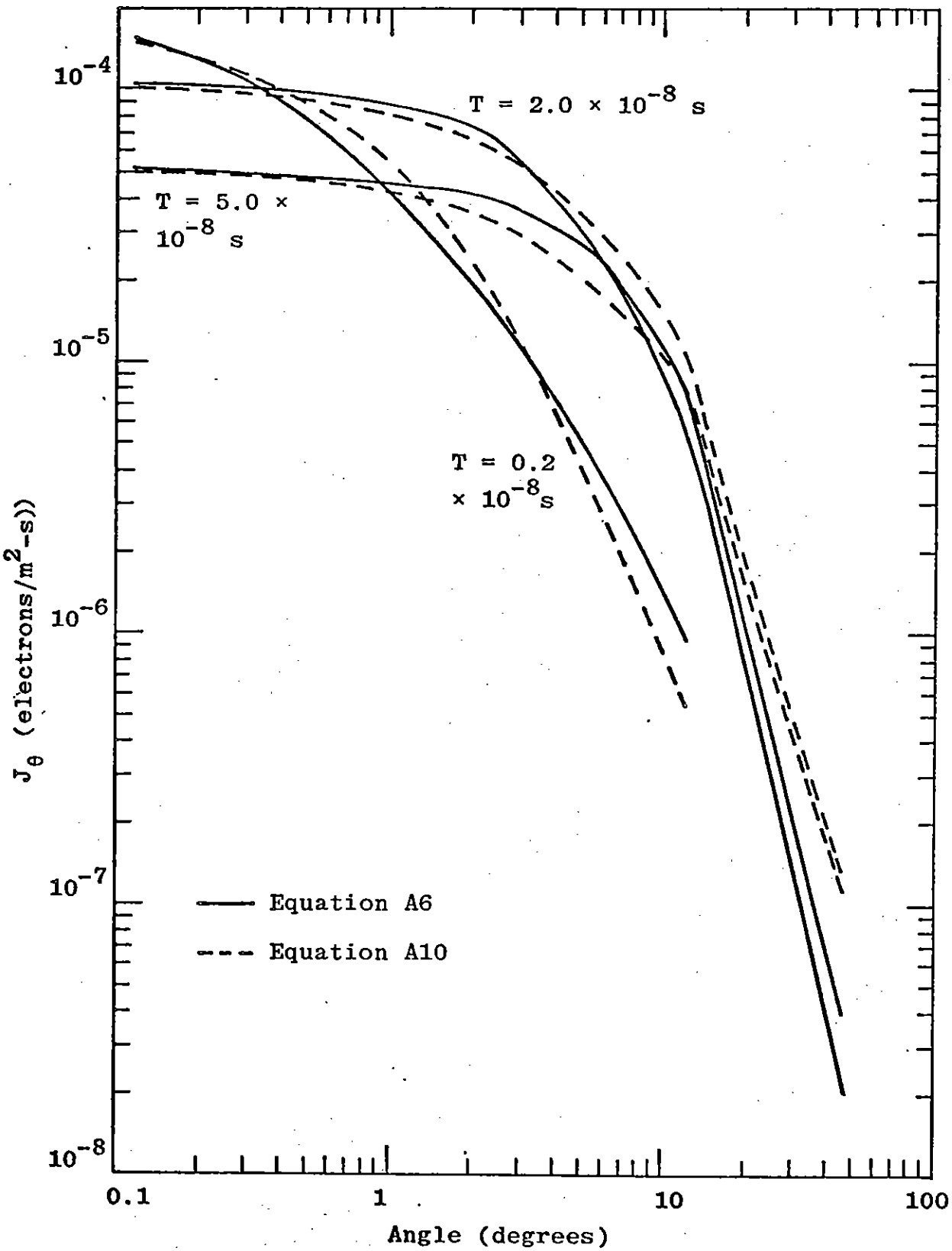

Figure A6. Transverse Current vs. Angle Above Surface, Range = 500 Meters, E_γ = 2 MeV